Ministry of Natural Resources
Ontario

Hon. Alan W. Pope
Minister

W. T. Foster
Deputy Minister

ONTARIO GEOLOGICAL SURVEY

Open File Report 5462

Ontario Geoscience Research Grant Program
Grant No. 82
Structural Controls of Uranium-Ore Bodies
In the Madawaska Mines
Bancroft Area

by

R.L. Bedell and W.M. Schwerdtner

1983

Ontario Geological Survey

OPEN FILE REPORT

ONTARIO GEOSCIENCE RESEARCH GRANT PROGRAM

Final Research Reports, 1983

Preface

This publication includes one final report on a research project that terminated March 31, 1982 and was funded under the Ontario Geoscience Research Grant Program. A requirement of the Program is that recipients of grants are to submit final reports within six months after termination of funding.

A final report is defined as a comprehensive summary stating the findings obtained during the tenure of the grant, together with supporting data. It may consist, in part, of reprints or preprints of publications and copies of addresses given at scientific meetings.

It is not the intent of the Ontario Geological Survey to formally publish the final reports for wide distribution but rather to encourage the recipients of grants to seek publication in appropriate scientific journals whenever possible. The Survey, however, also has an obligation to ensure that the results of the research are made available to the public at an early date. Although final reports are the property of the applicants and the sponsoring agencies, they may also be placed on an open file. This report is intended to meet this obligation.

E.G. Pye
Director
Ontario Geological Survey

Table of Contents Page

Maps (In Back Pocket)

Ontario Geoscience Research Grant Program
Grant No. 82
Structural Controls of Uranium-Ore Bodies
In the Madawaska Mines
Bancroft Area

by

R.L. Bedell[1] and W.M. Schwerdtner[1]

[1] University of Toronto
Department of Geology
Toronto, Ontario

Manuscript approved by E.G. Pye, Director, Ontario Geological Survey, April 22, 1983.

This report is published by permission of E.G. Pye, Director, Ontario Geological Survey.

ABSTRACT

Uranium-bearing pegmatite bodies in the Madawaska Mines area were emplaced preferrentially into the southwestern Faraday Metagabbro Complex. The pegmatite bodies are virtually undeformed. They were emplaced in the waning stages of Grenville Orogeny. Not dilation but replacement (partial assimilation) of host rock was the main mechanism of emplacement. The majority of the pegmatite bodies are subparallel to the internal structure and outer contact of the southwestern Faraday Metagabbro Complex.

All chemical elements that were predominantly incorporated into the mafic minerals of the pegmatite bodies have a positive correlation with uranium. All elements that were predominantly incorporated into the felsic minerals of pegmatite bodies have a negative correlation with uranium. Zirconium, a highly refractory element, has a correlation coefficient of 0.96 with uranium. This suggests that uranium precipitation occurred under magmatic conditions and while the host rocks were being assimilated.

INTRODUCTION

Most of the uranium in the Madawaska Mines is confined to a medium to coarse grained granite-syenite, collectively called pegmatite, which occurs predominantly as sheets and finger-like bodies (dikes, sills, and veins) in the southwestern portion of the Faraday Metagabbro Complex (Figure 1). We carried out field-based research with the aim of determining what structures and structural processes controlled the emplacement of these pegmatite bodies. Although the problem of uranium fixation was outside the scope of the original project, we felt compelled to pursue this subject sufficiently to develop a comprehensive model.

Two different processes lead to the emplacement of granitoid pegmatite bodies into common metamorphic host rocks: (1) dilation, and (2) replacement. Upon brittle fracture or other modes of discontinuous deformation of host rocks, one of the rival processes generally dominates in the development of quartzo-feldspathic veins and common pegmatitic bodies. Simple geometric criteria have benn established (Kretz, 1968) which permit the geologist to differentiate between dilation veins and replacement veins. These criteria are difficult to use where pegmatite bodies are quasi-concordant, non-planar, and/or severely deformed. It was, therefore, necessary to investigate whether the pegmatite bodies at Madawaska Mines had been severely strained, together with their gabbroic host rocks. As part of this investigation, we mapped the fabric pattern of the southwestern Faraday Metagabbro Complex (FMC) and studied a suite of large rock specimens in the laboratory. Apart from its tectonic importance, this work led to a structural map also reflecting the physical anisotropy pattern in the southwestern FMC. This pattern correlates broadly with the geometric pattern of the pegmatite bodies in the mine. In addition, we found convincing evidence underground that replacement of gabbroic host rock was the dominant mechanism of emplacement. As we had suspected, most pegmatite bodies in the FMC were emplaced into highly strained gabbroic rocks, and escaped severe deformation in situ.

PREVIOUS STRUCTURAL WORK AND REGIONAL SETTING

The FMC is located near the southeastern border of the crudely elliptical Faraday Granite (Hewitt and Satterly, 1957). The rocks at the southern margin of the Faraday Granite are fenitized, and belong to a long alkalic belt that traverses the Bancroft area (Schwerdtner and Lumbers 1980, figure 10; Bedell 1982, figure 16.1).

Diverse modal compositions and textures occur in the FMC. This prompted mine geologists to neglect the host rocks and monitor only the U, Th abundance and geometry of the pegmatite bodies. Little et al. (1972) suggested that the pegmatite bodies are associated with a plunging synform and an adjacent antiform to the north (Figure 2). We found no compelling evidence for these large folds in the foliation pattern of the host rocks. Owing to a northeasterly-trending regional foliation and the lobate character of the southeastern border of the southwestern FMC, quasi-concordant pegmatite sheets diverge and converge locally, and create fold-like forms in the pegmatite pattern of the mine. The origin of the lobate geometry of the southern contact of the FMC (Figure 3) is unknown and cannot be found without detailed study of the metasedimentary envelope of the FMC. We did not undertake such a study.

MACROSTRUCTURE OF THE SOUTHWESTERN FARADAY METAGABBRO COMPLEX

Lithologic and structural mapping of the southwestern FMC was carried out at surface as well as in easily accessible parts of the Madawaska Mines. We wanted to obtain a detailed picture of the macroscopic strain pattern in the FMC, and assess if, and to what degree, the system of the pegmatite bodies is concordant to the structure of the host rocks. The distribution, form and orientation of larger pegmatite bodies was determined at surface. More complete information about the pegmatite bodies has been obtained by mine geologists underground, and was readily available to us for use in this study.

In addition to the structural mapping, we collected oriented specimens of metagabbro for study of the mineral fabric and measurement of the magnetic anisotropy. We also judged the L, S strain fabric (Schwerdtner et al. 1977) of deformed mafic clots by visual inspection of orthogonally cut surfaces (Figure 4 a&b), and compared the results with those of the magnetic susceptibility anisotropy determinations.

Maps 1, 2, and 3 contain most of the data obtained by field mapping. Important structural results of this mapping will be discussed in the following paragraphs.

The attitude of foliations and lineations were measured in the field throughout the southwestern FMC. To represent the variation in attitude of foliation, the southwestern FMC was conveniently divided into five domains for which we constructed rose diagrams and contoured stereoplots (Figures 5 and 6 a-g). A synoptic rose diagram for all foliation strikes is shown in Figure 7a.

Figures 7a and 7b reveal that the regional foliation trend is approximately NE-SW, but that there are many local effects as well. Among the three northern domains, the trend shifts according to the northward-concave curvature of the foliation pattern (Figure 5). The scatter in the southwestern rose reflects the presence of a round nepheline syenite plug (map 1) and an interference between (1) the regional foliation, (2) a northwesterly-striking shear zone, also discernible in the central northern lobe, and (3) the lobate contact of the FMC. Although small folds in foliation were observed in several outcrops, we found no compelling evidence for macroscopic folding (see Previous Structural Work).

Stereoplots for the various surface domains as well as all accessible underground levels (Figures 6a-6g) reflect the prevailing SE dip of the region. Mineral lineations cluster strongly (Figure 8) and confirm the field observation that stretching is predominantly down-dip on the regional foliation plane.

Figure 3 shows that in the SE border region of the FMC, where Madawaska Mines is located, most uranium-ore bodies at the adit level of mining trend parallel to the NE regional grain. Near the lobate contact of the FMC, the ore bodies tend to follow the local pattern of the contact-parallel foliation. Apparently the foliation in the host rock controls the orientation of the pegmatite bodies in this small region. Throughout most of the southwestern FMC and the mine, the strike of the foliation tends to be subparallel to the pegmatite contacts (figure 9).

Joint attitudes, routinely obtained during field mapping, show considerable scatter in a synoptic stereoplot (Figure 10). However, a large number of joints are subvertical and trend NW-SE. The preferred orientation of joints is thus perpendicular to the regional structural grain.

Numerous specimens of deformed metagabbro were cut orthogonally to foliation and lineation (Figure 4). After visual inspection, specimens were grouped according to whether they were (1) predominantly lineated, (2) predominantly foliated, (3) as well lineated as foliated, or (4) virtually undeformed. The results were plotted on a map of the southwestern FMC, and reveal that there are several areas with consistent L, S fabric (Figure 11).

Our attempt to quantify the L, S fabric scheme by means of the magnetic susceptibility anisotropy method was not successful (Appendix 1). Results were not always consistent for individual large specimens. On the other hand, some of the consistent magnetic results clearly disagreed with the shape of the L, S fabrics as determined by inspection. We attempted to find the source of difficulty by studying heterogeneous samples and learnt that the primary compositional layering (at a mm to cm scale) has a strong influence on the shape of the susceptibility ellipsoid. For example, some lineated metagabbros have a fine mafic layering which results in an oblate ellipsoid of bulk magnetic susceptibility anisotropy. To be a reliable measure of the strain fabric, the susceptibility ellipsoid of this rock should be prolate. The main reason for analytical results inconsistent with the visual estimates appears to be the relatively coarse grain size of the magnetic minerals relative to the size of the drill cores measured in the torque meter. The inadequate size of the measured cores results in inhomogeneous magnetic fabrics. Tests of drill cores were made by shaving off minor portions of the sample. This procedure led to significant changes in the bulk magnetic susceptibility ellipsoid. In addition, the maximum deflections (which reflect the magnetic content of the rock) vary widely between the three cores used for each sample location (Appendix 1).

PETROGRAPHY AND MICROSTRUCTURE OF THE FMC

The Faraday Metagabbro Complex (FMC) is texturally and modally diverse. It ranges in composition from anorthositic gabbro to amphibolite and contains relict massive to layered enclaves reflecting its premetamorphic history. The rocks of some areas exhibit greater than 100% tensile strain.

In the anorthositic rocks the mafic minerals appear as aggregates of amphibole, some of which still contain relict clinopyroxene cores. Rare orthopyroxene can be found, and when plotted on the pyroxene quadrilateral phase diagram (Figure 12), the electron microprobe analyses fall within the 600-900^{o}C isotherms as outlined by Ross and Huebner (1975). These pyroxenes fall in the same temperature range and have similar compositions with respect to both major and minor elements as those reported by Ashwal (1982) in the Marcy Anorthosite Massif of the Adirondacks in New York, also of Grenville age and metamorphosed to granulite facies.

The pyroxenes are rimmed by a slightly more sodic amphibole that often occurs as randomly oriented aggregates. Associated with the amphibole are sporadic occurrences of opaques, including magnetite (showing no exsolution textures) and monoclinic pyrrhotite. Sphene aggregates are commonly associated with magnetite cores. Biotite is also associated with these mafic segregations but occurs as euhedral or kinked crystals indicative of a later origin relative to the bulk of the recrystallized mafic aggregates.

Morris (1956) reports a single occurence in the FMC of a mass of antigorite, chlorite and magnetite which he suggests may represent altered olivine.

Plagioclase occurs in diverse textural forms ranging from relict igneous laths, to grains dominated by mechanical twins to completely recrystallized equant grains (Bedell and Schwerdtner, 1981). The composition of the plagioclase as determined by electron microprobe analyses ranges from labradorite (An_{62} to oligoclase An_{20}).

Scapolite is a common constituent that starts to replace plagioclase along cleavage planes and twin boundaries until replacement is complete. The abundance of scapolite appears to increase in modal abundance with intensity of recrystallization of plagioclase as was also reported by Appleyard and Williams (1981). Apatite occurs sporadically and is found usually as subhedral grains within the plagioclase matrix.

In recent experimental work on gabbroic rocks

(Kronenberg and Shelton, 1980) at experimental strain rates of 3 x 10^{-6}/s and a confining pressure of 5kb, plagioclase was seen to become weaker than pyroxene at temperatures of about 700°C or greater. This would imply that deformation of plagioclase is chiefly responsible for the ductile behavior of the Faraday Metagabbro. In an effort to quantify the plagioclase microstructure, fifty length-width measurements of randomly selected grains were obtained per thin section. Employing conventional grain size statistics as used by sedimentologists, we assigned the various thin sections to three microstuctural states based on the dominating deformation mechanism operating in the plagioclase grains (Appendix 2). Assuming that the microstructural state in an outcrop can be represented by one or two thin sections, a map was drawn up depicting variations in the grain size of plagioclase throughout the southwestern FMC. The grain size of plagioclase is a function of the level of strain plus the degree of static recrystallization (Appendix 2).

EMPLACEMENT OF PEGMATITE BODIES

Detailed structural observations and measurements were made underground to find the dominant mode of emplacement of U-ore bodies (pegmatite), and determine at what stage in the structural history of the FMC this emplacement occurred. A systematic application of the simple criteria of Kretz (1968) was prevented by the irregular and gradational boundaries of the pegmatite bodies. In addition, the discordant structural markers required for application of the criteria are rarely seen in the Madawaska Mines.

However, ghost structures are common within the ore bodies as well as in narrow pegmatite veins throughout the Madawaska Mines. In most cases, oblique mineral foliation, distinct layers or other minor structures extend from the host rocks into pegmatite, generally fading out toward the middle of individual ore bodies or veins (Figures 13a and b). There is thus convincing evidence for widespread replacement of the metagabbro wall rocks. However, this does not rule out the possibility that dilation was a contributing factor to the emplacement of the uranium ore.

Although some of the narrow pegmatite veins and dikes display concordant internal foliation not obviously inherited from the wall rocks, most pegmatite bodies in the Madawaska Mines and at surface have escaped ductile deformation. Either the bodies were very competent while the host rocks were highly ductile, or pegmatite emplacement postdates most of the ductile deformation of the FMC.

To ascertain that the emplacement did not occur until most of the ductile deformation had been accumulated, we examined thin sections cut from regions of pegmatite bodies that were most susceptible to ductile deformation. For comparison we also made thin sections from regions least susceptible to ductile deformation. Details about this approach follow.

It is a well known fact, that most pegmatite dikes and veins are prone to bifrucation, branching and splaying along their length. This is related to the style of fracture propagation in brittle and semi-brittle rocks (Price, 1966) and is independent of whether dilation is the vein-generating mechanism. Starting with an undeformed system of branching dikes and veins replete with knees and bifrucation structures that resemble open kink folds, it is intuitively obvious that the "hinge" regions of the competent pegmatite bodies are most susceptible to mechanical failure at the onset of a subsequent regional deformation. If the dikes are statistically subparallel on the scale of individual domains or a large structure like the FMC, then the pegmatite system will either be extended or compressed, and possibly also sheared. No matter whether the longitudinal strain is tensile or compressive, the hinge regions of fold-like structures in the pegmatite system will be prone to deformation. Accentuation of "folds" or "kink" structures leads to compression of the concave "hinge" zones, while the "unbending" of the same structures leads to compression of the convex "hinge" zones.

As shown mathematically by Chapple (1969), the tangential stress needed to tighten the curvature of a crooked (or already folded) layer is much smaller than that required to initiate folding of a planar layer. Thus even if the tectonic stress level is low, the "hinge" regions of kink fold-like structures in dike systems can deform severely while the planar "limbs" of the same structures rotate quasi-rigidly within their incompetent host rocks.

Field evidence in other regions of the Canadian shield suggests that, under upper-amphibolite facies conditions, coarse pegmatite dikes are more competent than their amphibolite hosts (e.g. Schwerdtner et al. 1971, boudinage structure 2). If the (virtually undeformed) pegmatites of the Madawaska Mines area were potentially less competent than their metagabbroic host rocks then they would be even more susceptible to deformation at the "hinges" of pseudo-folds (bifrucation points, knees of dikes, etc.).

We sampled the straight "limbs" as well as the convex and concave hinge regions of several fold-like crooks and bifrucation structures in the Madawaska Mines (Figure 14 and 15a,b,c). At none of these structural sites do the pegmatite textures show macroscopic or microscopic signs of significant ductile deformation. Unlike in most rocks of the FMC, there is no evidence of significant ductile deformation of feldspar in the pegmatites. Quartz ribbons, however, are occasionally found indicating a low to moderate level of granular strain. The amount of deformation in concave, convex, and intermediate areas of "hinge" zones of pegmatite bodies appears to be the same as that found in the "limbs".

There seems to be no doubt that the uranium-ore bodies at Madawaska Mines were indeed emplaced after, or in the waning stages of, the Grenville tectonism that caused the penetrative deformation in the FMC.

GEOCHEMICAL AFFINITY OF URANIUM

This study has been concerned with the structural control of uranium-ore bodies rather than the fixation of the uranium. However, emplacement of the pegmatites occurred by replacement of metagabbro host rock and various observations suggest that this may control the bulk of uranium mineralization.

In the Madawaska Mines the high-grade uranium ore is believed to occur within pegmatite rich in mafic minerals and along the contact between pegmatite bodies and highly mafic host rocks. Also, where mafic xenoliths occur in the pegmatite, uranium is apparently concentrated at the rims of the xenoliths (Ralph Alexander, Chief Geologist, Madawaska Mines, personal communication, 1981). We were able to confirm these observations by systematic sampling, chemical analysis, and correlation between the amount of uranium and those of major and minor chemical elements in the granitoid rocks.

Thirty-one whole-rock chemical analyses were obtained from the mine area, and the amount of U_3O_8 compared with that of 21 other elements plus loss on ignition (Figure 16).

Thorium shows the best correlation with a coeficient of 0.97 because it crystallizes in the dominant uranium-bearing species, uraninite. Madawaska Mines employees who analyzed the rocks for uranium and thorium, found that they occur consistently in a ratio of 2:1. Zirconium, which is highly immobile due to its insolubility and extremely high melting point has the second-highest correlation coefficient of 0.96. This demonstrates that the present distribution of uranium was mainly attained by primary magmatic precipitation. The remaining elements can be divided into two groups depending on whether they were predominantly incorporated into mafic or felsic minerals. All elements in mafic minerals have a positive correlation with uranium, whereas all those in felsic minerals have a negative correlation.

As evident in numerous exposures (Figures 13a and b), most of the mafic constituents in the pegmatites are structural and/or compositional relics of the mafic host rocks. Figure 17 shows that the mechanical disaggregation of host rocks can lead to pegmatites with more evenly dispersed mafic constituents. In combination with these geological observations, the chemical correlations support the hypothesis that uranium was precipitated during pegmatite genesis and concomitant replacement of mafic host rock.

MAJOR CONCLUSIONS

Our field-based structural study of the southwestern Faraday Metagabbro Coomplex (FMC) and the Madawaska Mines area has led to the folowing major conclusions.

(1) Pegmatite bodies were emplaced preferentially into the FMC and similar mafic units in the Bancroft region.

(2) The pegmatite bodies of the Madawaska Mines area are virtually undeformed. They were emplaced in the waning stages of the Grenville orogeny.

(3) The pegmatite bodies were mainly formed by replacement (partial assimilation) of metagabbro.

(4) Most pegmatite bodies are subparallel to the internal structure and outer contact of the FMC.

(5) All chemical elements that were predominantly incorporated into mafic minerals of the pegmatite bodies have a positive correlation with uranium. All elements that were predominantly incorporated into felsic minerals have a negative correlation with uranium. Zirconium, a highly refractory element has a correlation coefficient of 0.96 with uranium. This suggests that uranium precipitation occurred

under magmatic conditions and while the host rocks were being assimilated.

FIGURE CAPTIONS

Fig. 1 Generalized geological map of the western Bancroft area (after Bedell, 1982), and location of Madawaska Mines (formerly called Faraday Uranium Mines).

Fig. 2 Previously postulated folds in the subsurface within and adjacent to Madawaska Mines (redrawn from Little et al., 1972).

Fig. 3 Simplified structural map of the Madawaska Mines area (after Bedell, 1982).

Fig. 4 Strained metagabbro cut parallel normal to the planer shape fabric of the strained mafic aggregates; (a) section parallel to the stretching lineation, (b) section perpendicular to the stretching lineation.

Fig. 5 Local dispersion and areal variation in trend of the mineral fabric in the western Faraday Metagabbro Complex. Black regions are pegmatite bodies mapped at surface.

Fig. 6 Azimuth frequency plots and fabric diagrams contoured by Kamb's method. Further explanation on the individual plots and diagrams. For geographic location at surface, see Figure 5.

Fig. 7 Synoptic plots and diagrams of foliation data obtained underground (a) and at surface (b).

Fig. 8 Synoptic diagram of all mineral lineation directions measured at surface and underground; and contours according to Kamb's method.

Fig. 9 Obliquity between foliation strike in wall rocks and strike of adjacent pegmatite contacts.

Fig. 10 Point diagram of joint normals obtained at surface (see text).

Fig. 11 (larger map) L-S fabric pattern in southwestern Faraday Metagabbro Complex as judged by inspection of sawn hand specimens and structures in outcrops.

Fig. 12 Quadrilateral phase diagram for pyroxene (see text).

Fig. 13a Replacement of layered metagabbro (8a) by pegmatite (7b). The pegmatite dyke is about 20 cm wide. Code and date refers to a sketch in Bedell's field notes.

Fig. 13b Pegmatite lobe with ghost foliation parallel to gneissosity in wall rock. Note late dykelet cutting the pegmatite. Sketch made on 1200' level of mine.

Fig. 14 Bifurcating pegmatite bodies with fold-like regions sampled for textural study.

Fig. 15 No textural differences are apparent in thin sections from (a) intermediate, (b) convex or concave areas of "hinges" or (c) "limbs". Also note the relatively low amount of ductile strain relative to that found within the FMC (see text).

Fig. 16 Correlation of uranium with other chemical elements in U-rich pegmatites.

Fig. 17 Mechanical disaggregation of gabbroic xenoliths within a pegmatite body. Location in mine as indicated.

Figure 1. Generalized geological map of the western Bancroft area (after Bedell, 1982), and location of Madawaska Mines (formerly called Faraday Uranium Mines).

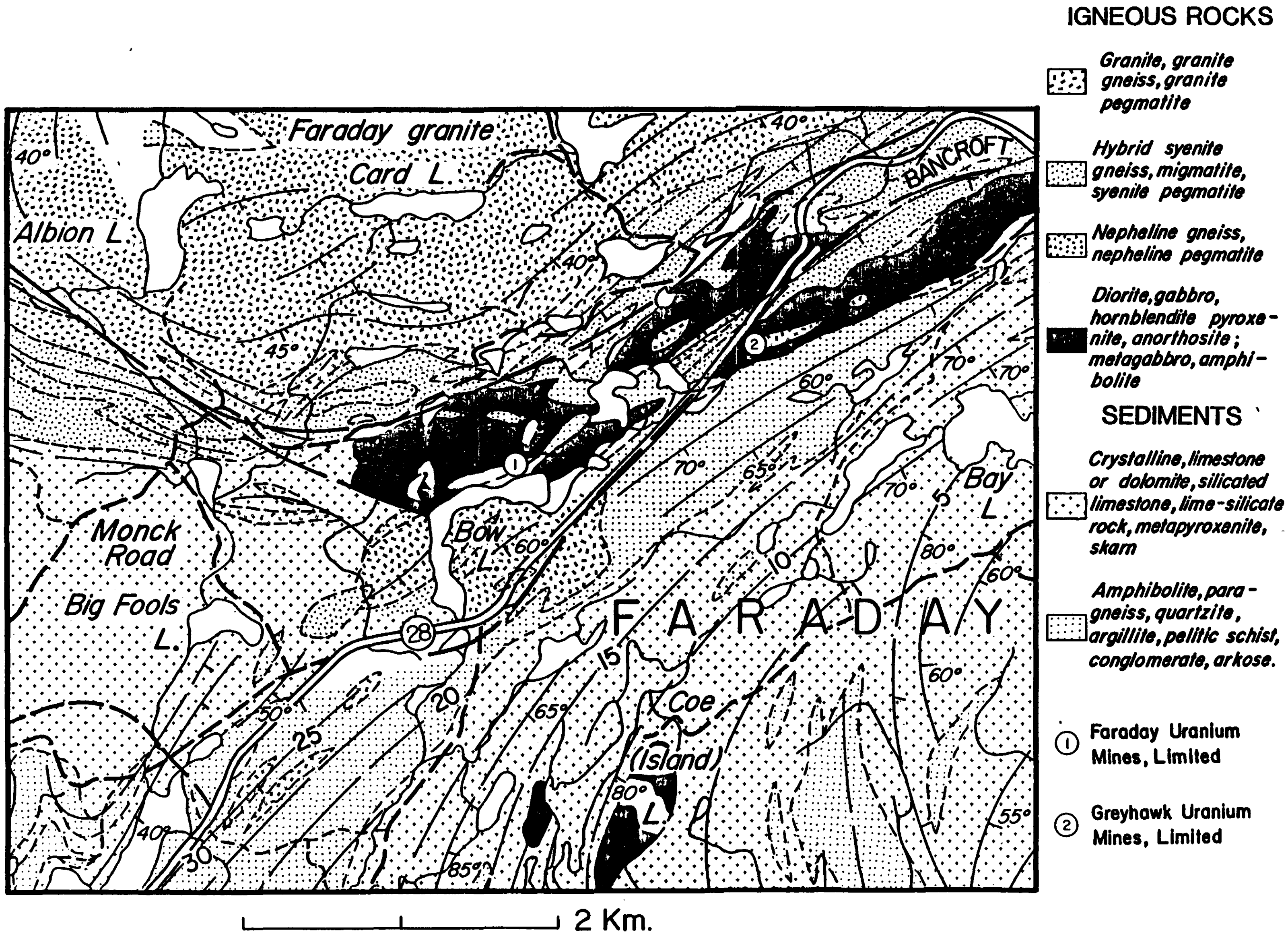

Figure 2. Previously postulated folds in the subsurface within and adjacent to Madawaska Mines (redrawn from Little et al., 1972).

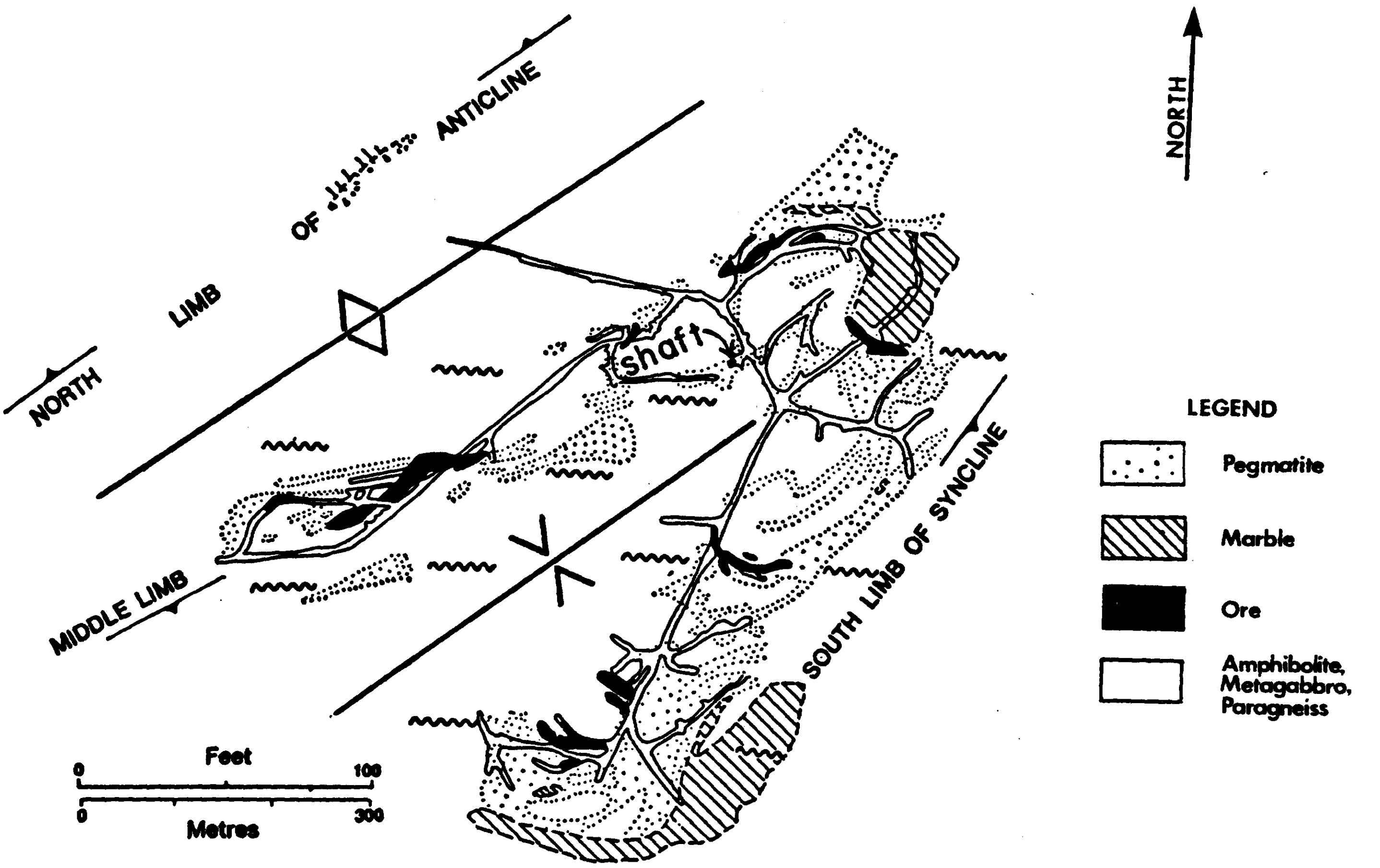

Figure 3. Simplified structural map of the Madawaska Mines area (after Bedell, 1982).

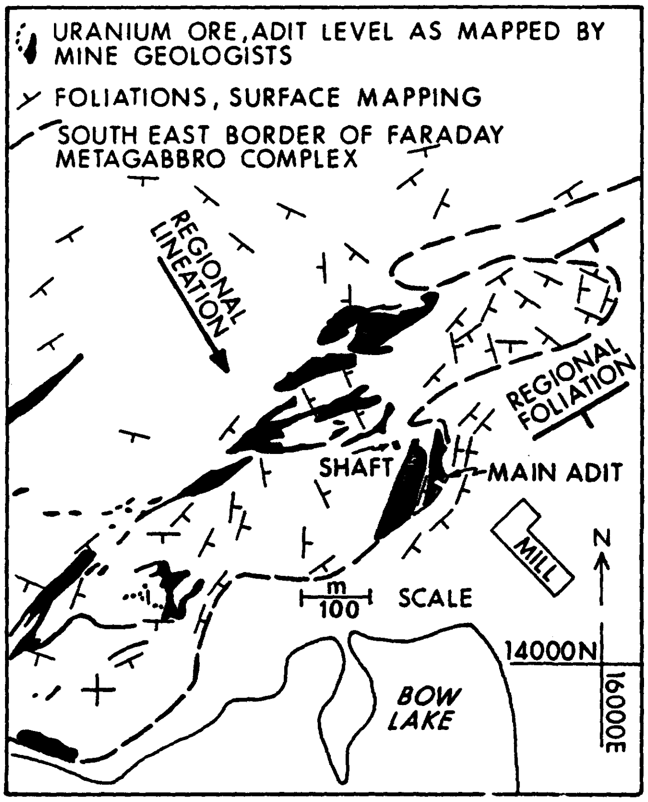

Figure 4. Strained metagabbro cut parallel normal to the planer shape fabric of the strained mafic aggregates;
(a) section parallel to the stretching lineation,

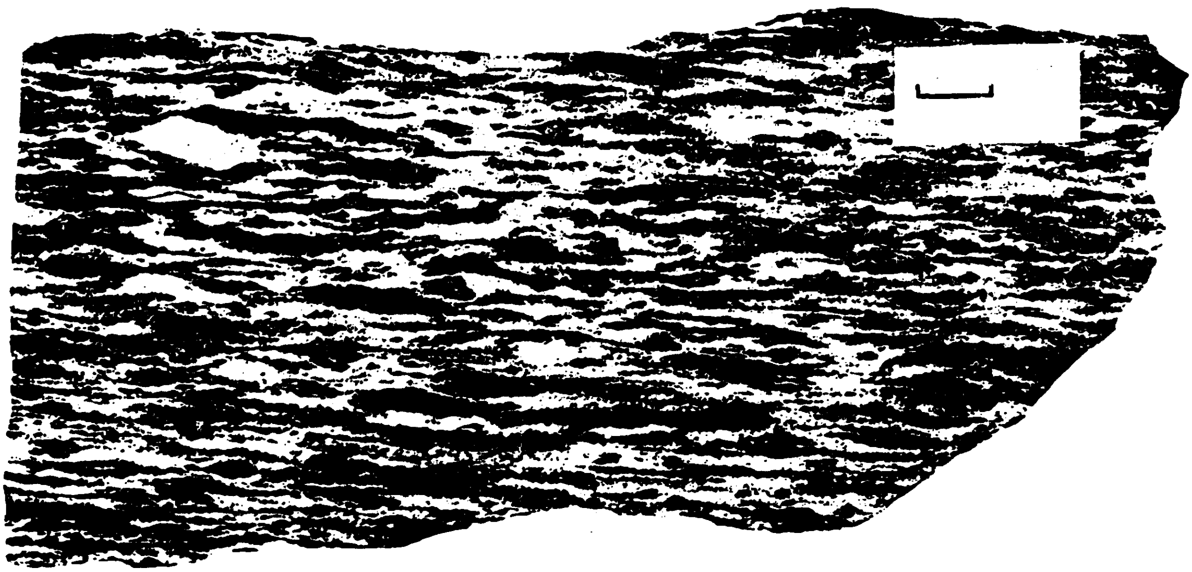

Figure 4. Strained metagabbro cut parallel normal to the planer shape fabric of the strained mafic aggregates; (b) section perpendicular to the stretching lineation.

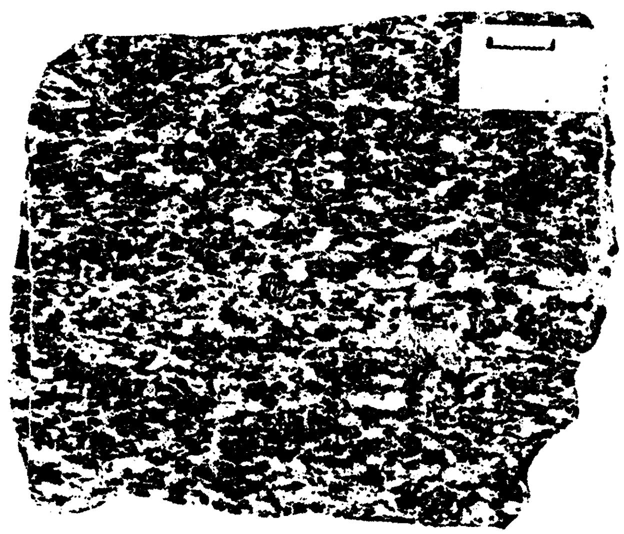

Figure 5. Local dispersion and areal variation in trend of the mineral fabric in the western Faraday Metagabbro Complex. Black regions are pegmatite bodies mapped at surface.

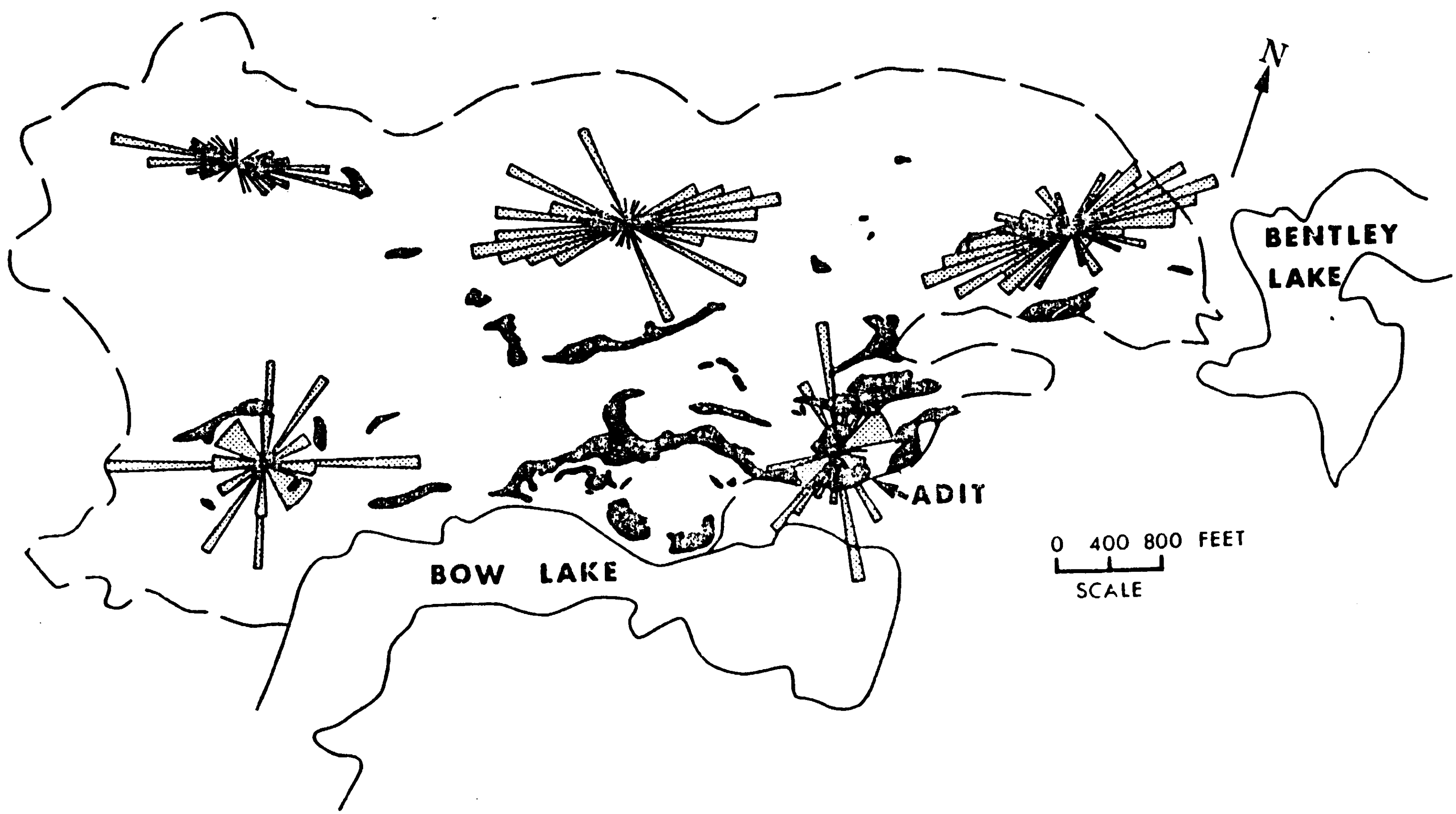

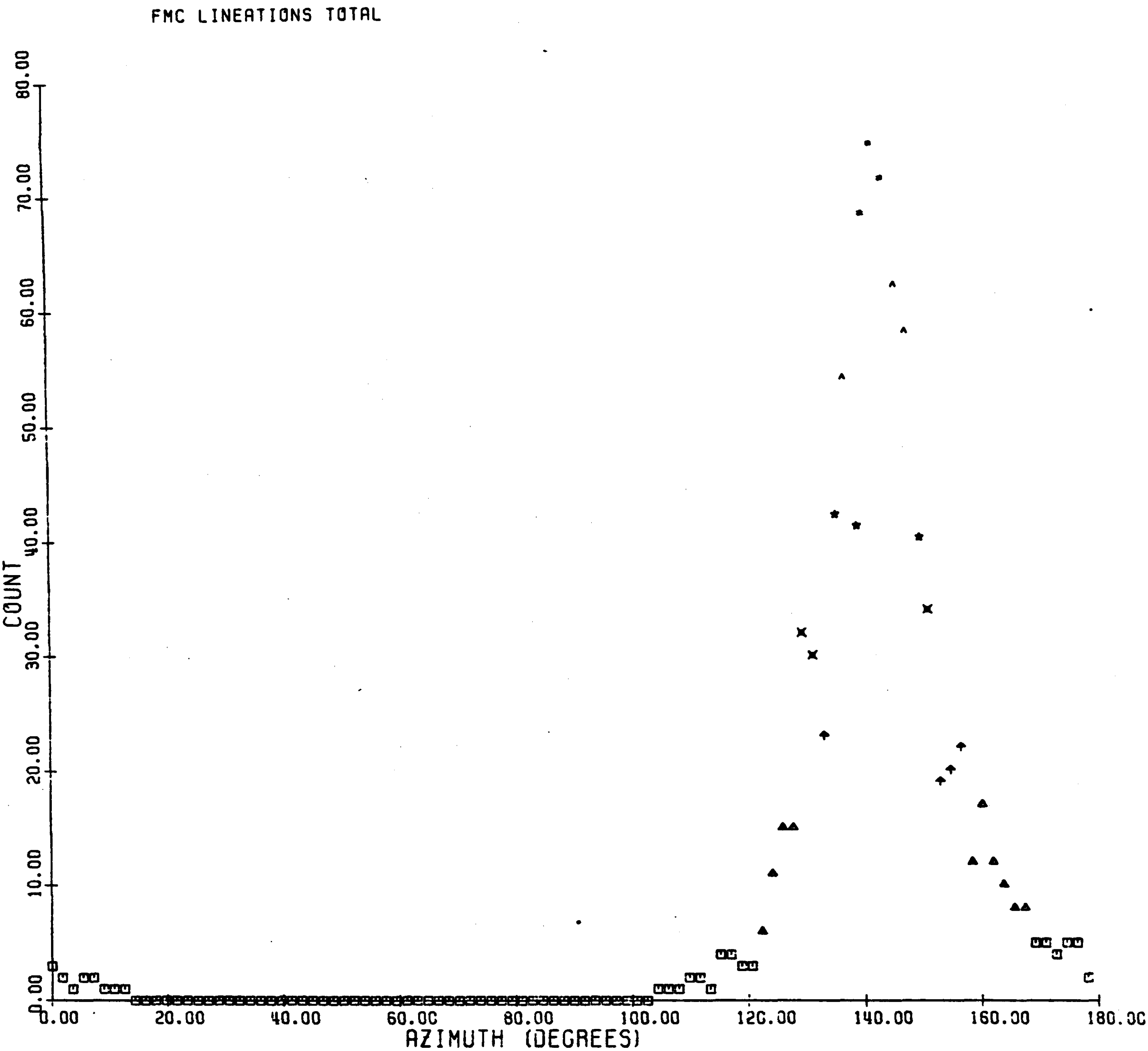

Figure 6. Azimuth frequency plots and fabric diagrams contoured by Kamb's method. Further explanation on the individual plots and diagrams. For geographic location at surface, see Figure 5.

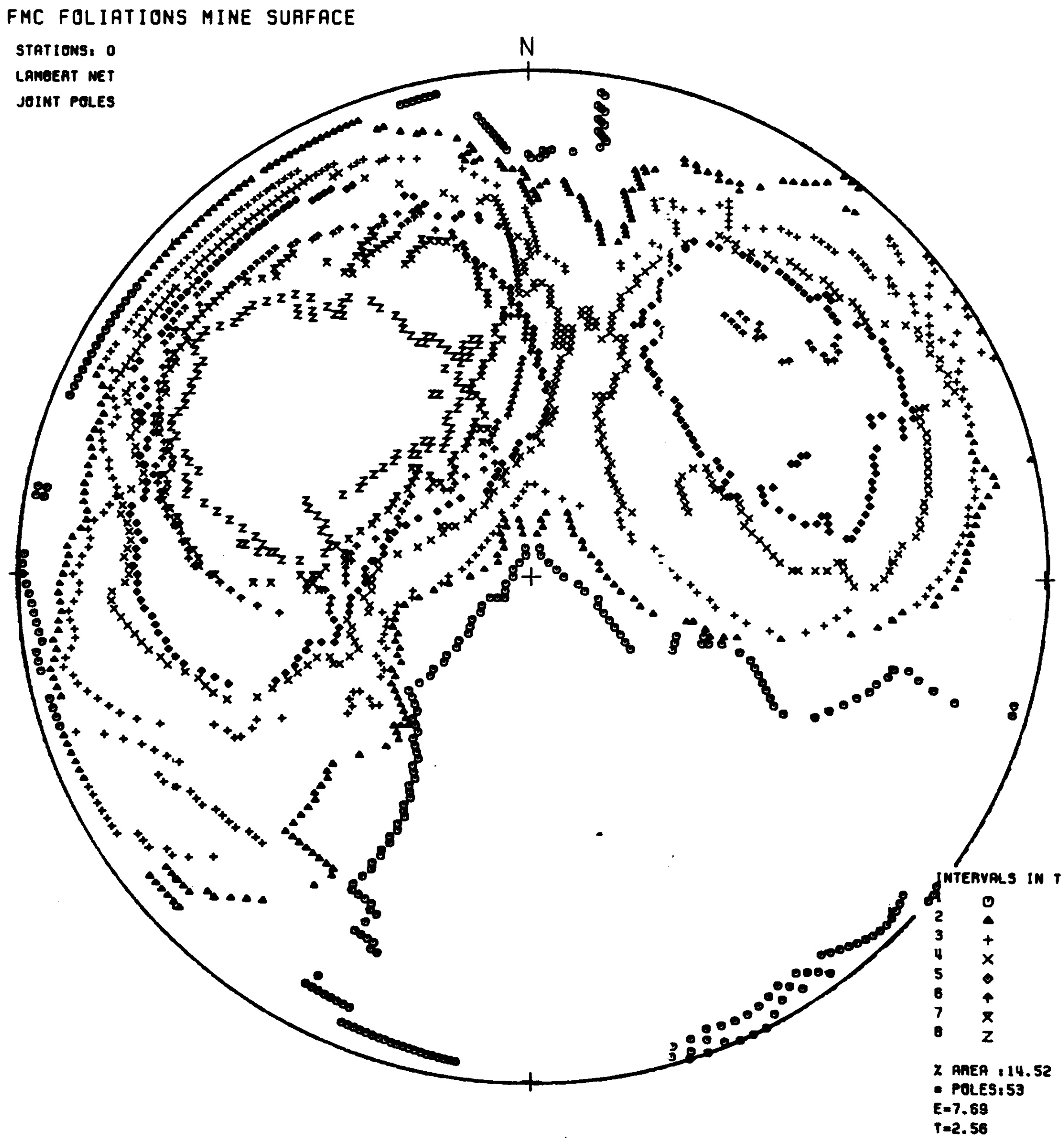

Figure 6a. Azimuth frequency plots and fabric diagrams contoured by Kamb's method.

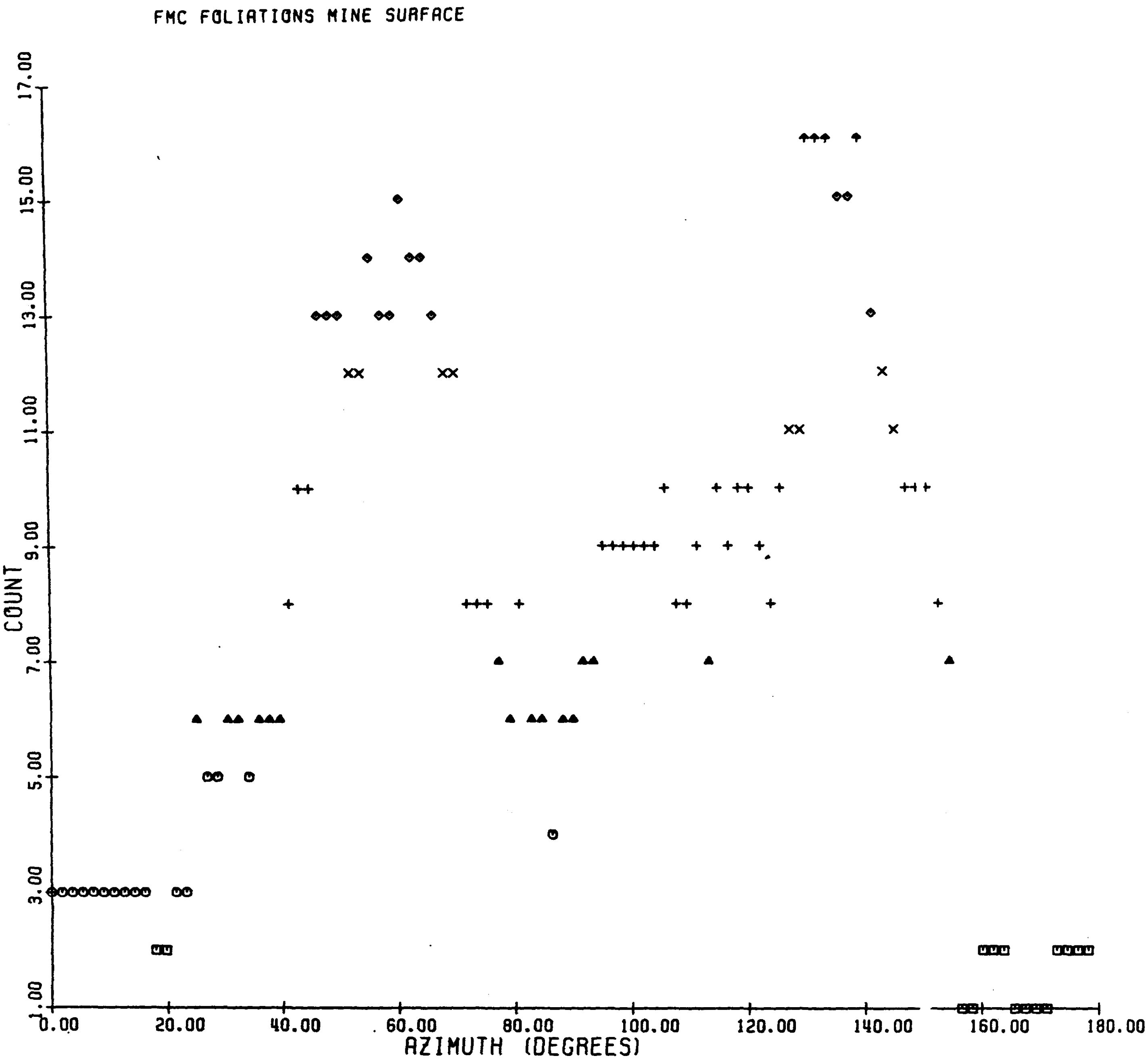

Figure 6b. Azimuth frequency plots and fabric diagrams contoured by Kamb's method.

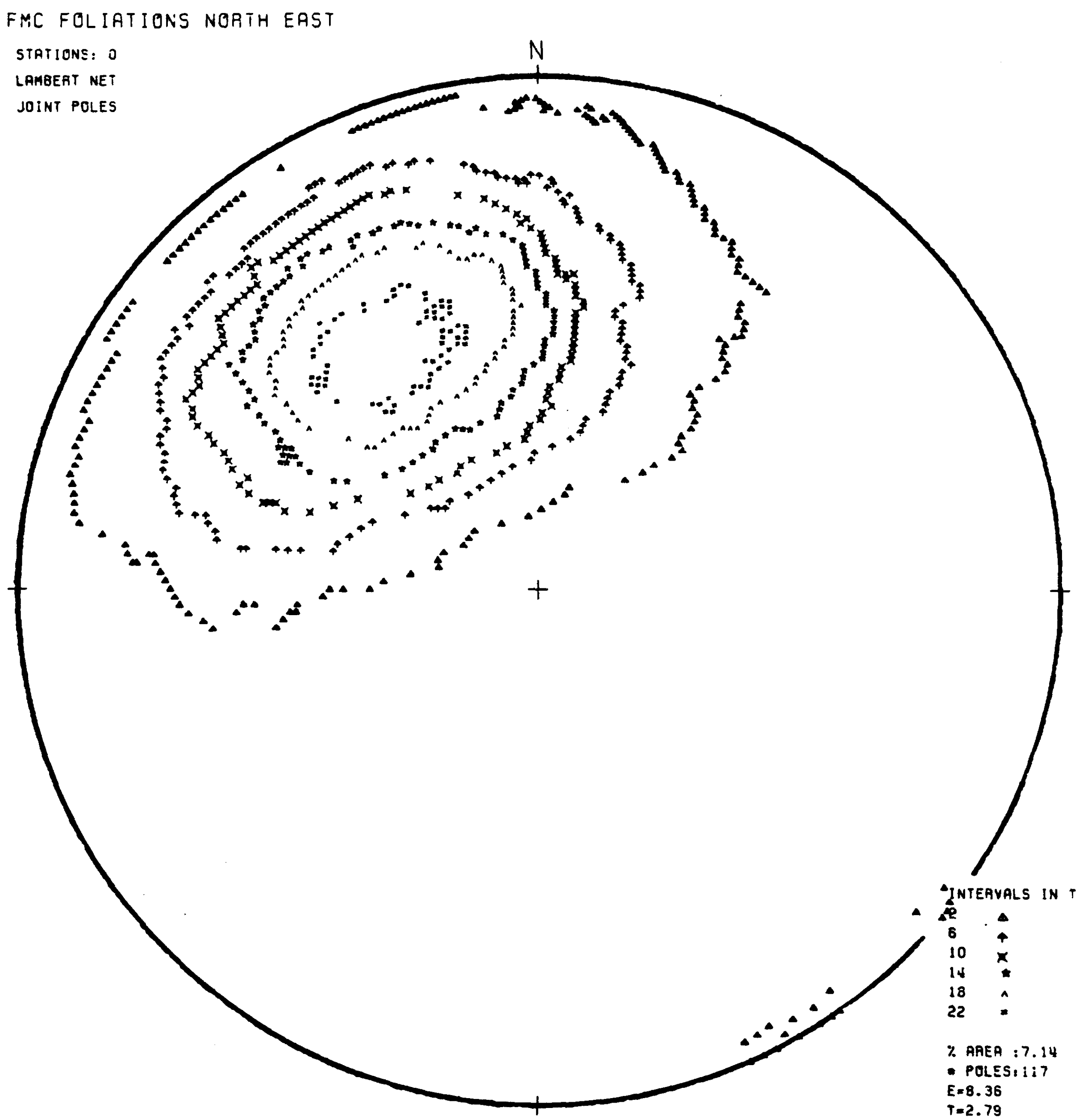

Figure 6c. Azimuth frequency plots and fabric diagrams contoured by Kamb's method.

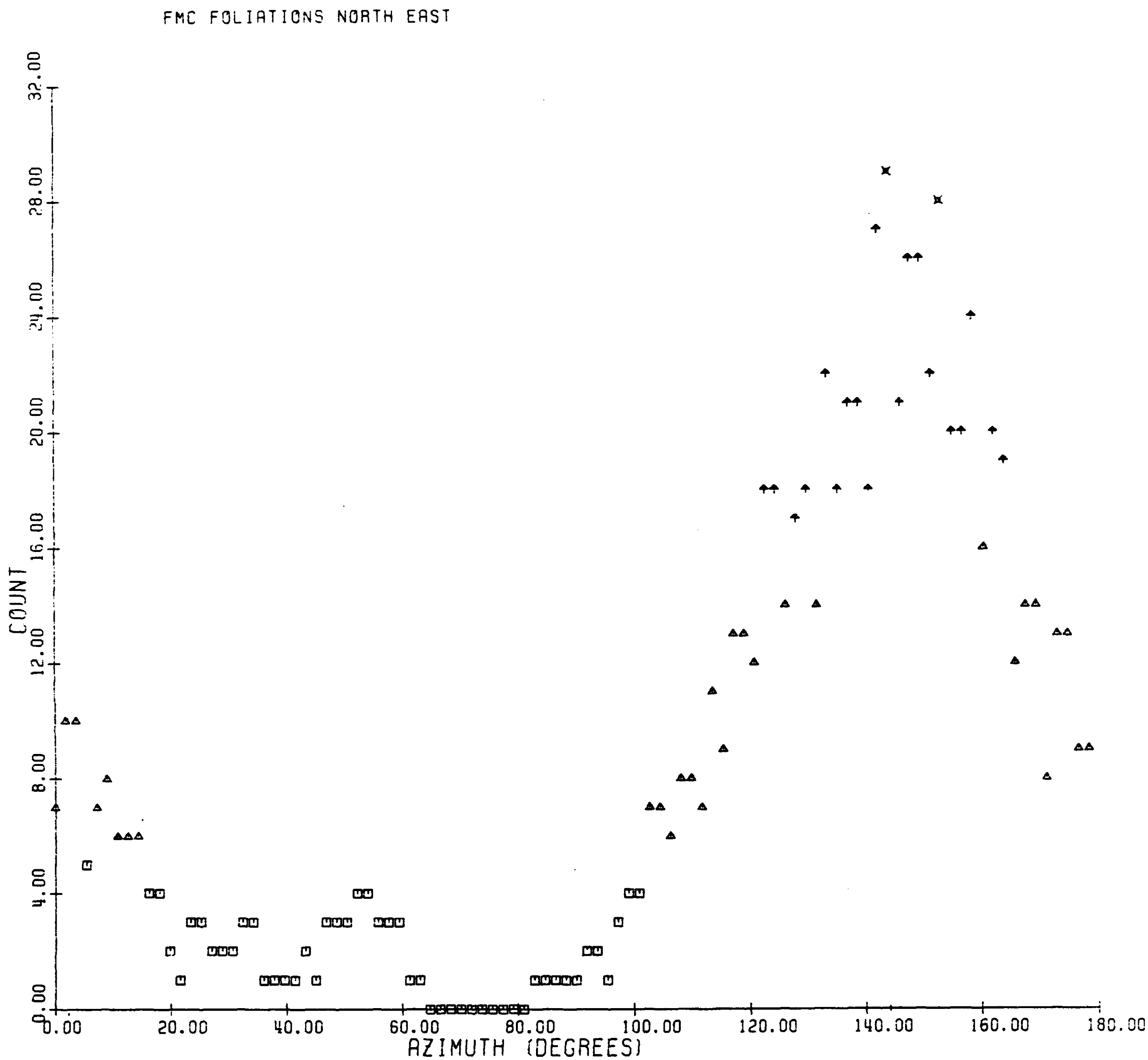

Figure 6c. Azimuth frequency plots and fabric diagrams contoured by Kamb's method.

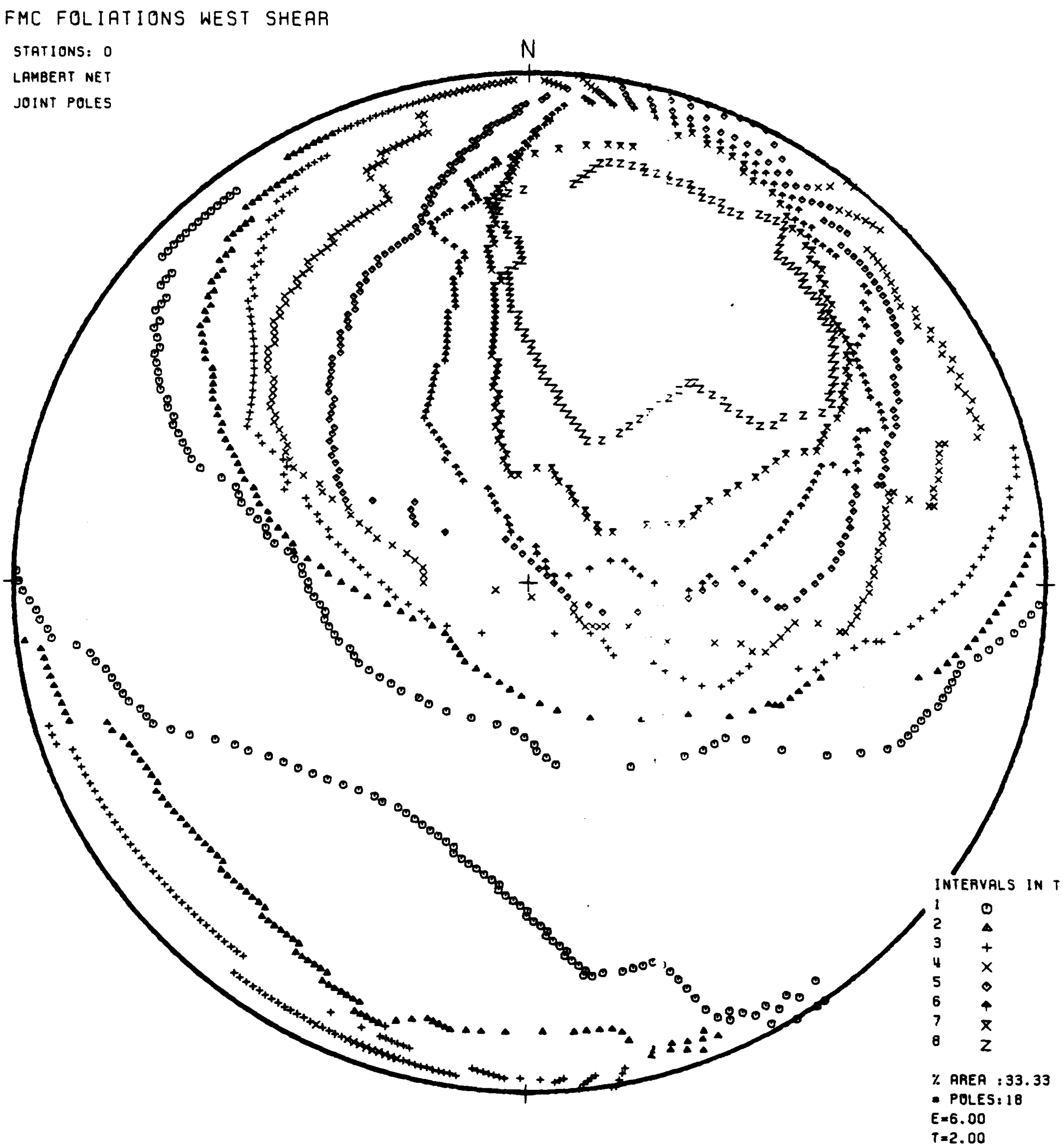

Figure 6c. Azimuth frequency plots and fabric diagrams contoured by Kamb's method.

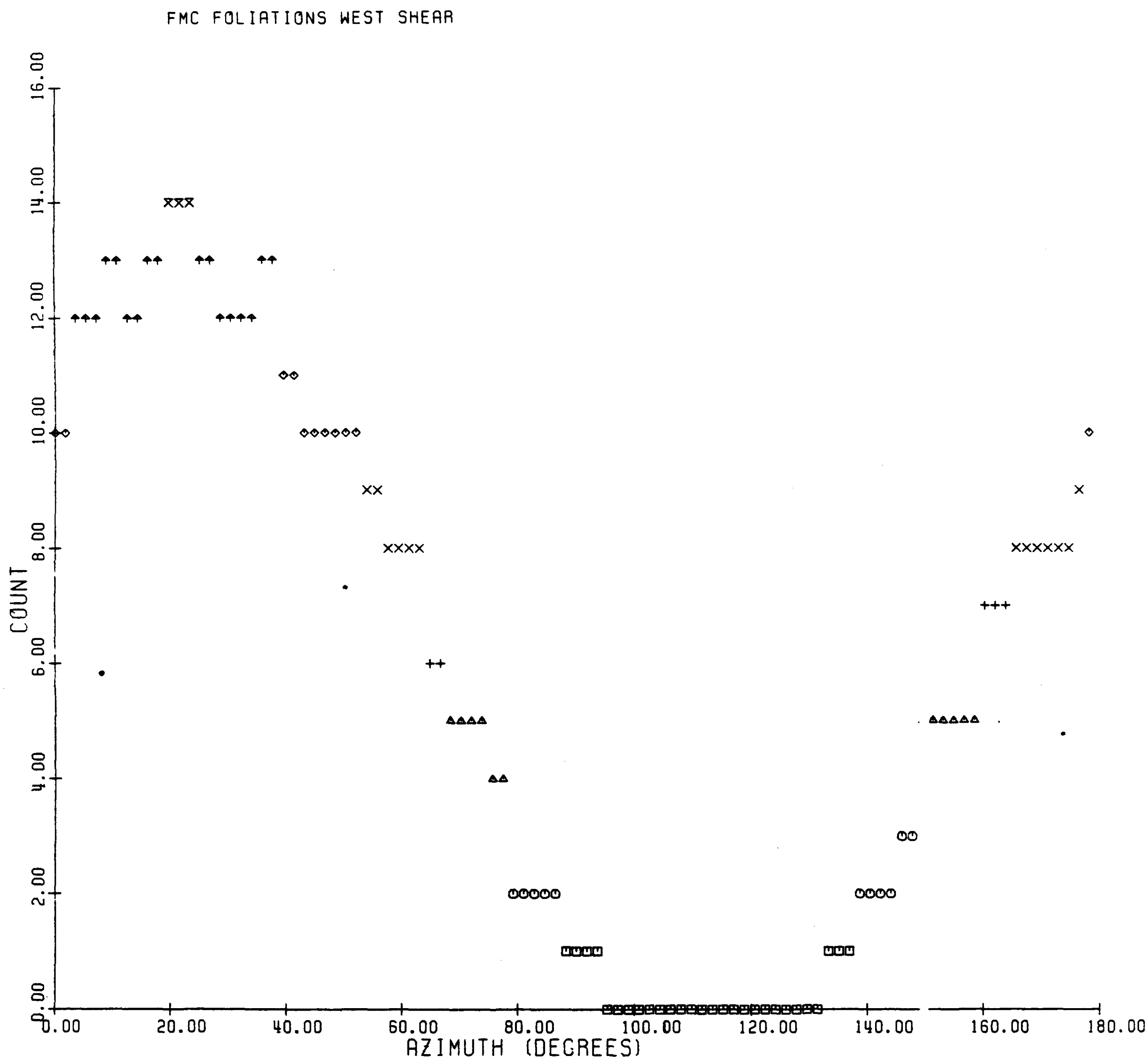

Figure 6d. Azimuth frequency plots and fabric diagrams contoured by Kamb's method.

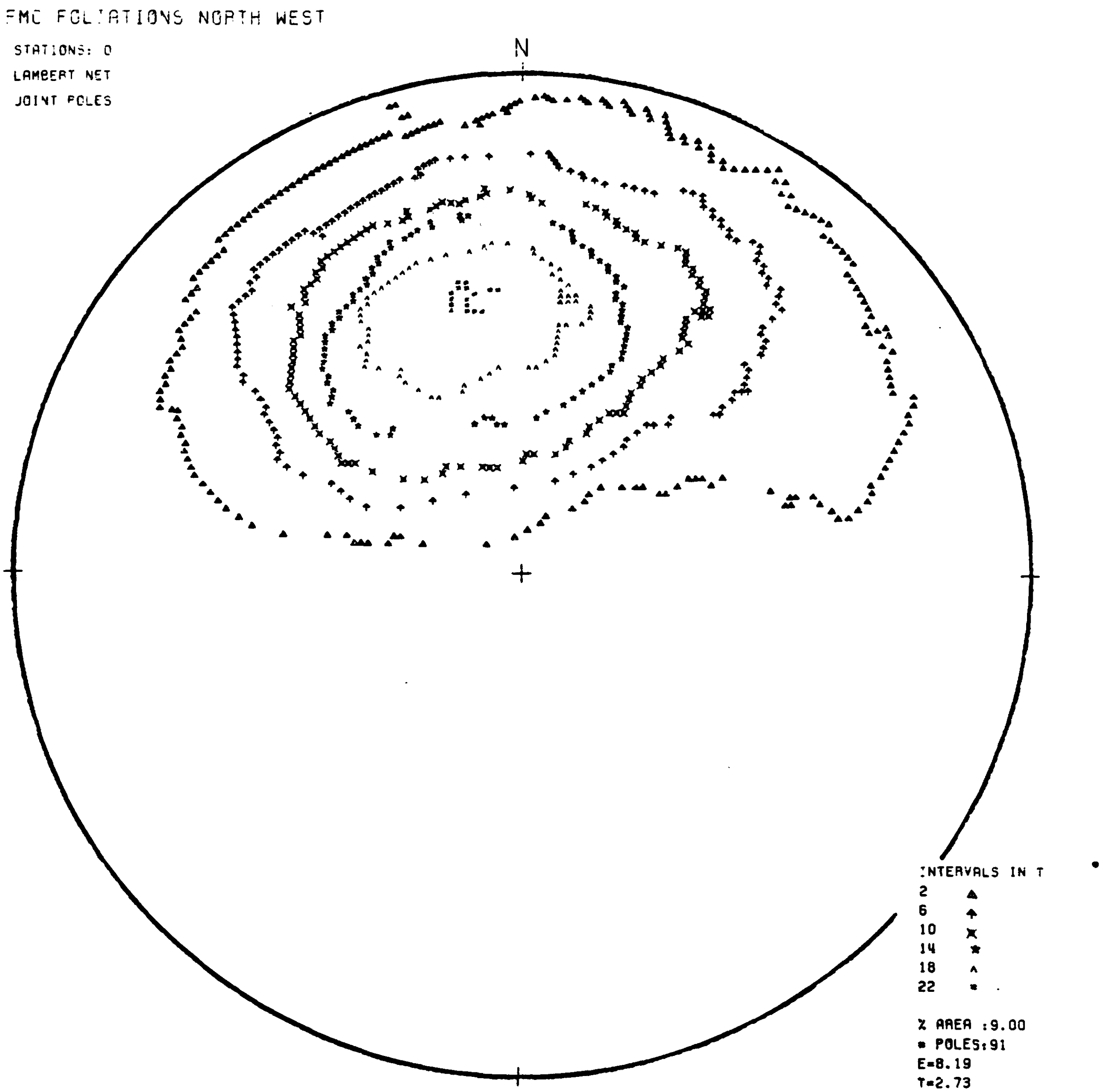

Figure 6d. Azimuth frequency plots and fabric diagrams contoured by Kamb's method.

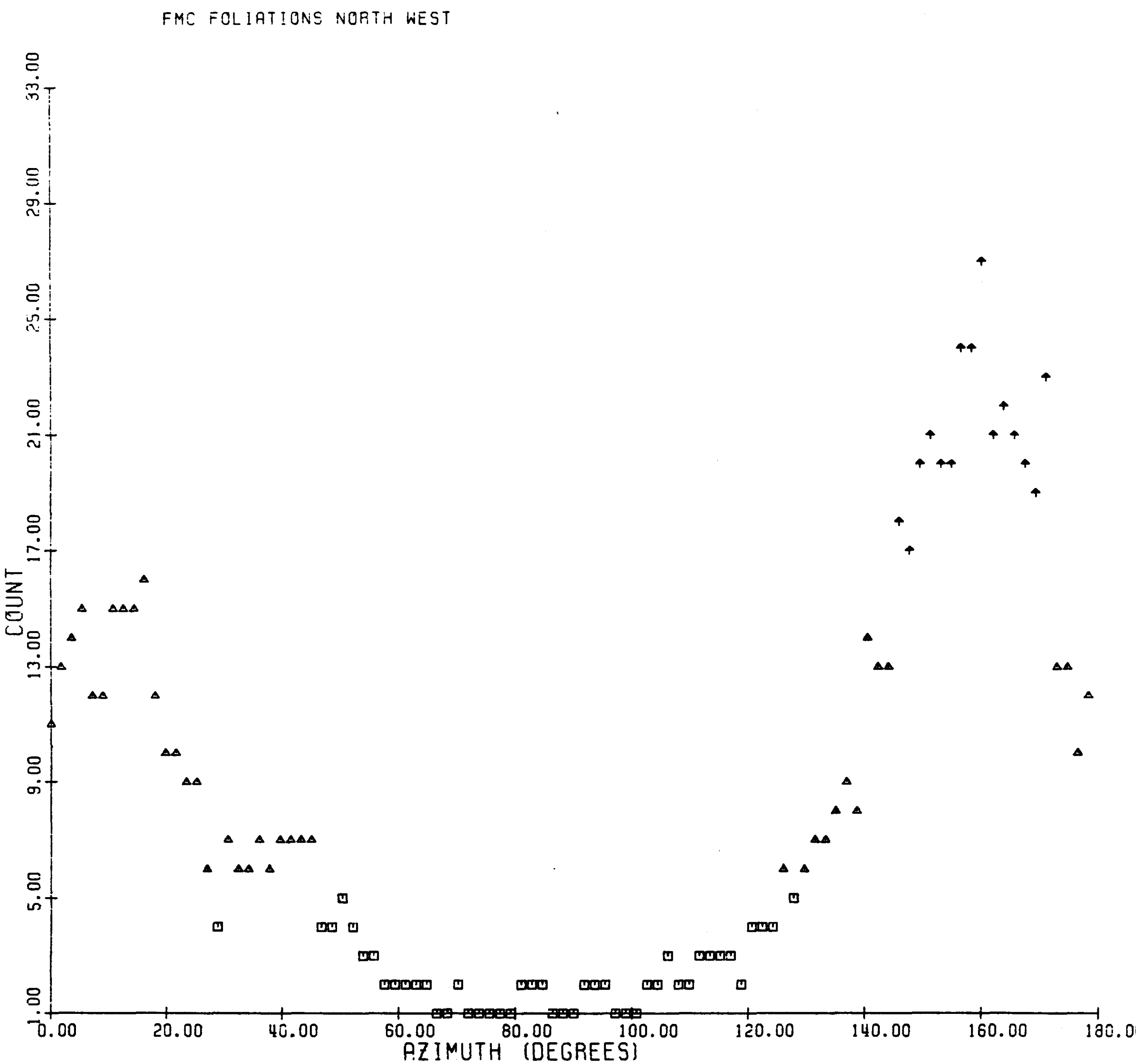

Figure 6e. Azimuth frequency plots and fabric diagrams contoured by Kamb's method.

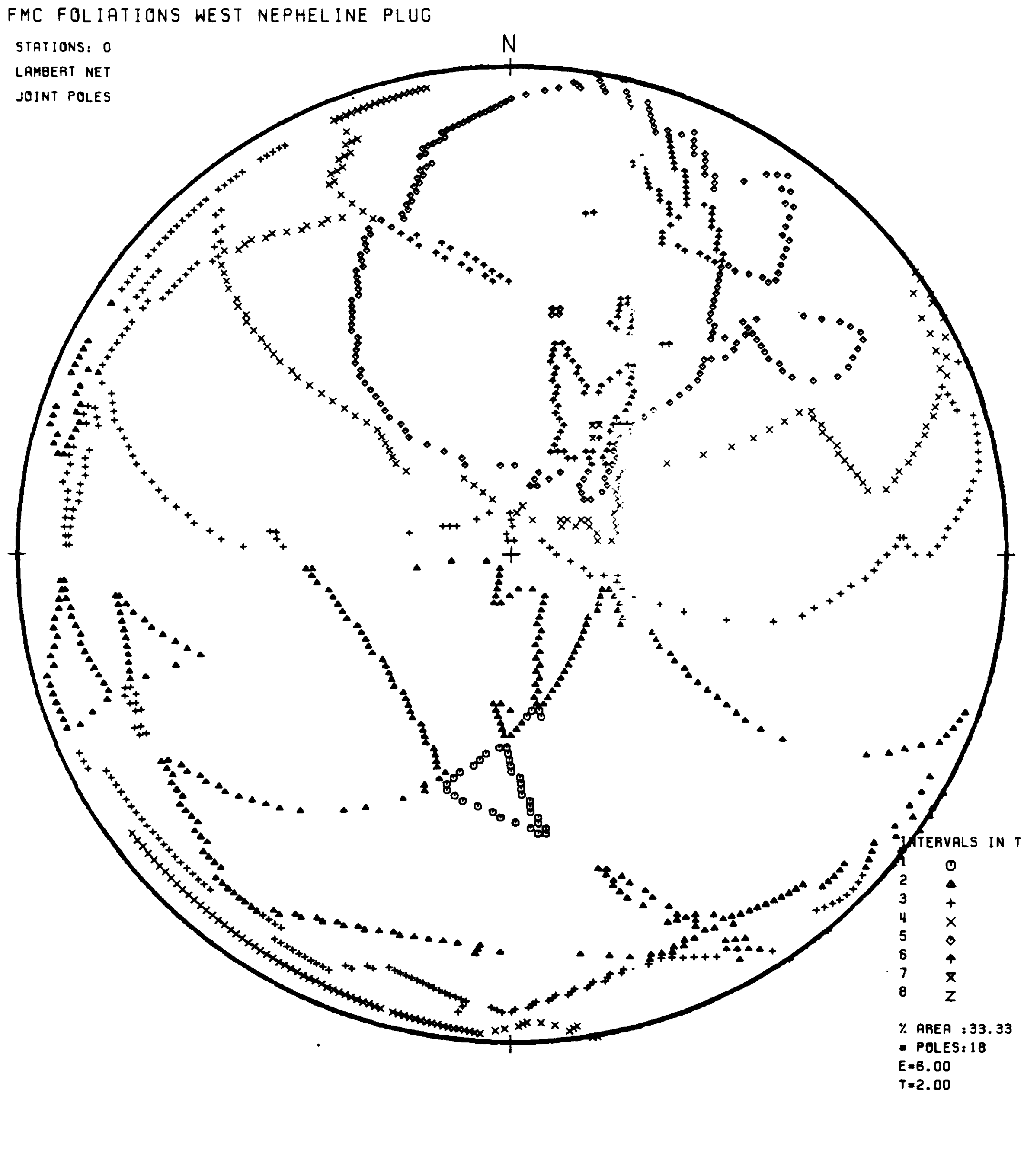

Figure 6e. Azimuth frequency plots and fabric diagrams contoured by Kamb's method.

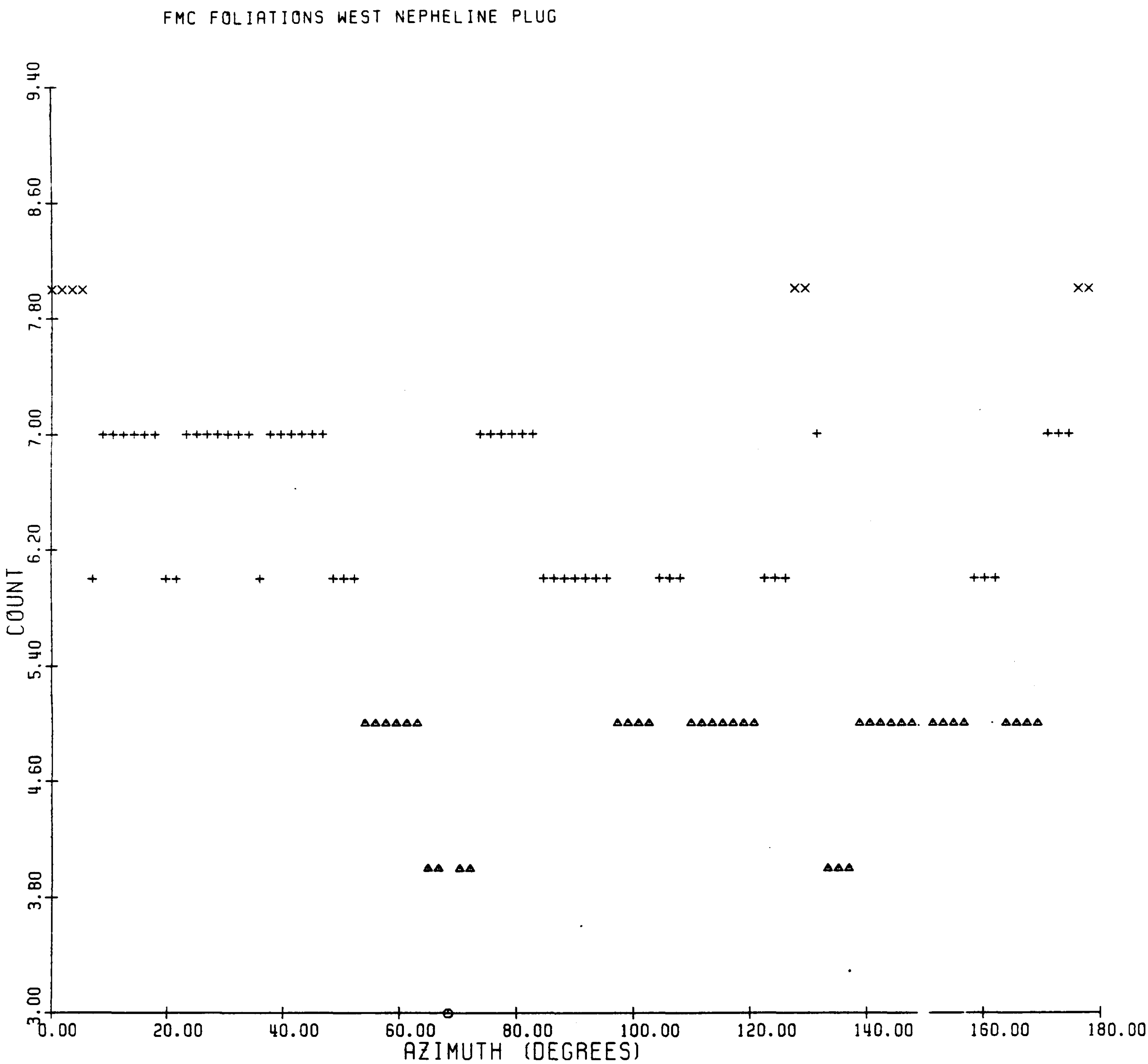

Figure 6f. Azimuth frequency plots and fabric diagrams contoured by Kamb's method.

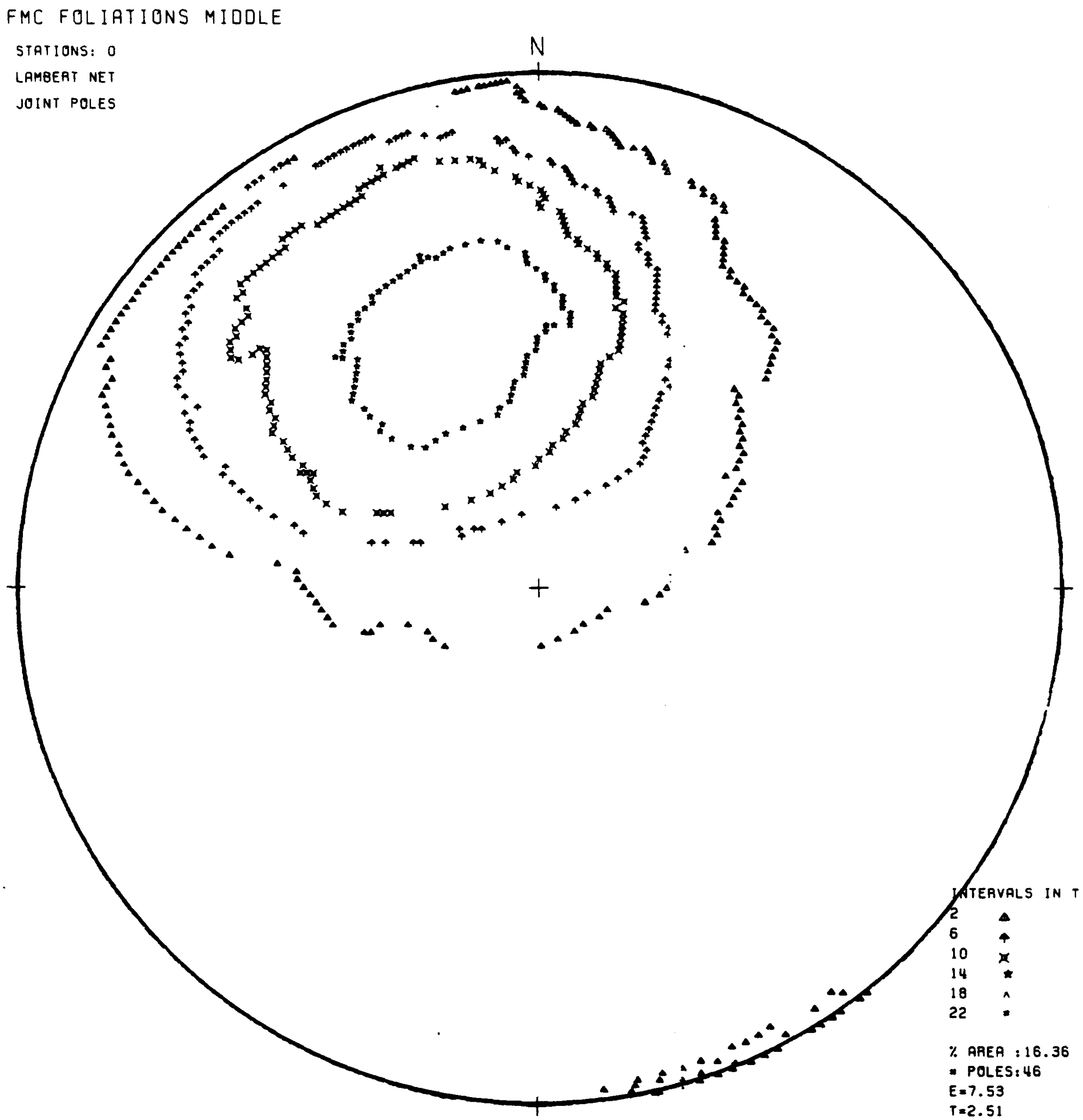

Figure 6f. Azimuth frequency plots and fabric diagrams contoured by Kamb's method.

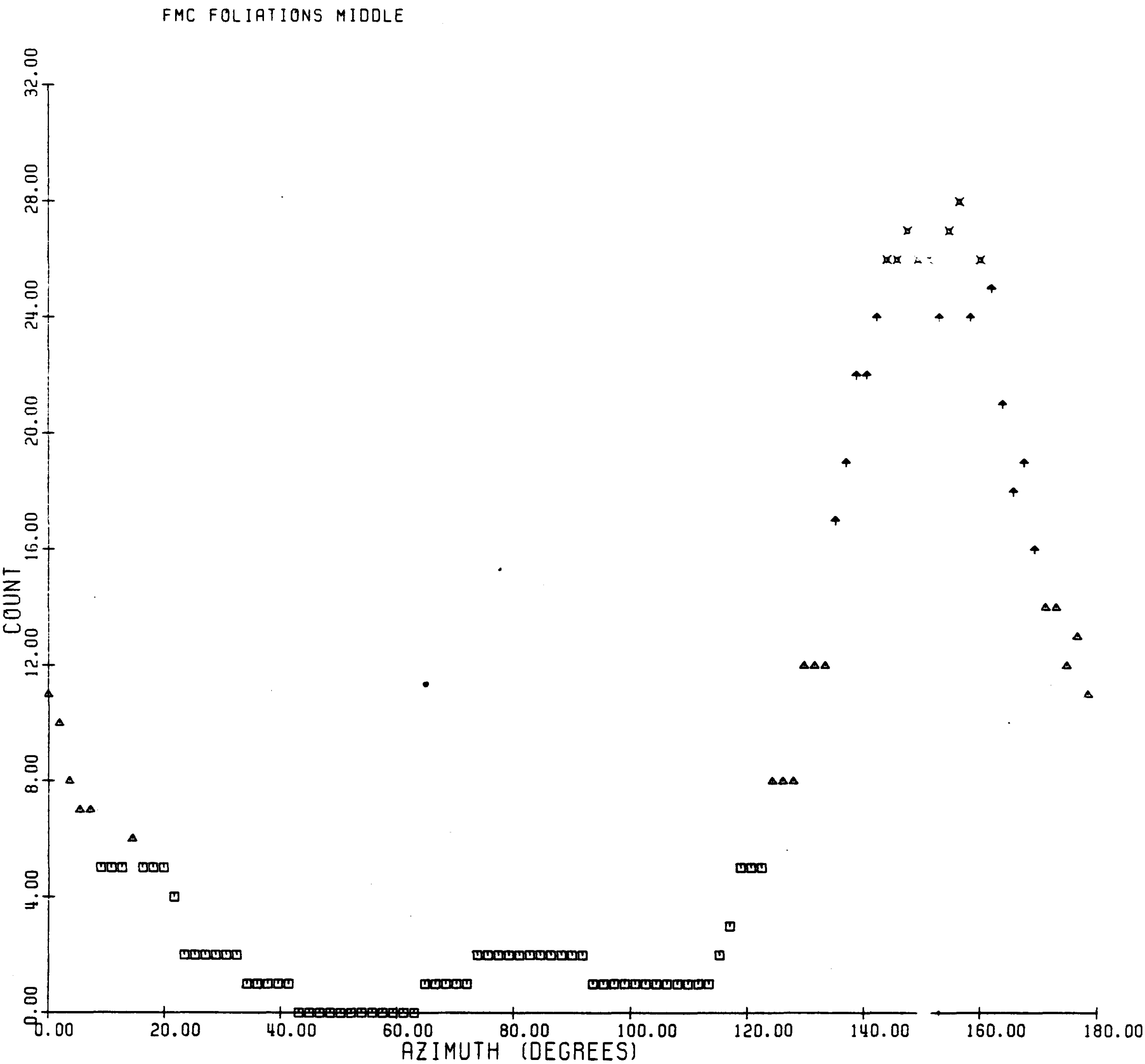

Figure 6g. Azimuth frequency plots and fabric diagrams contoured by Kamb's method.

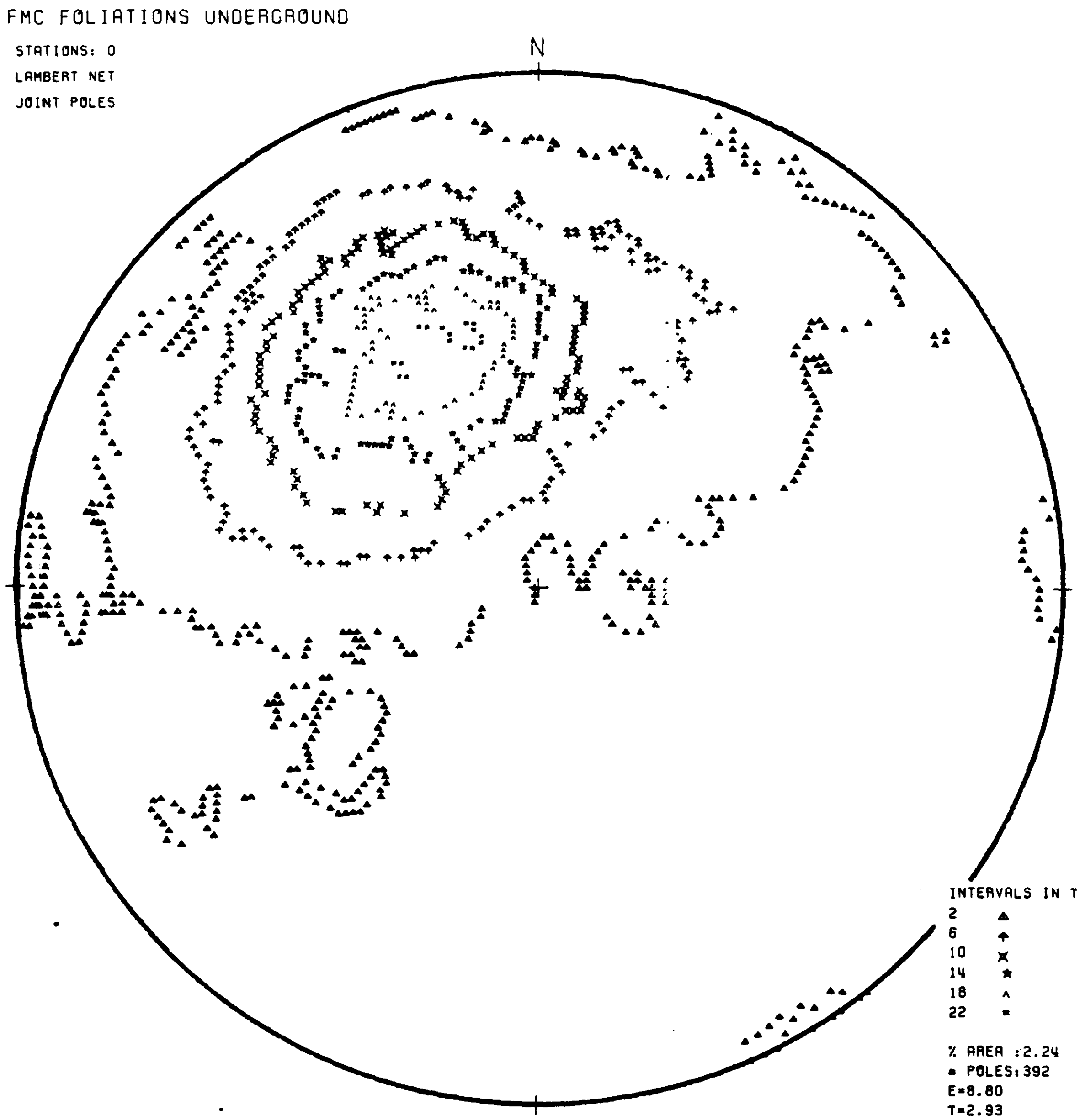

Figure 6g. Azimuth frequency plots and fabric diagrams contoured by Kamb's method.

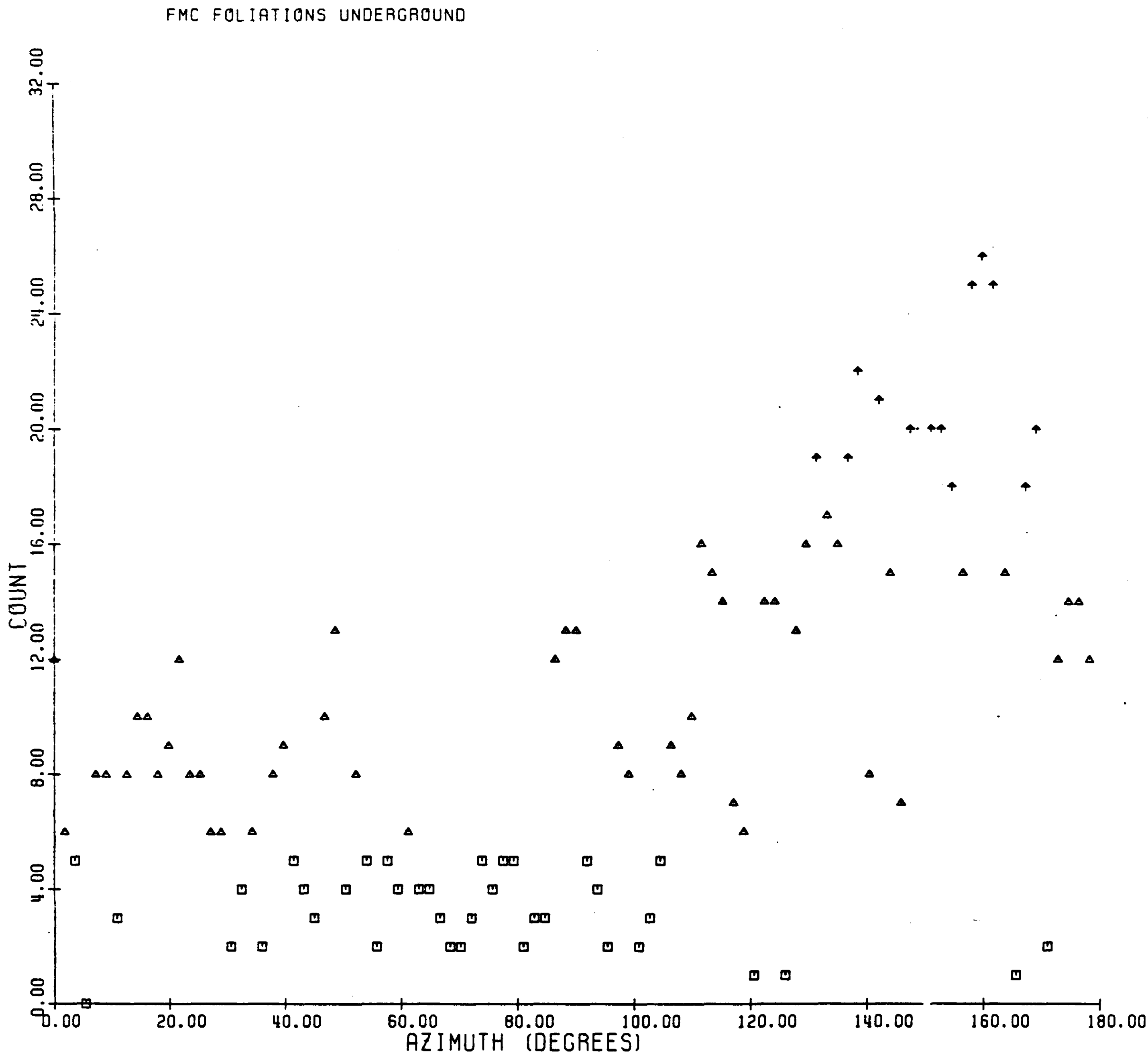

Figure 7a. Synoptic plots and diagrams of foliation data obtained underground.

Kamb's Method

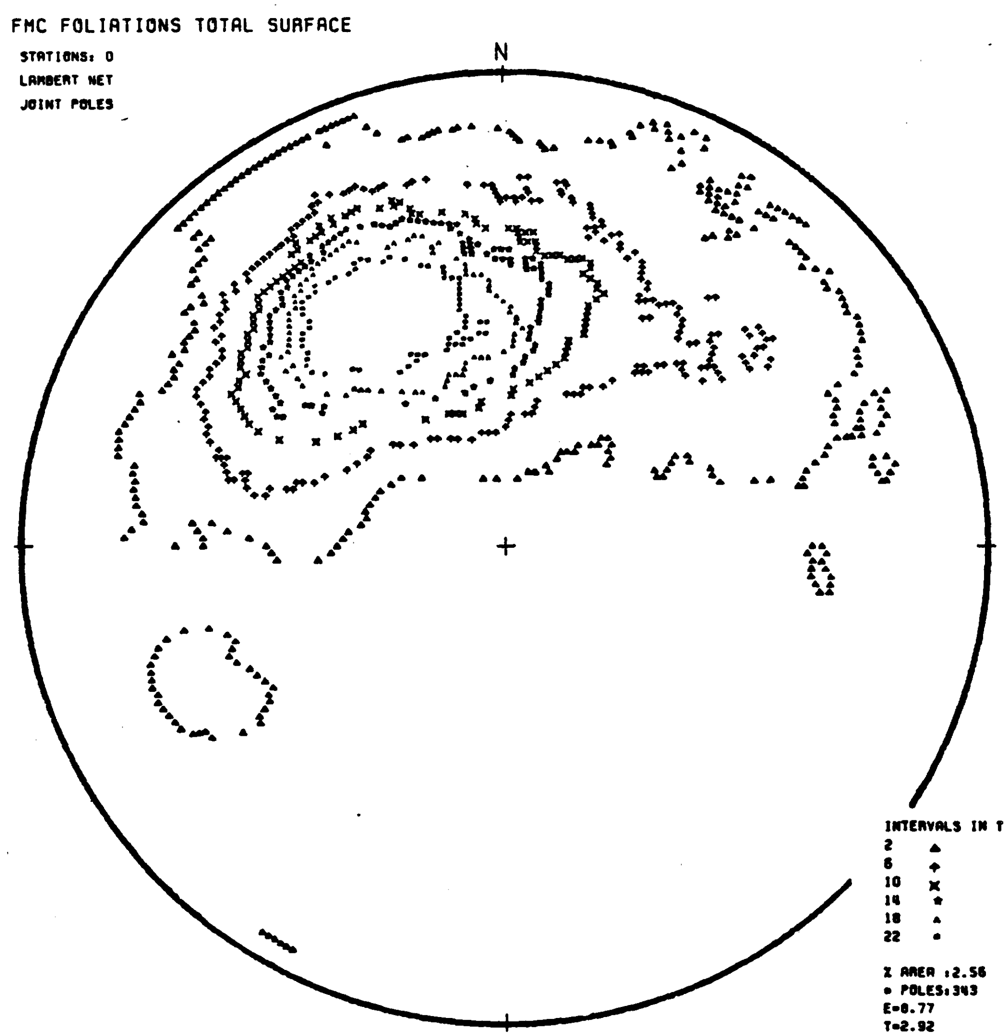

Figure 7b. Synoptic plots and diagrams of foliation data obtained at surface.

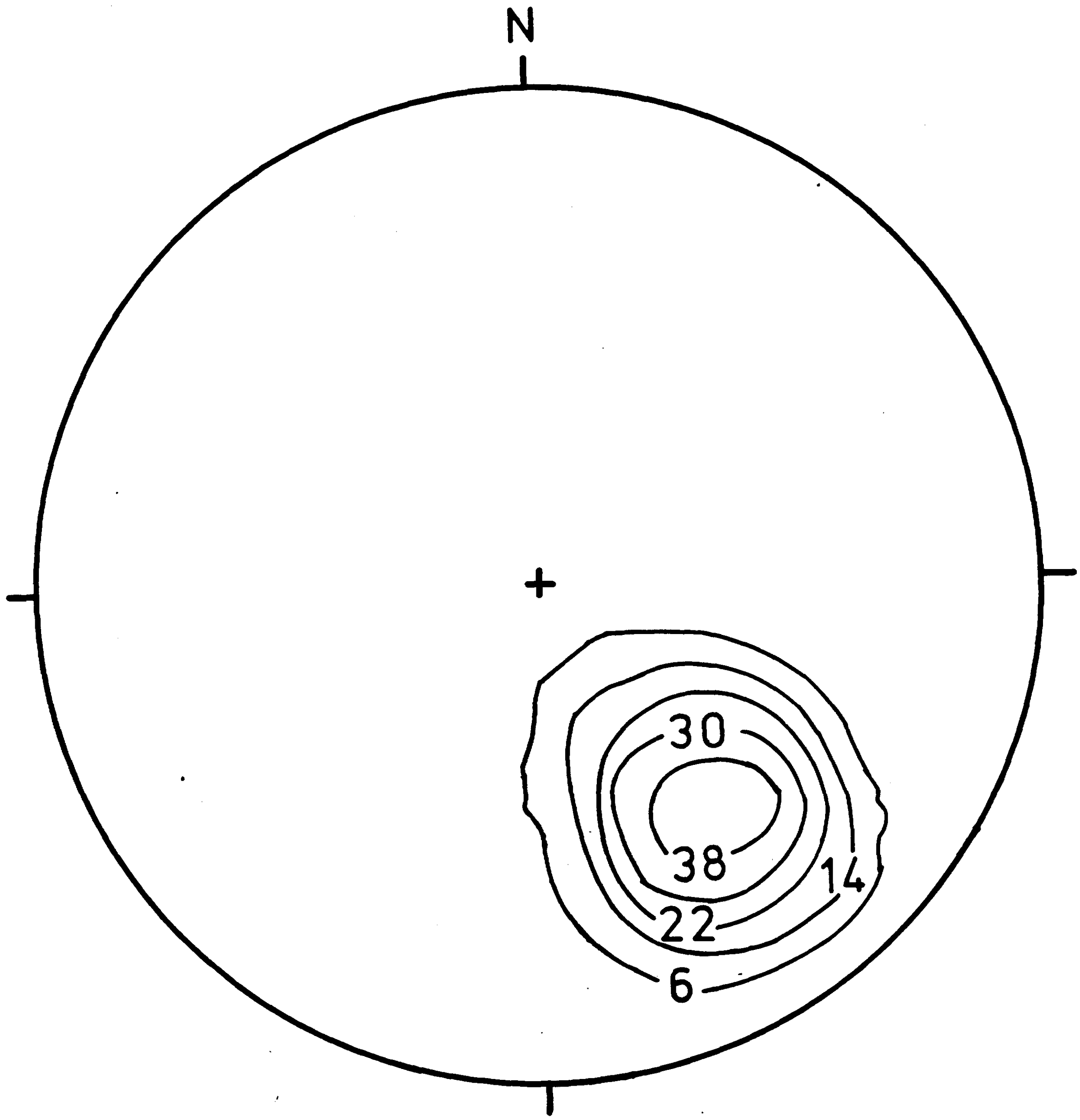

Figure 8. Synoptic diagram of all mineral lineation directions measured at surface and underground; and contours according to Kamb's method.

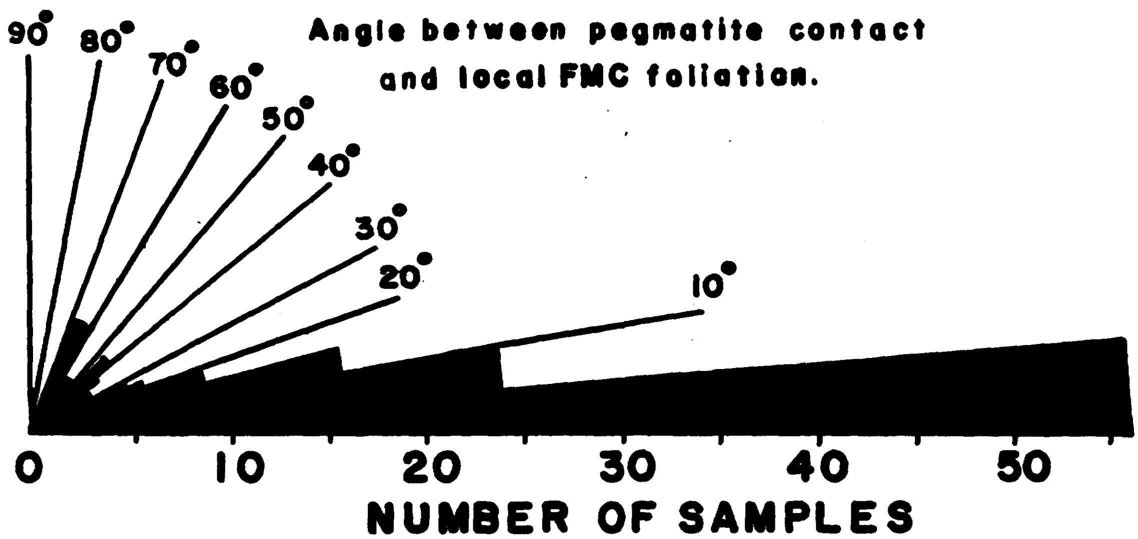

Figure 9. Obliquity between foliation strike in wall rocks and strike of adjacent pegmatite contacts.

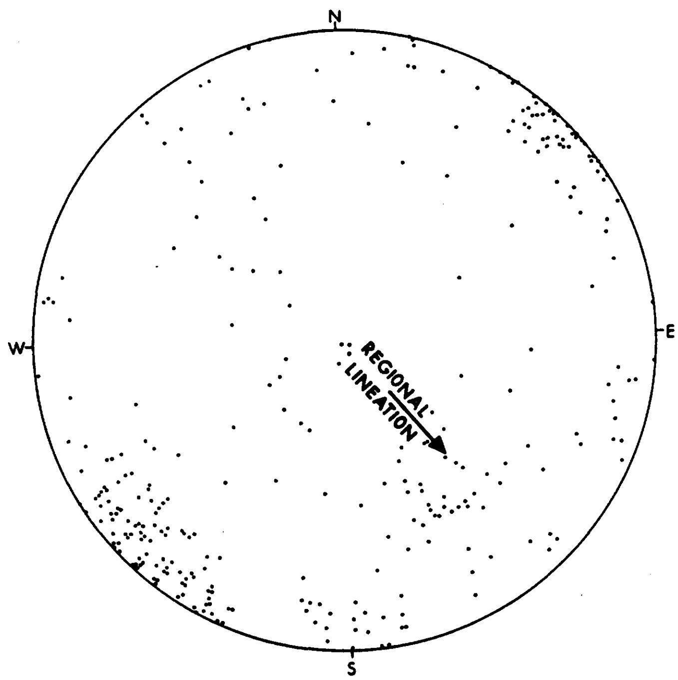

Figure 10. Point diagram of joint normals obtained at surface (see text).

Figure 11. L-S fabric pattern in southwestern Faraday Metagabbro Complex as judged by inspection of sawn hand specimens and structures in outcrops.

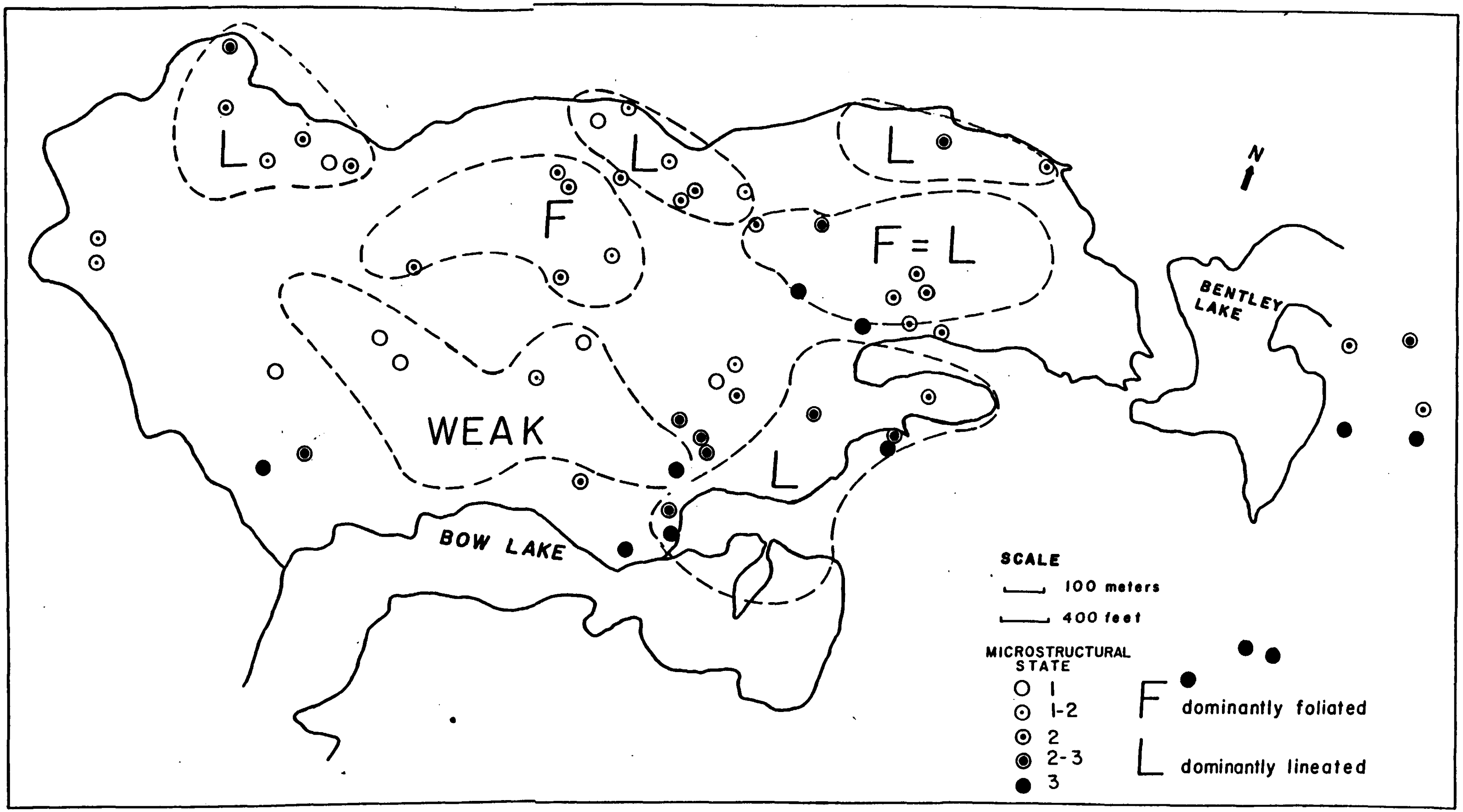

Figure 12. Quadrilateral phase diagram for pyroxene (see text).

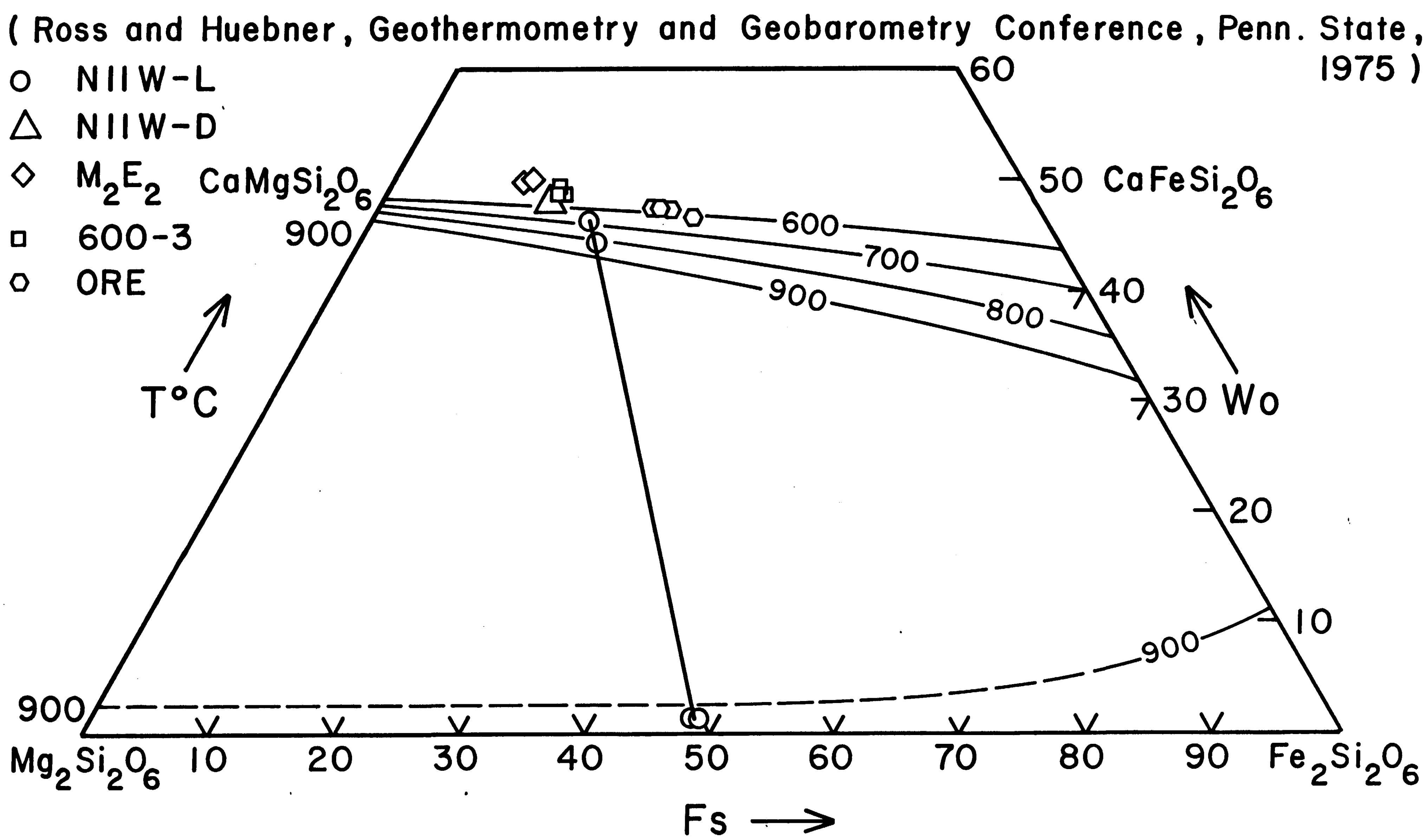

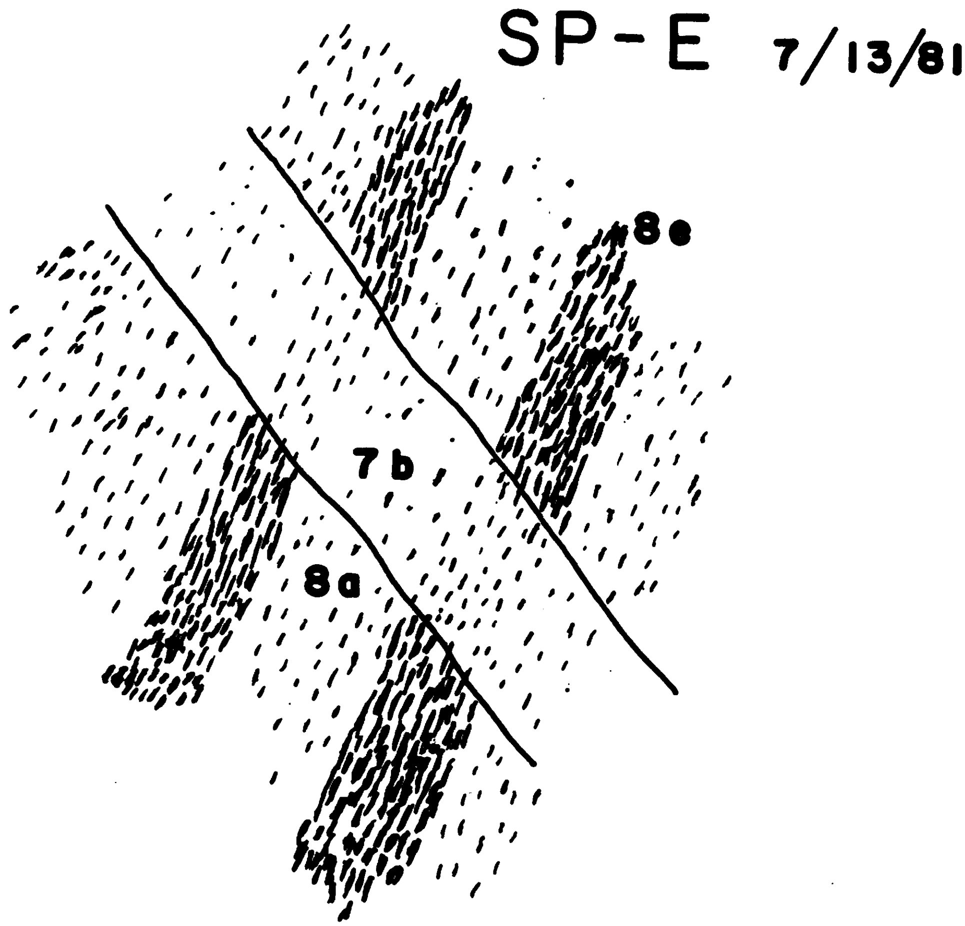

Figure 13a. Replacement of layered metagabbro (8a) by pegmatite (7b). The pegmatite dyke is about 20 cm wide. Code and date refers to a sketch in Bedell's field notes.

Figure 13b. Pegmatite lobe with ghost foliation parallel to gneissosity in wall rock. Note late dykelet cutting the pegmatite. Sketch made on 1200' level of mine.

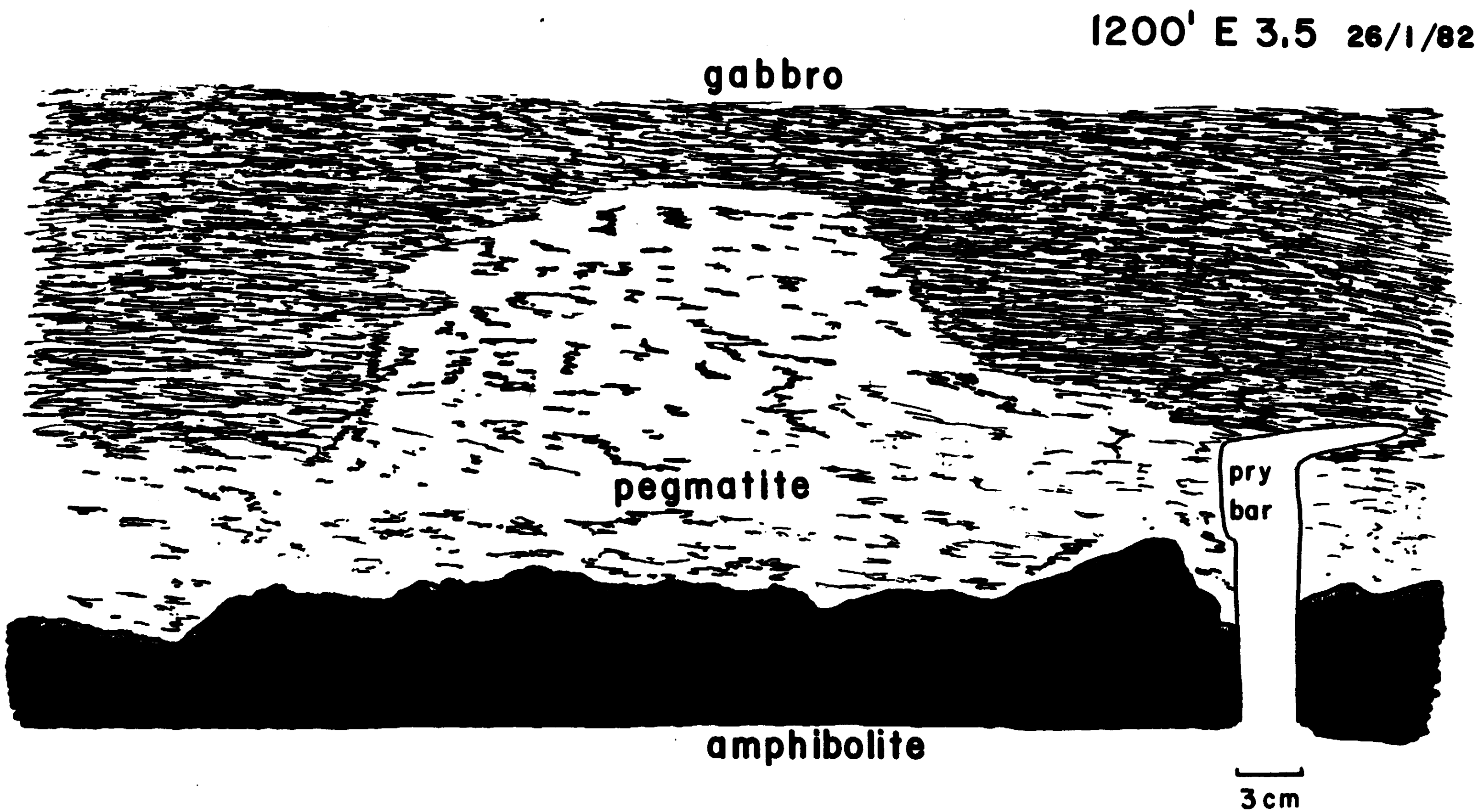

Figure 14. Bifurcating pegmatite bodies with fold-like regions sampled for textural study.

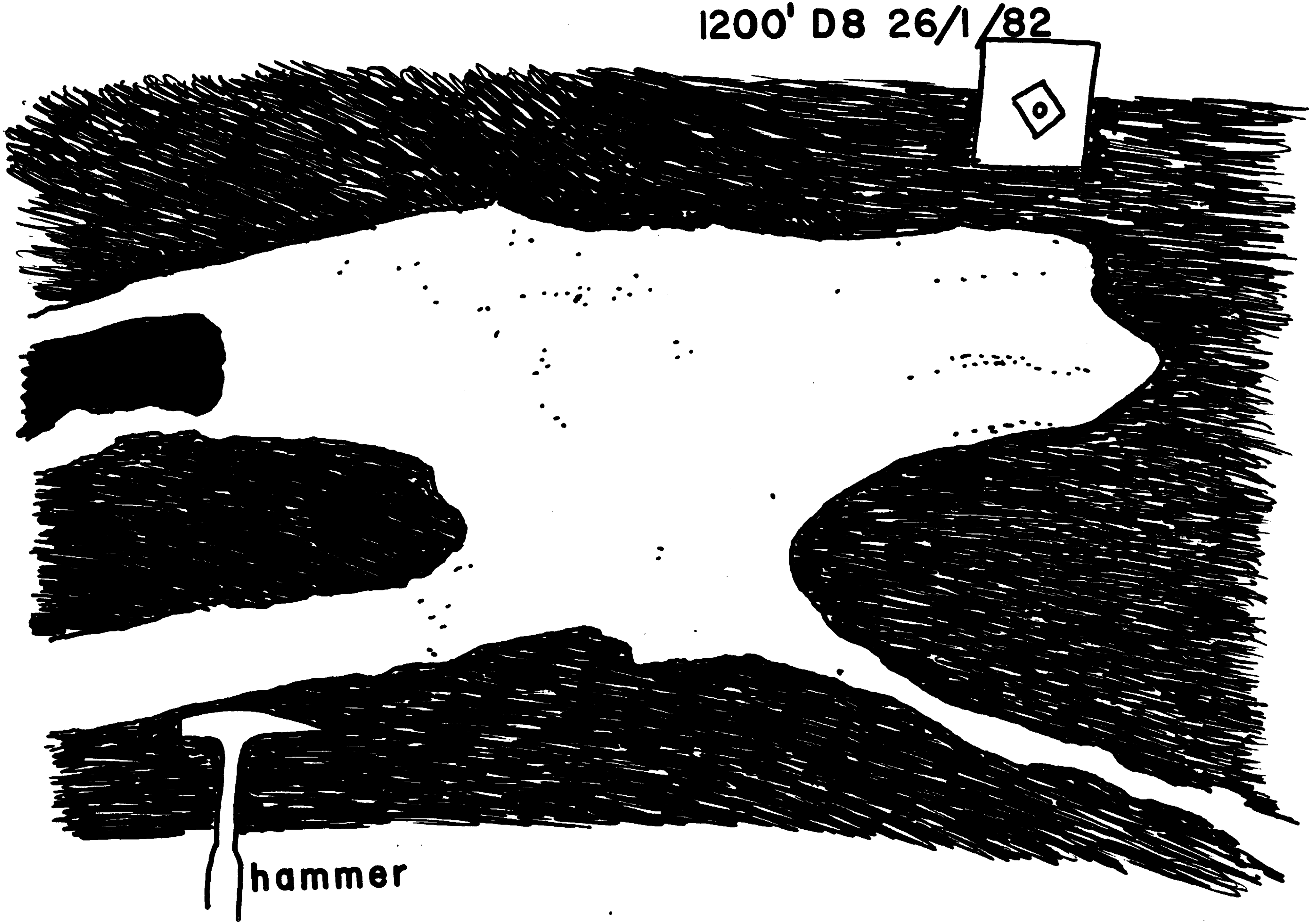

Figure 15. No textural differences are apparent in thin section from
(a) intermediate

(b) convex ore concave areas of "hinges" or

(c) "limbs".

Also note the relatively low amount of ductile strain relative to that found within the FMC (see text).

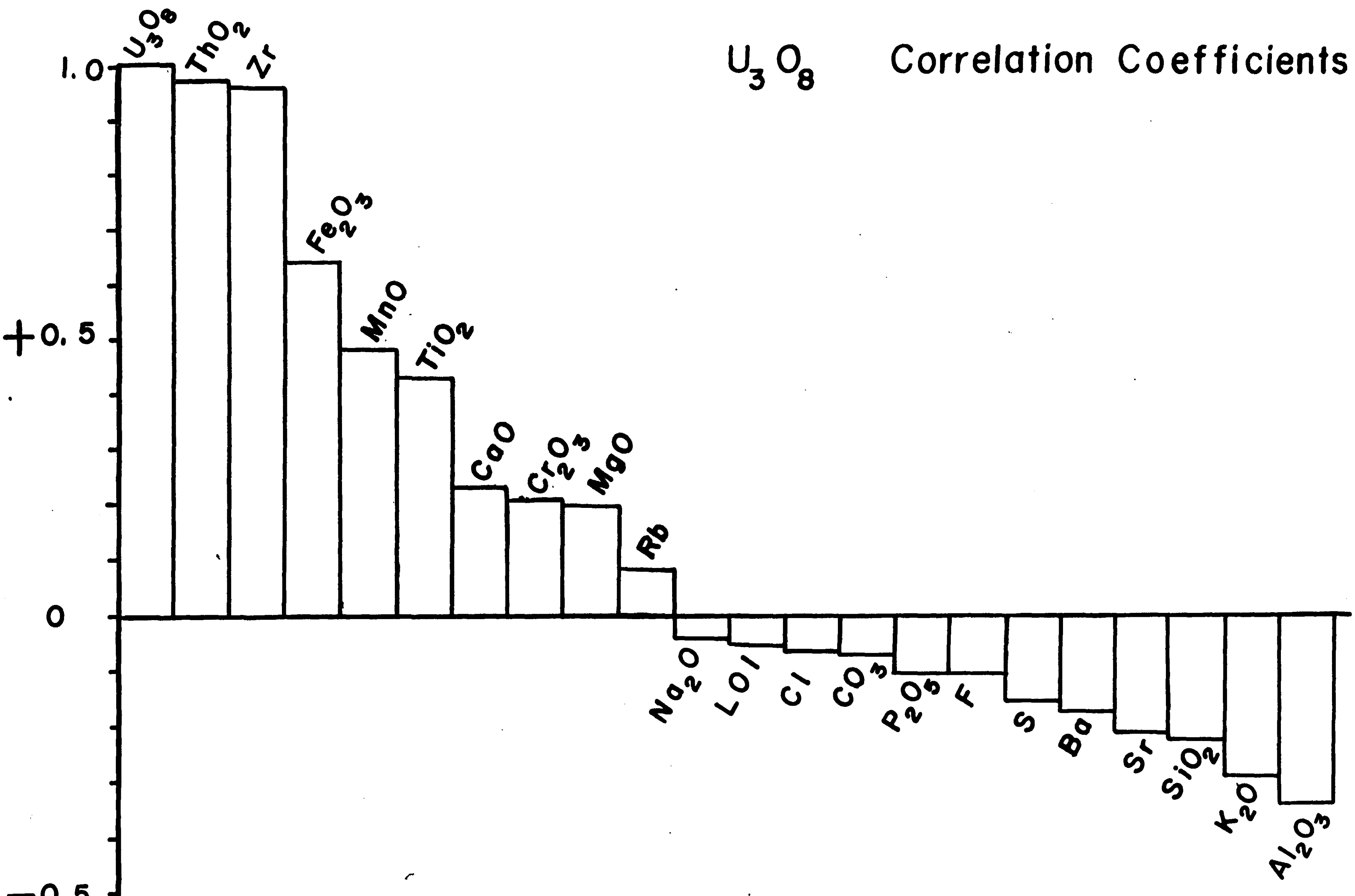

Figure 16. Correlation of uranium with other chemical elements in U-rich pegmatites.

Figure 17. Mechanical disaggregation of gabbroic xenoliths within a pegmatite body. Location in mine as indicated.

Appendix 1

Magnetic Fabric of Matagabbros

APPENDIX 1

Bulk magnetic susceptibility anisotropy (BMSA) of metagabbros was studied with a torque meter made at the University of Toronto. This instrument determines the magnetic susceptibility ellipsoid in cylindrical samples of (drill core) 1" diameter and .85" length. The susceptibility ellipsoid reflects the fabric of ferrimagnetic grains which presumably correspond with the total mineral fabric of a rock.

The ferrimagnetic grains in the FMC consist of magnetite and monoclinic pyrrhotite. These magnetic grains are commonly associated with the mafic clots (Figure 4) that act as markers of the rock fabric throughout the FMC. When visual rock fabric directions are compared with those obtained from the BMSA there is good agreement. Cores were oriented so that the mineral lineation should be at approximately 0° or 180°.

The problem with the BMSA application in this study is that the observed L, S fabric (predominantly lineated, foliated, or lineation = foliation) often does not agree with the shape of the magnetic susceptibility ellipsoid.

The shape of the magnetic susceptibility ellipsoid is determined by measuring the differences between the principal susceptibilities and determining the ratio:

$$P = (K_{max} - K_{int}) / (K_{int} - K_{min})$$

Therefore, if P is greater than unity the ellipsoid is dominantly lineated, if less than unity it is dominantly foliated, or approximately unity it is equally foliated and lineated.

A plot of observed rock fabric against measured susceptibility ellipsoid is shown in Figure A. There seems to be a weak correlation between the observed and measured fabrics, and significant variation in measured P-values between cylindrical specimens from the same sample.

Inhomogeneity of magnetic material within a given sample may be a problem. This is indicated by Figure B and C where the maximum deflection (amount sample is rotated within an applied magnetic field) out of 15 measurements for each core was plotted against deviation (in degrees) of the maximum susceptibility axis from 0^{o} or 180^{o}. One can observe for any given sample that the maximum deflection may vary considerably from core to core. The average silicate grain size is approximately .5 mm but the mafic aggregates are commonly up to 5 mm across and may be up to 10 cm long. The large grain size could explain the great variations in magnetic content which may effect P-values.

Figures D and E demonstrate how core reorientation within the sample chamber gives similar P-values as should be expected. Figure E, core B contains a fine grained layering and this effect seems to be detected by the BMSA as a more oblate P-value. Therefore, the method appears to be working with respect to orientations and local perturbations of the pervasive L and S tectonite fabrics.

Another source for error are variations in the length/diameter (l/d) of the cylindrical specimens. The effect of l/d variations in the FMC was examined by progressively reducing a single specimen (sample SPDA) from

.90 to .70" in steps of .05". A small but consistent variation was found among BMSA ellipsoid directions and P-values (Figure F). For the interval .85 to .75" the exact same axis orientations and P-values were found. At .70" a significant change in P-value and maximum susceptibility axis suggests inhomogeneity with respect to magnetic mineral content.

Collectively the petrographic observations, plots of maximum susceptibility, and l/d data suggest inhomogeneity to be the main source of difficulty. The amount of opaques within the mafic aggregates suggests that we may be dealing with magnetic shape anisotropy. Given the coarse grained nature of these magnetic aggregates with respect to the relatively small specimens, compositional inhomogeneities prevent reliable P-values, but may yield accurate BMSA ellipsoid orientations.

Figure A: A plot of fabric "observed" against P-values. $P > 1$ represents a lineated magnetic fabric, $P < 1$ foliated, P approximately 1 equally foliated and lineated. If the magnetic fabric matched the observed mafic mineral fabric, the analyses should ideally cluster in an envelope from the lower left origin extending to the upper right corner of the plot. This is clearly not the case. For instance, only one sample (M-G6) that has an observable strong lineation actually recorded a well lineated magnetic fabric. Individual cores are plotted as dots and cores from the same sample are connected by a horizontal line. The large variation in P between cores from the same sample suggests an inhomogeneous magnetic fabric.

Figures B and C: Plots of maximum deflection against degree variation of maximum susceptibility axis from ideal alignment along 0 or 180°. This plot indicates that most samples show reasonable agreement between observed mineral fabric lineation and maximum magnetic susceptibility trend (e.g. 0 - 15°). Note how variation between observed and measured fabric orientation tends to increase with decreased maximum deflection. At low susceptibility differences the error of the analysis increases. The maximum deflection found in the 15 measurements taken per core (usually 3 cores taken per sample) is variable. The amount of deflection is related to the amount of oriented magnetic minerals in the core. Hence, variable deflections in cores from the same sample, of the same orientation, represent inhomogeneity of magnetic material.

Figure D: Cores drilled at different orientations. Typically cores were drilled perpendicular, on to the plane of foliation. A core drilled along lineation (P = 1.48) shows a 90° flip of the maximum susceptibility trend from 0 or 180° to approximately vertical. This demonstrates the ability of the BMSA to give accurate directions of the magnetic fabric coincident with the observed mafic mineral fabric.

Figure E: Variation in principle susceptibility axes with reorientation of drill core. Core B shows a fine (mm scale) relic igneous layering that is discernible by the BMSA method with an oblate P-value of 0.47.

Figure F: Variation in maximum susceptibility trend with Length/Diameter (L/D) of drill core. A single core originally 1" x 1" was shaven in 0.05" intervals and analyzed. At 0.95" the sample was realigned in the sample chamber and replicate analyses were taken to determine accuracey. A consistent trend of principle susceptibility axes with decreasing core length was observed. At L/D = 0.70 there is a flip in the principal susceptibility direction. This trend and P-value suggests a more prolate ellipsoid parallel to the length of the drill core.

fp

BMSA SAMPLE LOCATIONS

Sample numbers for BMSA analyses were designed to accomodate the FORTRAN computer that reduced the data. The following list should clarify the location of those specimens not readily located by their sample number.

LFB1: LFB12

15WA: N15W-A

WN11B: N11W-B

WN11A: N11W-A

M1-C: Mag 1-C

M1DA: Mag 1-D_A

M1DB: Mag 1-D_B

M1DC: Mag 1-D_C

70E1: N70E-A (near baseline)

72EA: N72W-A (near baseline)

BL-5: Bentley Lake Domain station E

BL-8: Bentley Lake Domain station B

SPBL: Sand pit on North Shore of Bow Lake station SP-A

SP13: Sand pit station D

150A:	150'	level	of	mine station	A
4A34:	450'	"	"	"	34
4A41:	"	"	"	"	41
4A42:	"	"	"	"	42
4A43:	"	"	"	"	43
4A44:	"	"	"	"	44
7516:	750'	level	of	mine station	at entrance to 516 drift
7SHT:	750'	"	"	"	at shaft
7SPT:	750'	"	"	"	at entrance to 537 stope
75XC:	750'	"	"	"	at 502 cross cut
12-D:	1200'	"	"	"	D_{10}

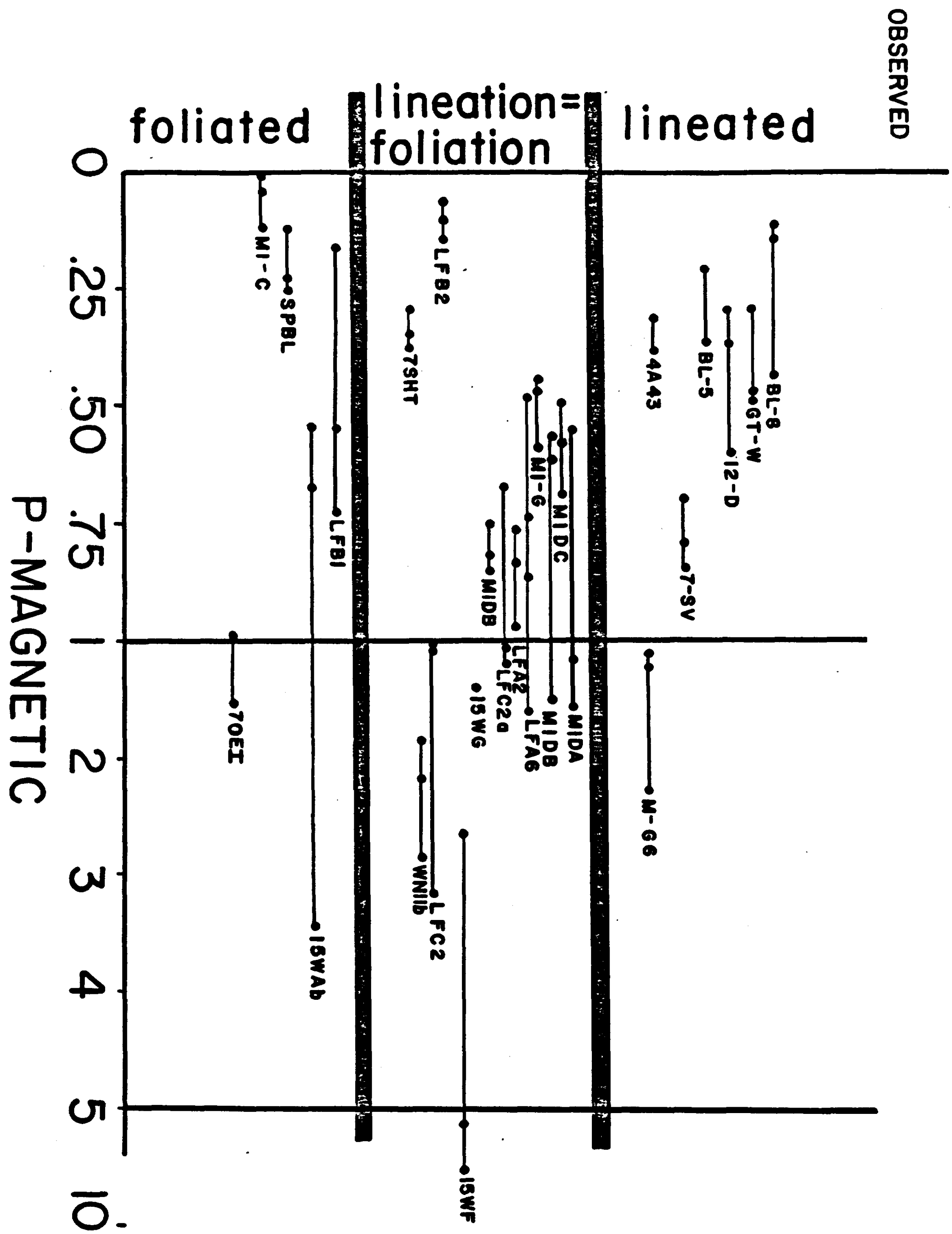

Appendix 1, Figure A.

Appendix 1, Figure B.

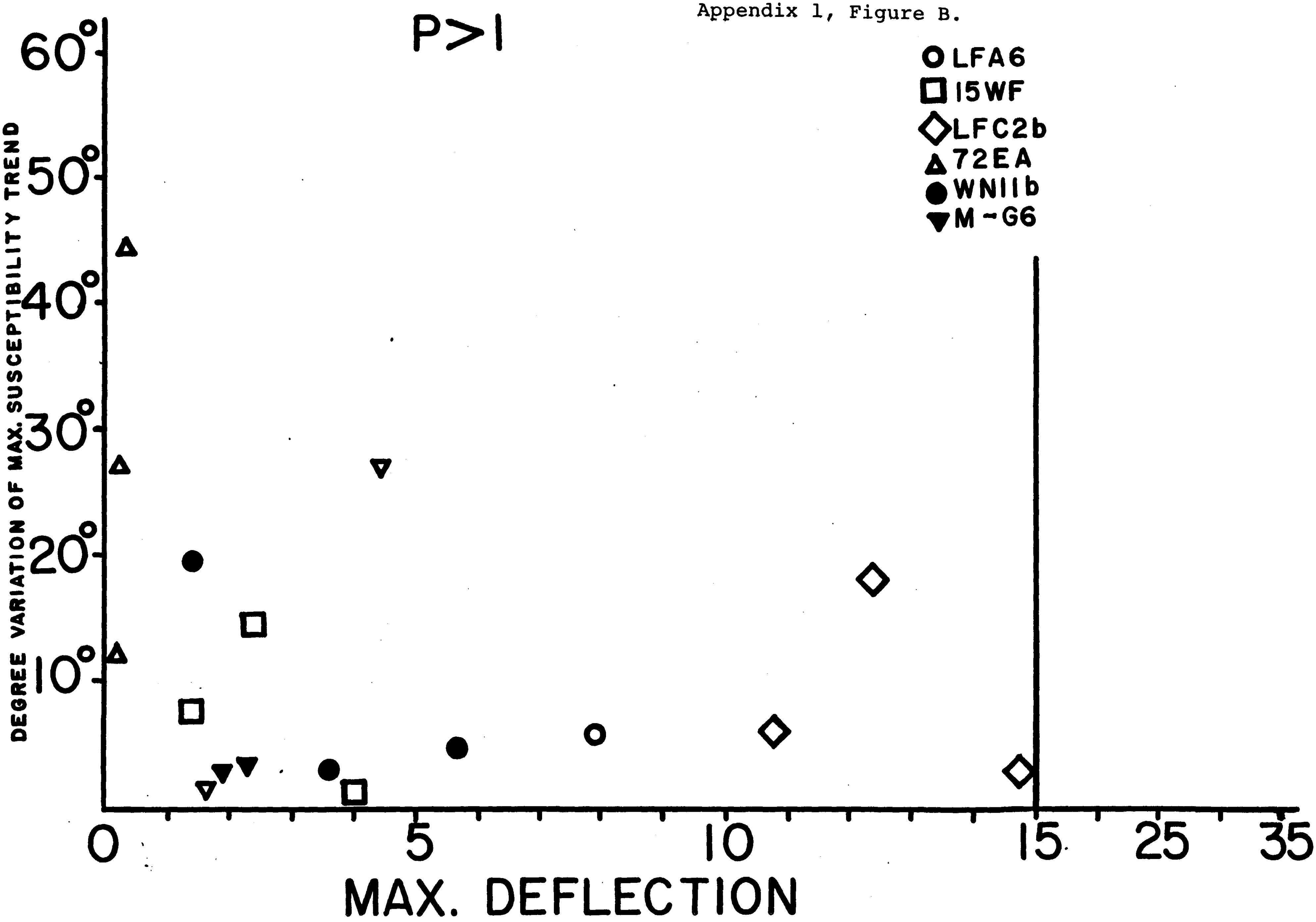

Appendix 1, Figure C.

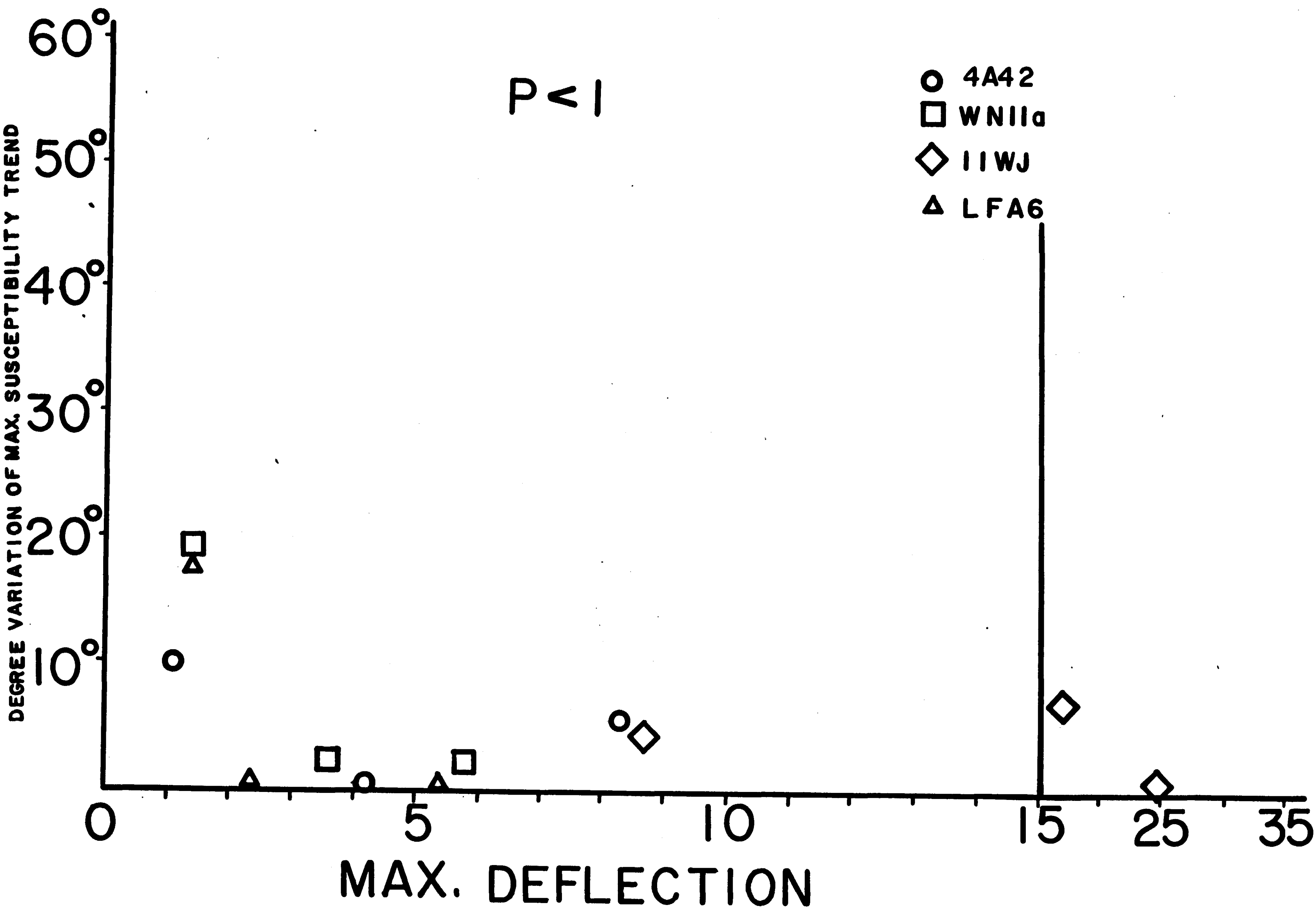

Appendix 1, Figure D.

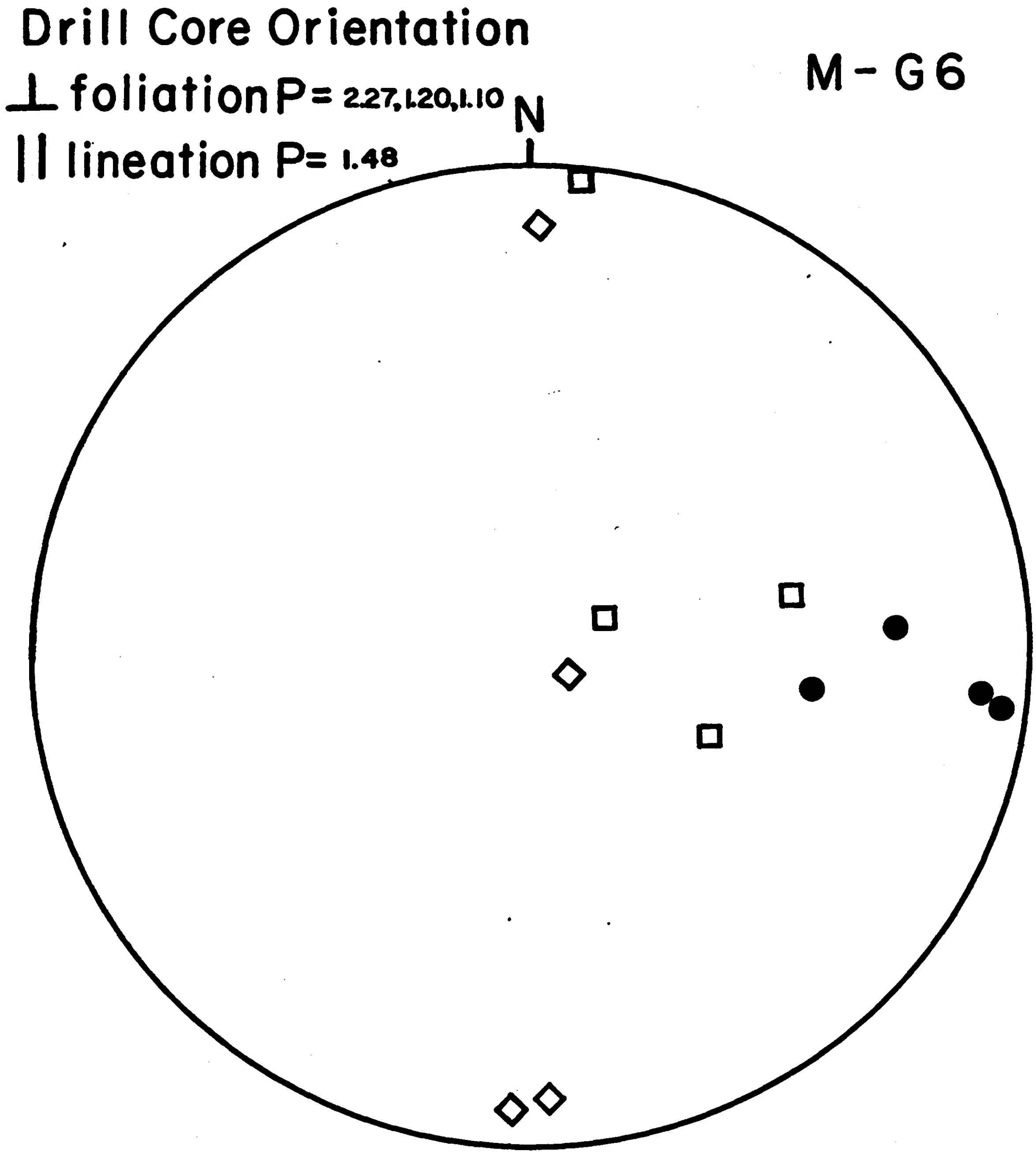

```
SPECIMEN NO. IS M-G6
DATA FROM 0 TO 180 DEGREES, READING POSITIONS 1,2,3
   -0.3      -1.9       0.3       1.8      -0.3
   -0.7       1.9       0.7      -1.8      -0.6
   -0.6      -1.8       0.7       1.7      -0.6
ERROR=  -0.31797
ROOTS=      -4.468     -3.062      0.130
SUSC= -4.47 CHECK=          -0.
TREND IS   77.31  PLUNGE IS    46.10
SUSC= -3.06 CHECK=          -0.
TREND IS   96.57  PLUNGE IS   -42.26
SUSC=  0.13 CHECK=           0.
TREND IS  177.59  PLUNGE IS     9.77
 P=    2.27183
ROCK IS PREDOMINANTLY LINEATED.

SPECIMEN NO. IS
DATA FROM 0 TO 180 DEGREES, READING POSITIONS 1,2,3
    0.1      -1.3      -0.1       1.3       0.1
   -0.5       2.3      -0.6      -2.3      -0.5
   -0.4      -2.2       0.4       2.2      -0.4
ERROR=  -0.21212
ROOTS=      -4.691     -2.532      0.074
SUSC= -4.69 CHECK=          -0.
TREND IS   59.48  PLUNGE IS    77.46
SUSC= -2.53 CHECK=          -0.
TREND IS   94.51  PLUNGE IS   -10.33
SUSC=  0.07 CHECK=           0.
TREND IS  183.24  PLUNGE IS     7.06
 P=    1.20727
ROCK IS PREDOMINANTLY LINEATED.

SPECIMEN NO. IS
DATA FROM 0 TO 180 DEGREES, READING POSITIONS 1,2,3
    0.3      -1.1      -0.2       1.3       0.3
    0.9       1.7      -0.8      -1.6      -0.9
   -0.8      -1.7       0.8       1.7      -0.8
ERROR=  -0.27174
ROOTS=      -3.999     -2.000      0.199
SUSC= -4.00 CHECK=          -0.
TREND IS  113.70  PLUNGE IS    58.75
SUSC= -2.00 CHECK=           0.
TREND IS   84.43  PLUNGE IS   -27.90
SUSC=  0.20 CHECK=           0.
TREND IS    1.42  PLUNGE IS    12.97
 P=    1.10005
ROCK IS PREDOMINANTLY LINEATED.

SPECIMEN NO. IS M-G6
DATA FROM 0 TO 180 DEGREES, READING POSITIONS 1,2,3
   -0.4       1.8       0.4      -1.3      -0.4
   -0.4      -4.5       0.4       4.4      -0.4
    0.5       2.8      -0.6      -2.8       0.4
ERROR=   0.01657
ROOTS=      -0.057      3.584      8.973
SUSC= -0.06 CHECK=          -0.
TREND IS    5.93  PLUNGE IS     2.20
SUSC=  3.58 CHECK=           0.
TREND IS   95.68  PLUNGE IS    -6.94
SUSC=  8.97 CHECK=           0.
TREND IS  115.83  PLUNGE IS    83.59
 P=    1.47999
ROCK IS PREDOMINANTLY LINEATED.
```

9

Appendix 1, Figure E.

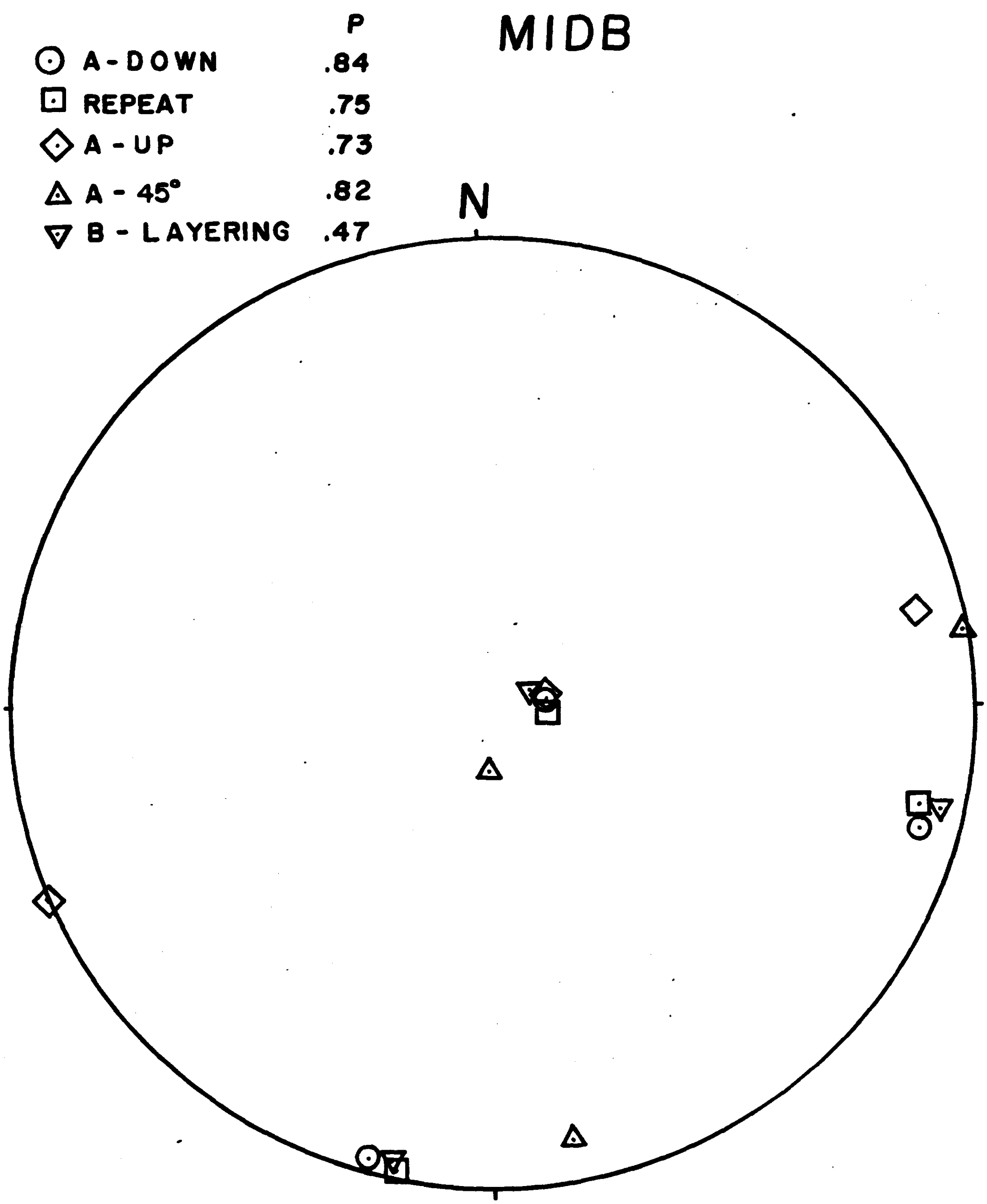

```
SPECIMEN NO. IS M1DB
DATA FROM 0 TO 180 DEGREES, READING POSITIONS 1,2,3
     0.5      -0.8      -0.4       0.8       0.5
    -0.2       1.9       0.2      -1.9      -0.2
    -0.4      -1.0       0.4       1.0      -0.4
ERROR=    0.02703
ROOTS=     -3.874     -1.679      0.153
SUSC= -3.87 CHECK=         -0.
TREND IS   79.70  PLUNGE IS    80.24
SUSC= -1.68 CHECK=         -0.
TREND IS  106.79  PLUNGE IS    -8.72
SUSC=  0.15 CHECK=          0.
TREND IS  196.13  PLUNGE IS     4.39
 P=    0.83508
ROCK IS PREDOMINANTLY FOLIATED.

SPECIMEN NO. IS
DATA FROM 0 TO 180 DEGREES, READING POSITIONS 1,2,3
     0.4      -0.8      -0.4       0.8       0.4
    -0.1       1.9       0.1      -1.9       0.0
    -0.4      -1.0       0.4       1.0      -0.4
ERROR=    0.02703
ROOTS=     -3.871     -1.609      0.080
SUSC= -3.87 CHECK=         -0.
TREND IS   88.88  PLUNGE IS    80.05
SUSC= -1.61 CHECK=          0.
TREND IS  102.70  PLUNGE IS    -9.68
SUSC=  0.08 CHECK=          0.
TREND IS  192.32  PLUNGE IS     2.34
 P=    0.74669
ROCK IS PREDOMINANTLY FOLIATED.

SPECIMEN NO. IS
DATA FROM 0 TO 180 DEGREES, READING POSITIONS 1,2,3
    -0.4      -0.8       0.4       0.8      -0.4
    -0.1       1.9       0.1      -1.9       0.0
    -0.4      -1.0       0.4       1.0      -0.4
ERROR=    0.02703
ROOTS=     -3.875     -1.598      0.073
SUSC= -3.88 CHECK=         -0.
TREND IS   78.87  PLUNGE IS    79.55
SUSC= -1.60 CHECK=          0.
TREND IS   78.15  PLUNGE IS   -10.47
SUSC=  0.07 CHECK=          0.
TREND IS  348.15  PLUNGE IS     0.13
 P=    0.73392
ROCK IS PREDOMINANTLY FOLIATED.

SPECIMEN NO. IS
DATA FROM 0 TO 180 DEGREES, READING POSITIONS 1,2,3
     0.3       0.9      -0.3      -0.9       0.3
     0.4       1.1      -0.4      -1.1       0.4
    -0.1      -1.9       0.0       1.9       0.1
ERROR=    0.01935
ROOTS=     -2.218      0.019      1.850
SUSC= -2.22 CHECK=         -0.
TREND IS  175.73  PLUNGE IS    79.98
SUSC=  0.02 CHECK=         -0.
TREND IS  170.44  PLUNGE IS    -9.99
SUSC=  1.85 CHECK=          0.
TREND IS   80.62  PLUNGE IS     0.91
 P=    0.81845
ROCK IS PREDOMINANTLY FOLIATED.

SPECIMEN NO. IS
DATA FROM 0 TO 180 DEGREES, READING POSITIONS 1,2,3
     0.3      -0.7      -0.3       0.7       0.3
    -0.3       2.3       0.3      -2.3      -0.3
    -0.4      -1.6       0.4       1.6      -0.4
ERROR=   -0.01075
ROOTS=     -4.658     -1.433      0.091
SUSC= -4.66 CHECK=         -0.
TREND IS   62.44  PLUNGE IS    82.95
SUSC= -1.43 CHECK=          0.
TREND IS  102.92  PLUNGE IS    -5.38
SUSC=  0.09 CHECK=          0.
TREND IS  192.51  PLUNGE IS     4.56
 P=    0.47235
ROCK IS PREDOMINANTLY FOLIATED.
```

Appendix 1, Figure F.

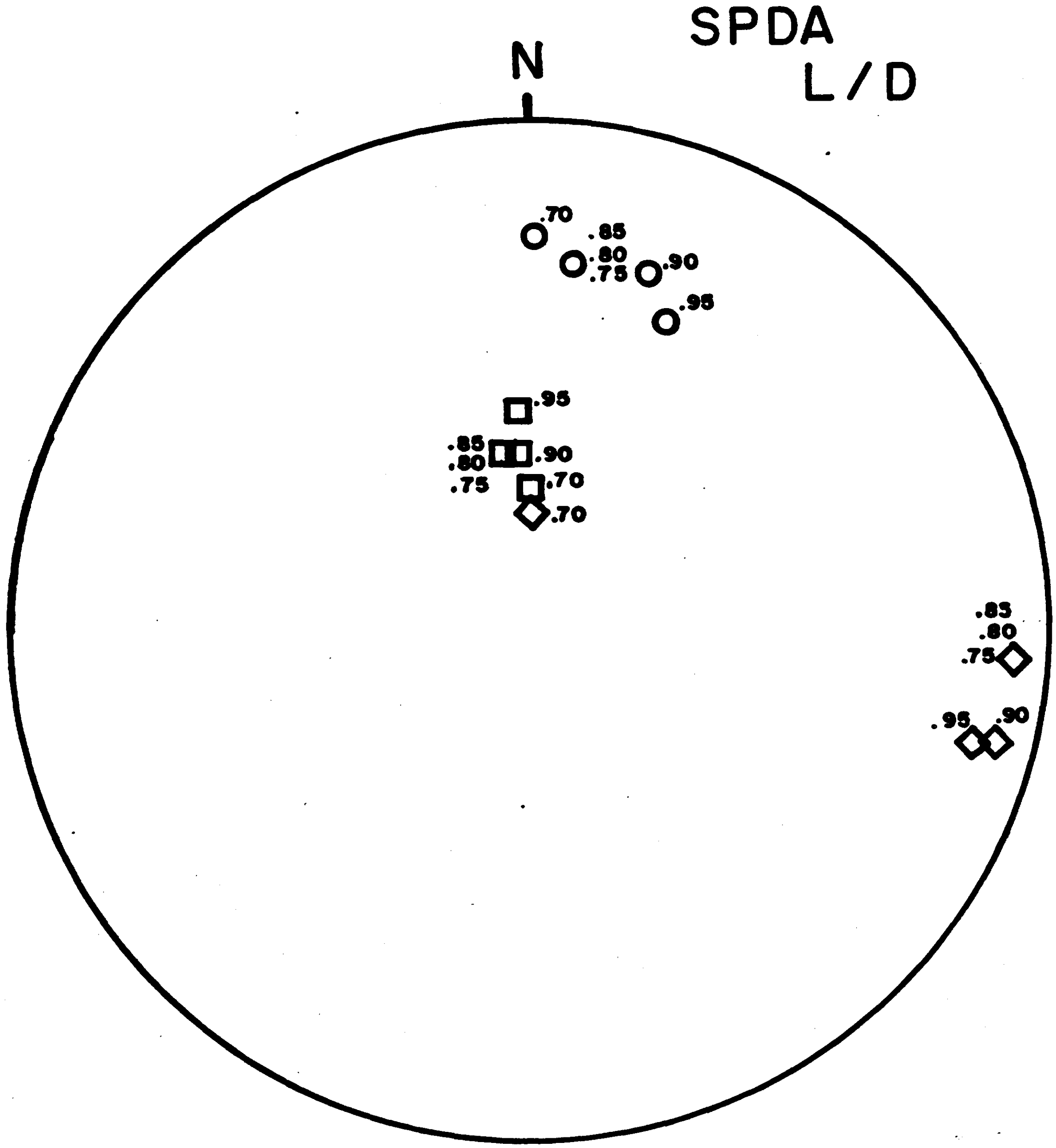

```
SPECIMEN NO. IS
DATA FROM 0 TO 180 DEGREES, READING POSITIONS 1,2,3
    0.0       0.3       0.0      -0.3       0.0
   -0.3       0.2       0.3      -0.2      -0.3
    0.1      -0.4      -0.1       0.4       0.1
ERROR=   0.11111
ROOTS=      -0.567        0.156        0.612
SUSC= -0.57 CHECK=           0.
TREND IS  350.80  PLUNGE IS     61.83
SUSC=  0.16 CHECK=          -0.
TREND IS    6.66  PLUNGE IS   -27.27
SUSC=  0.61 CHECK=           0.
TREND IS   93.23  PLUNGE IS      6.59
 P=   0.63066
ROCK IS PREDOMINANTLY FOLIATED.
```

L/D = .85

```
SPECIMEN NO. IS
DATA FROM 0 TO 180 DEGREES, READING POSITIONS 1,2,3
    0.0       0.3       0.0      -0.3       0.0
   -0.3       0.2       0.3      -0.2      -0.3
    0.1      -0.4      -0.1       0.4       0.1
ERROR=   0.11111
ROOTS=      -0.567        0.156        0.612
SUSC= -0.57 CHECK=           0.
TREND IS  350.80  PLUNGE IS     61.83
SUSC=  0.16 CHECK=          -0.
TREND IS    6.66  PLUNGE IS   -27.27
SUSC=  0.61 CHECK=           0.
TREND IS   93.23  PLUNGE IS      6.59
 P=   0.63066
ROCK IS PREDOMINANTLY FOLIATED.
```

L/D = .80

9

```
SPECIMEN NO. IS
DATA FROM 0 TO 180 DEGREES, READING POSITIONS 1,2,3
    0.0       0.3       0.0      -0.3       0.0
   -0.3       0.2       0.3      -0.2      -0.3
    0.1      -0.4      -0.1       0.4       0.1
ERROR=   0.11111
ROOTS=      -0.567        0.156        0.612
SUSC= -0.57 CHECK=           0.
TREND IS  350.80  PLUNGE IS     61.83
SUSC=  0.16 CHECK=          -0.
TREND IS    6.66  PLUNGE IS   -27.27
SUSC=  0.61 CHECK=           0.
TREND IS   93.23  PLUNGE IS      6.59
 P=   0.63066
ROCK IS PREDOMINANTLY FOLIATED.
```

L/D = .75

```
SPECIMEN NO. IS
DATA FROM 0 TO 180 DEGREES, READING POSITIONS 1,2,3
    0.0       0.3       0.0      -0.3       0.0
   -0.2       0.2       0.2      -0.2      -0.2
    0.0      -0.3       0.0       0.3       0.0
ERROR=   0.25000
ROOTS=      -0.483        0.083        0.600
SUSC= -0.48 CHECK=          -0.
TREND IS    0.0   PLUNGE IS     67.51
SUSC=  0.08 CHECK=          -0.
TREND IS    0.0   PLUNGE IS   -22.50
SUSC=  0.60 CHECK=           0.
TREND IS    0.0   PLUNGE IS   -71.58
 P=   0.91421
ROCK IS PREDOMINANTLY FOLIATED.
```

L/D = .70

```
SPECIMEN NO. IS SPDA
DATA FROM 0 TO 180 DEGREES, READING POSITIONS 1,2,3
      0.1        0.3        0.0       -0.3        0.1
     -0.3        0.1        0.3       -0.1       -0.3
      0.1       -0.4       -0.1        0.4        0.1
ERROR=     0.00000
ROOTS=        -0.433         0.214         0.619
SUSC= -0.43 CHECK=              0.
TREND IS   347.67   PLUNGE IS     53.96
SUSC=  0.21 CHECK=             -0.
TREND IS     5.46   PLUNGE IS    -34.73
SUSC=  0.62 CHECK=              0.
TREND IS    89.54   PLUNGE IS      8.51
 P=    0.62718
ROCK IS PREDOMINANTLY FOLIATED.
```

L/D = .95

ARROW UP

```
SPECIMEN NO. IS
DATA FROM 0 TO 180 DEGREES, READING POSITIONS 1,2,3
     -0.1        0.3        0.1       -0.3       -0.1
     -0.3        0.1        0.3       -0.1       -0.3
      0.1       -0.4       -0.1        0.4        0.1
ERROR=     0.00000
ROOTS=        -0.417         0.171         0.646
SUSC= -0.42 CHECK=              0.
TREND IS   357.73   PLUNGE IS     54.50
SUSC=  0.17 CHECK=             -0.
TREND IS    21.64   PLUNGE IS    -33.13
SUSC=  0.65 CHECK=              0.
TREND IS   104.08   PLUNGE IS     11.37
 P=    0.80819
ROCK IS PREDOMINANTLY FOLIATED.
```

L/D = .95

```
SPECIMEN NO. IS
DATA FROM 0 TO 180 DEGREES, READING POSITIONS 1,2,3
     -0.1        0.3        0.1       -0.3       -0.1
     -0.3        0.1        0.4       -0.1       -0.3
      0.1       -0.4       -0.1        0.4        0.1
ERROR=     0.00000
ROOTS=        -0.464         0.213         0.651
SUSC= -0.46 CHECK=             -0.
TREND IS   358.19   PLUNGE IS     53.18
SUSC=  0.21 CHECK=             -0.
TREND IS    24.21   PLUNGE IS    -33.95
SUSC=  0.65 CHECK=              0.
TREND IS   105.54   PLUNGE IS     12.60
 P=    0.64581
ROCK IS PREDOMINANTLY FOLIATED.
```

L/D = .95

REPEAT

```
SPECIMEN NO. IS
DATA FROM 0 TO 180 DEGREES, READING POSITIONS 1,2,3
     -0.1        0.3        0.1       -0.3       -0.1
     -0.3        0.2        0.3       -0.2       -0.3
      0.1       -0.4       -0.1        0.4        0.1
ERROR=     0.11111
ROOTS=        -0.562         0.122         0.640
SUSC= -0.56 CHECK=             -0.
TREND IS   355.57   PLUNGE IS     62.17
SUSC=  0.12 CHECK=             -0.
TREND IS    17.59   PLUNGE IS    -26.09
SUSC=  0.64 CHECK=              0.
TREND IS   103.10   PLUNGE IS      9.04
 P=    0.75574
ROCK IS PREDOMINANTLY FOLIATED.
```

L/D = .90

Appendix 2

Microstructural Study

APPENDIX 2

In an effort to quantify the three microstructural states as determined from the dominant plagioclase texture in thin section, 50 length and width measurements of randomly selected plagioclase grains were made per section. Using 20 representative thin sections from throughout the southwestern FMC, ANOVA (Table A) determined that the three microstructural states were statistically independent populations with >95% confidence.

Average cumulative curves (Folk, 1974) were constructed for each of the three microstructural states (Figure A). The advantage of this construction is that numerous quantitative statistical parameters can be derived (Table B). These statistics are pictorially presented for ease of visual interpretation.

Microstructural state #1 is characterized by the presence of relic igneous plagioclase laths indicating a low level of deformation. State #2 is characterized by an absence of igneous laths. The original laths have been dismembered and transformed by progressive rotation into the grains of aggregates dominated by mechanical twins. This process suggests a relatively high level of deformation. State #3 is characterized by a recrystallized groundmass dominated by strain free equant plagioclase grains that have become optically positive. The lack of optically discernible strain effects in these grains reveals that recovery and recrystallization was static.

We will now examine the results of the grain size statistics in relation to the three microstructural states. The median value (Table B, derived from Figure A) is variable because of variable initial grain size. However, the mean value decreases progressively as one changes from microstructural state #1 to #3, owing to greater changes in fabric. This is strong evidence for the dominance of the mechanism of recrystallization by subgrain formation coupled with progressive rotation of the subgrains as seen in thin section. Recrystallization by nucleation and growth tends to increase the grain size.

The value of the Inclusive Graphic Standard Deviation can be correlated with the relative degree of sorting as determined by sedimentologists. In the present context, we are not dealing with processes of mechanical sorting but are attaining uniform grain size by deformation and recovery.

The value of Inclusive Graphic Skewness expresses the degree to which the grain size population approaches a normal distribution. As expected, skewness decreases with increasing fabric modification.

Kurtosis is a function of "peakedness" of the normal distribution curve. The present data demonstrate that microstructural state #1 is better sorted at the center than the tails of the statistical curve, while #2 and #3 show approximately equal sorting in the center and tails of that curve.

In conclusion, these statistics are useful in demonstrating the operation of different mechanisms of microstructural grain modification and their relative significance in fabric development.

Figure A: Plot of cumulative percent of grains that make it through a sieve of a given mm. grain size (Folk, 1974). In this study, grain size represents the longest dimension measured in plagioclase. Each curve represents an average cumulative curve for one of three microstructural states.

Table A: Analysis of Variance (ANOVA) of all the raw data from measured plagioclase grains demonstrates that each one of the three microstructural states is a statistically independent population with > 95% confidence. This allows us to construct three average cumulative curves for the three microstructural states (Figure A).

Table B: Statistical data obtained from the three average cumulative curves shown in Figure A.

MAP #1

This lithologic map is a modified version of that produced by Morris (1956). The scheme of rock types is that outlined by Dr. S.B. Lumbers who is doing exstensive regional mapping throughout the Grenville province of Ontario.

In this legend the main catagories of rock types are listed and only those subdivisions which are applicable to this study are presented.

11- Alkalic Rock - Carbonatite and Related Dikes

(a) Carbonatite

10- Paleozoic and Sedimentary Rocks

9- Post Metamorphic and Late Metamorphic Intrusive Rocks

(a) Diabase dikes

8- Anorthosite Suite

(a) Gneissic anorthositic gabbro and gabbroic anorthosite with layering and ultramafics

(b) Metagabbro and metadiorite

7- Late Granitic and Syenitic Rocks

(a) Massive quartz monzonite

(a') Gneissic quartz monzonite

(b) Granite pegmatite

(b') Syenitic pegmatite poor in quartz with pyroxene, amphibole, magnetite, apatite, calcite, uranium ?, pyrite, (brick red colour)

(b'') Calcite-rich pegmatite with apatite, fluorite, K-feldspar

(c) Massive syenite

(d) Gneissic syenite

(e) Gneissic nepheline syenite

(f) Gneissic syenite with apatie, pyroxene, amphibole

(g) Gneissic, alkalic, corundum-bearing syenite

(h) Nepheline bearing syenite pegmatite

(j) Albite syenite

(k) Leucosyenite pegmatite

6- Early Granite Rocks

5- Migmatitic Varieties of Clastic Siliceous Metasediments

4- Mafic Intrusive Rocks

(a) Metagabbro and metadiorite

(b) Metadiabase

3- <u>Carbonate Metasediments</u>

(a) Calcite marble

(é) siliceous marble

(f) fine grained dark grey marble

(h) skarn

2- <u>Clastic Siliceous Metasediments</u>

(a) Metagreywacke

(b) Orthoquartzite

1- <u>Calcareous Metasediments</u>

DEFORM VS GRAINS 13:55 FRIDAY, JANUARY 8, 1982 2

GENERAL LINEAR MODELS PROCEDURE

DEPENDENT VARIABLE: GRAINS

SOURCE	DF	SUM OF SQUARES	MEAN SQUARE	F VALUE	PR > F	R-SQUARE	C.V.
MODEL	2	0.15846750	0.07923375	3.73	0.0455	0.304830	24.6495
ERROR	17	0.36138750	0.02125809		STD DEV		GRAINS MEAN
CORRECTED TOTAL	19	0.51985500			0.14580154		0.59150000

SOURCE	DF	TYPE I SS	F VALUE	PR > F	DF	TYPE IV SS	F VALUE	PR > F
DEFORM	2	0.15846750	3.73	0.0455	2	0.15846750	3.73	0.0455

Using the data from the interval 5 to 95 cumulative percent the following confidence limits apply to the given F values:

90% (α = .1) = 2.64
95% (α = .05)= 3.59
99% (α = .01)= 6.11

F value 3.73, therefore greater than 95% confidence.

Appendix 2, Table A.

Appendix 2, Table B.

Microstructural State	#1	#2	#3
Median	.52mm	.56mm	.42mm
Mean 16-84	.69mm	.56mm	.42mm
5-95	.72mm	.60mm	.43mm
Inclusive Graphic Standard Deviation	1.09Ø (poorly sorted)	.60Ø (moderately well sorted)	.50Ø (moderately well to well sorted)
Inclusive Graphic Skewness	-0.250 (excess coarse)	+0.010 (nearly symmetrical)	-0.009 (nearly symmetrical)
Kurtosis	1.15 (leptokurtic)	1.07 (mesokurtic)	1.04 (mesokurtic)

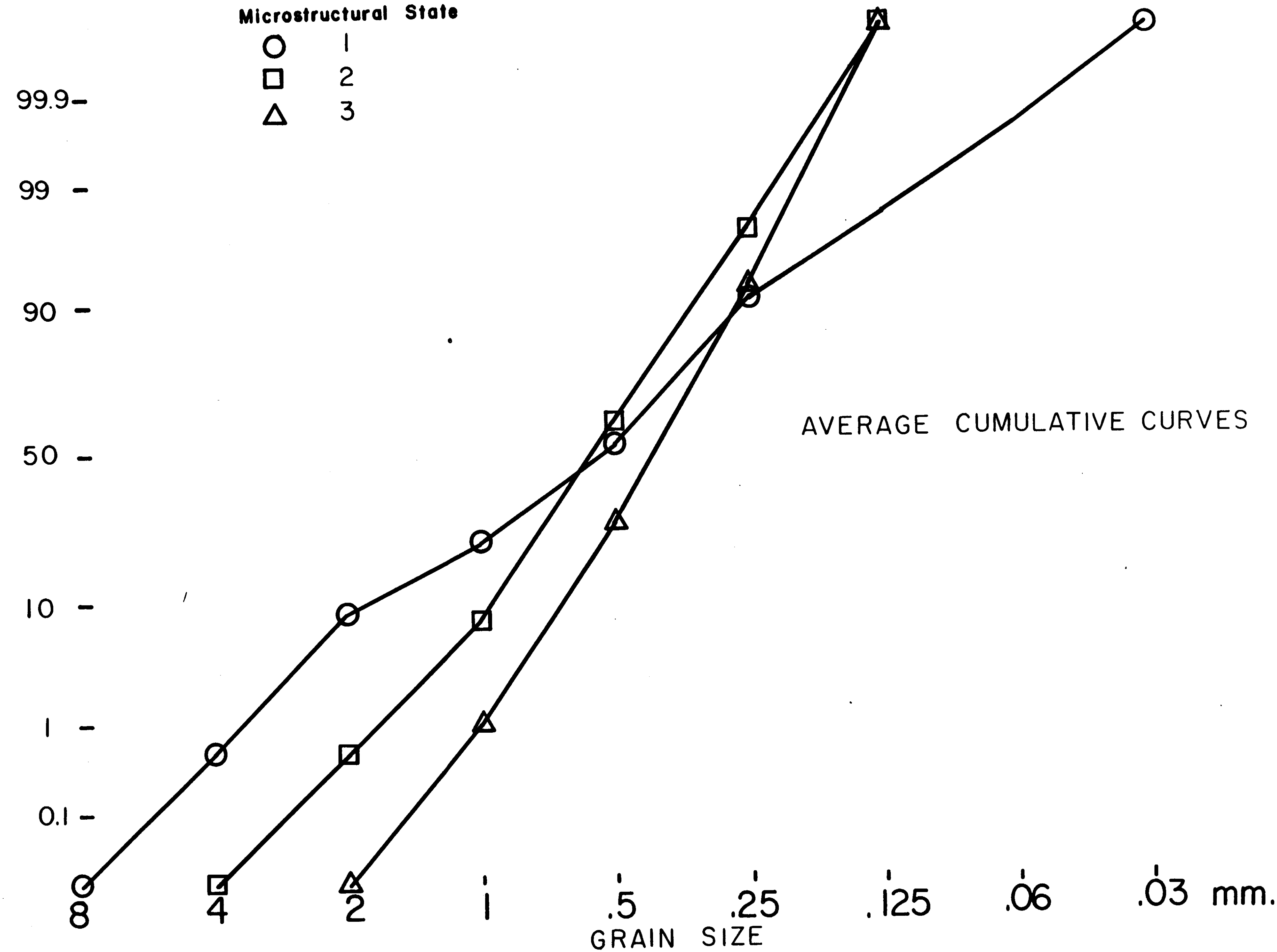

Appendix 2, Figure A.

Appendix 3

Data and Statistics used for Summary Display and Correlation in Figure 16

S T A T I S T I C A L   A N A L Y S I S   S Y S T E M

VARIABLE	N	MEAN	STANDARD DEVIATION	MINIMUM VALUE	MAXIMUM VALUE	STD ERROR OF MEAN	SUM	VARIANCE	C.V.
SIO2	31	68.12258065	10.38266856	45.40000000	84.2000000	1.86478232	2111.800000	107.7998	15.241
AL2O3	31	13.09677419	3.76824308	5.80000000	21.4000000	0.67679644	406.000000	14.1997	28.772
CAO	31	3.16516129	4.55517133	0.10000000	20.3000000	0.81813292	98.120000	20.7496	143.916
MGO	31	1.12419355	1.66270217	0.19000000	7.3000000	0.29863012	34.850000	2.7646	147.902
NA2O	31	5.22935484	1.50704111	2.16000000	8.7500000	0.27067257	162.110000	2.2712	28.819
K2O	31	3.02387097	2.78701116	0.29000000	10.8000000	0.50056198	93.740000	7.7674	92.167
FE2O3	31	2.95161290	4.36657539	0.43000000	18.4000000	0.78426009	91.500000	19.0670	147.939
MNO	31	0.07741935	0.12785324	0.01000000	0.4800000	0.02296312	2.400000	0.0163	165.144
TIO2	31	0.14161290	0.15895695	0.02000000	0.6100000	0.02854951	4.390000	0.0253	112.248
P2O5	31	0.21096774	0.78069779	0.00000000	4.2800000	0.14021746	6.540000	0.6095	370.056
LOI	31	0.75377419	0.77190603	0.00000000	3.3100000	0.13863842	23.367000	0.5958	102.405
BA	31	804.51612903	1875.28635806	30.00000000	8220.0000000	336.81137273	24940.000000	3516698.9247	233.095
CR2O3	31	194.83870968	78.86152284	20.00000000	370.0000000	14.16394763	6040.000000	6219.1398	40.475
ZR	31	425.80645161	928.17661464	0.00000000	5130.0000000	166.70544121	13200.000000	861511.8280	217.981
SR	31	850.64516129	1018.47577449	230.00000000	4380.0000000	182.92364908	26370.000000	1037292.9032	119.730
RB	31	212.58064516	153.73066799	20.00000000	450.0000000	27.61084305	6590.000000	23633.1183	72.316
F	31	810.32258065	1450.66992311	150.00000000	6800.0000000	260.54800968	25120.000000	2104443.2258	179.024
CL	31	114.42580645	38.63620899	56.90000000	191.0000000	6.93926798	3547.200000	1492.7566	33.765
U3O8	31	0.03790323	0.07263808	0.00000000	0.4000000	0.01304618	1.175000	0.0053	191.641
THO2	31	0.01645161	0.03033682	0.00000000	0.1600000	0.00544865	0.510000	0.0009	184.400
CO3	31	0.29677419	0.66205935	0.00000000	3.2000000	0.11890937	9.200000	0.4383	223.085
S	31	0.53909677	1.09526944	0.00000000	4.7700000	0.19671620	16.712000	1.1996	203.168
SYMBOL	29	1.00000000	0.00000000	1.00000000	1.0000000	0.00000000	29.000000	0.0000	0.000

SAMPLE	BA	CR2O3	ZR	SR	RB
1	90	230	1230	320	450
2	200	230	150	980	90
3	1020	70	380	1130	80
4	30	60	800	1460	350
5	110	310	460	460	30
6	60	150	40	860	20
7	150	260	870	280	100
8	410	220	60	480	220
9	280	120	470	2290	40
10	420	180	0	470	260
11	110	290	460	570	20
12	60	370	870	450	30
13	380	260	60	590	140
14	240	190	320	1160	370
15	530	200	120	540	250
16	7290	30	80	4380	440
17	8220	20	80	4270	370

SAMPLE	BA	CR2O3	ZR	SR	RB
18	120	220	5130	310	370
19	130	210	490	600	40
20	300	150	40	290	300
21	660	190	0	330	440
22	600	180	50	450	350
23	620	120	0	340	440
24	480	200	10	370	280
25	600	220	0	280	350
26	530	200	410	510	140
27	70	230	260	400	60
28	80	220	60	490	50
29	40	290	20	360	30
30	520	240	210	460	170
31	590	180	70	490	310

SAMPLE	F PPM	CL PPM	U3O8 %	THO2 %	CO3 %
1	820	104.	0.085	0.025	0.2
2	5100	170.	0.005	NIL	0.3
3	620	165.	NIL	TRACE	0.4
4	400	96.6	0.035	0.025	0.1
5	260	155.	0.040	0.035	<0.1
6	6800	180.	0.005	TRACE	0.8
7	300	115.	0.090	0.055	0.4
8	280	146.	0.010	TRACE	<0.1
9	190	191.	0.015	0.010	0.3
10	240	56.9	0.025	TRACE	<0.1
11	220	74.9	0.050	0.015	0.2
12	270	73.9	0.050	0.025	<0.1
13	190	88.2	0.010	0.005	<0.1
14	230	83.8	0.015	TRACE	<0.1
15	260	110.	0.025	0.010	<0.1
16	1200	100.	TRACE	TRACE	1.8
17	1560	116.	TRACE	NIL	3.2
18	720	110.	0.400	0.160	0.4
19	820	172.	0.025	0.015	0.1
20	1900	88.5	0.010	TRACE	1.0
21	220	81.8	TRACE	TRACE	<0.1
22	260	147.	0.010	NIL	<0.1
23	210	74.5	NIL	TRACE	<0.1
24	310	66.5	0.010	0.005	<0.1
25	160	93.0	NIL	NIL	<0.1
26	210	106.	0.090	0.030	<0.1
27	360	88.1	0.070	0.040	<0.1
28	360	103.	0.020	0.025	<0.1
29	310	124.	TRACE	TRACE	<0.1
30	150	185.	0.050	0.015	<0.1
31	190	81.5	0.030	0.015	<0.1

SAMPLE	S %
1	0.064
2	0.420
3	0.024
4	4.77
5	0.048
6	0.960
7	0.026
8	0.004
9	NIL
10	0.022
11	0.840
12	0.770
13	0.010
14	3.39
15	0.370
18	0.078
19	0.220
20	0.360
21	0.018
22	0.058
23	NIL
24	0.002
25	0.008
26	0.002
27	0.070
28	0.010
29	0.130
30	NIL
31	0.038

SAMPLE	SIO2	AL2O3	CAO	MGO	NA2O	K2O	FE2O3	MNO	TIO2	P2O5	LOI	SUM
18	49.5	8.91	9.22	3.75	4.57	0.77	18.4	0.40	0.48	0.09	0.85	96.5
19	72.8	14.1	1.09	0.30	7.65	0.91	0.88	0.02	0.04	0.00	0.93	98.7
20	58.3	6.94	8.46	4.63	3.56	1.72	12.6	0.48	0.15	0.01	2.77	99.6
21	73.1	14.1	0.18	0.26	4.84	5.12	0.45	0.01	0.03	0.00	0.31	98.3
22	72.0	14.4	0.40	0.42	4.93	5.21	0.94	0.01	0.05	0.00	0.39	98.7
23	69.1	16.7	0.10	0.71	5.50	6.32	0.45	0.01	0.07	0.00	0.31	98.7
24	71.5	15.5	0.23	0.38	6.30	3.95	0.64	0.01	0.03	0.00	0.23	98.7
25	76.0	12.4	0.10	0.19	4.65	4.03	0.43	0.01	0.02	0.00	0.31	98.1
26	73.2	13.6	0.43	0.30	4.94	4.52	0.91	0.02	0.12	0.00	0.47	98.6
27	73.4	14.1	1.07	0.41	7.79	0.46	0.98	0.04	0.10	0.00	0.47	98.7
28	74.5	13.7	0.83	0.28	7.51	0.47	0.76	0.02	0.06	0.00	0.31	98.4
29	78.9	10.6	1.09	0.40	6.02	0.32	1.00	0.03	0.09	0.00	0.47	99.0
30	74.4	12.7	0.31	0.31	4.61	4.42	0.81	0.01	0.07	0.00	0.31	98.0
31	72.7	13.9	0.49	0.29	4.72	5.48	1.01	0.03	0.06	0.00	0.23	98.5

SAMPLE	SIO2	AL2O3	CAO	MGO	NA2O	K2O	FE2O3	MNO	TIO2	P2O5	LOI	SUM
1	53.6	8.47	11.9	4.27	4.51	0.65	13.4	0.42	0.61	0.14	0.23	98.7
2	60.0	15.5	4.94	2.33	6.80	0.83	5.20	0.11	0.57	0.10	1.85	98.2
3	61.9	17.9	1.58	0.69	4.92	7.02	2.96	0.05	0.31	0.09	0.47	98.0
4	53.5	12.7	10.1	1.34	6.79	0.32	4.19	0.16	0.14	0.04	1.16	90.4
5	78.8	9.60	1.27	0.22	4.27	0.55	3.67	0.02	0.08	0.00	0.00	98.5
6	45.4	7.35	20.3	7.30	2.78	0.39	8.27	0.23	0.11	4.28	1.85	98.3
7	76.2	10.7	1.75	0.57	5.59	1.39	1.76	0.05	0.22	0.05	0.54	98.3
8	75.0	13.1	0.25	0.24	5.09	3.82	0.65	0.01	0.06	0.02	0.08	98.3
9	64.8	20.1	2.42	0.23	8.75	0.72	0.46	0.02	0.03	0.01	0.47	98.0
10	72.7	14.1	0.64	0.33	5.84	3.77	1.05	0.05	0.05	0.00	0.16	98.6
11	78.7	9.53	1.74	0.37	5.30	0.56	0.84	0.02	0.04	0.02	1.16	98.3
12	84.2	5.80	1.98	0.38	3.44	0.29	1.10	0.03	0.09	0.07	0.85	98.2
13	76.9	12.4	0.73	0.27	5.47	2.77	0.62	0.01	0.05	0.00	0.39	99.1
14	67.3	11.9	5.43	0.20	4.92	2.54	1.16	0.03	0.07	0.02	1.31	94.8
15	72.7	13.6	0.95	0.30	5.11	4.54	0.77	0.02	0.06	0.00	0.93	99.0
16	51.2	21.4	4.89	2.18	2.16	9.08	2.58	0.04	0.29	0.73	2.47	97.0
17	50.0	20.2	4.25	1.95	2.78	10.8	2.56	0.03	0.29	0.87	3.31	97.0

		METHOD	DETECTION LIMIT
S	%	XRF	0.002
F	PPM	WET	100.000
NA2O	%	XRF	0.010
MGO	%	XRF	0.010
AL2O3	%	XRF	0.010
SIO2	%	XRF	0.010
P2O5	%	XRF	0.010
CL	PPM	WET	0.100
K2O	%	XRF	0.010
CAO	%	XRF	0.010
TIO2	%	XRF	0.010
MNO	%	XRF	0.010
FE2O3	%	XRF	0.010
RB	PPM	XRF	10.000
SR	PPM	XRF	10.000
ZR	PPM	XRF	10.000
BA	PPM	XRF	20.000
U3O8	%	XRF	0.005
THO2	%	XRF	0.005
LOI	%	XRF	0.010
CR2O3	PPM	XRF	10.000
CO3	%	WET	0.100

CORRELATION COEFFICIENTS / PROB > |R| UNDER HO:RHO=0 / NUMBER OF OBSERVATIONS

	SIO2	AL203	CAO	MGO	NA20
SIO2	1.00000 0.0000 31	-0.17440 0.3481 31	-0.80056 0.0001 31	-0.78379 0.0001 31	0.32114 0.0781 31
AL203	-0.17440 0.3481 31	1.00000 0.0000 31	-0.36892 0.0411 31	-0.34552 0.0569 31	0.21789 0.2390 31
CAO	-0.80056 0.0001 31	-0.36892 0.0411 31	1.00000 0.0000 31	0.92347 0.0001 31	-0.34149 0.0601 31
MGO	-0.78379 0.0001 31	-0.34552 0.0569 31	0.92347 0.0001 31	1.00000 0.0000 31	-0.45044 0.0110 31
NA20	0.32114 0.0781 31	0.21789 0.2390 31	-0.34149 0.0601 31	-0.45044 0.0110 31	1.00000 0.0000 31
K20	-0.18324 0.3238 31	0.67455 0.0001 31	-0.28794 0.1162 31	-0.16452 0.3765 31	-0.46375 0.0086 31
FE203	-0.67243 0.0001 31	-0.44425 0.0123 31	0.72955 0.0001 31	0.78087 0.0001 31	-0.30596 0.0942 31
MNO	-0.63540 0.0001 31	-0.49312 0.0048 31	0.74294 0.0001 31	0.80141 0.0001 31	-0.25764 0.1617 31
TIO2	-0.62325 0.0002 31	-0.01563 0.9335 31	0.47379 0.0071 31	0.52468 0.0025 31	-0.20187 0.2761 31
P205	-0.53176 0.0021 31	-0.14984 0.4211 31	0.72592 0.0001 31	0.73286 0.0001 31	-0.42269 0.0178 31
LOI	-0.52053 0.0027 31	-0.08161 0.6625 31	0.48559 0.0056 31	0.52992 0.0022 31	-0.28942 0.1143 31
BA	-0.43118 0.0154 31	0.59806 0.0004 31	0.02207 0.9062 31	0.10627 0.5694 31	-0.50054 0.0041 31
CR203	0.69963 0.0001 31	-0.67969 0.0001 31	-0.26419 0.1509 31	-0.24576 0.1827 31	0.14632 0.4322 31

	K20	FE203	MNO	TIO2
SIO2	-0.18324 0.3238 31	-0.67243 0.0001 31	-0.63540 0.0001 31	-0.62325 0.0002 31
AL203	0.67455 0.0001 31	-0.44425 0.0123 31	-0.49312 0.0048 31	-0.01563 0.9335 31
CAO	-0.28794 0.1162 31	0.72955 0.0001 31	0.74294 0.0001 31	0.47379 0.0071 31
MGO	-0.16452 0.3765 31	0.78087 0.0001 31	0.80141 0.0001 31	0.52468 0.0025 31
NA20	-0.46375 0.0086 31	-0.30596 0.0942 31	-0.25764 0.1617 31	-0.20187 0.2761 31
K20	1.00000 0.0000 31	-0.27869 0.1290 31	-0.32210 0.0772 31	-0.01976 0.9160 31
FE203	-0.27869 0.1290 31	1.00000 0.0000 31	0.95222 0.0001 31	0.69523 0.0001 31
MNO	-0.32210 0.0772 31	0.95222 0.0001 31	1.00000 0.0000 31	0.59904 0.0004 31
TIO2	-0.01976 0.9160 31	0.69523 0.0001 31	0.59904 0.0004 31	1.00000 0.0000 31
P205	-0.01443 0.9386 31	0.24482 0.1844 31	0.22070 0.2328 31	0.06722 0.7194 31
LOI	0.06510 0.7279 31	0.34149 0.0601 31	0.38934 0.0304 31	0.26435 0.1507 31
BA	0.75394 0.0001 31	-0.06437 0.7308 31	-0.12984 0.4863 31	0.22168 0.2307 31
CR203	-0.62654 0.0002 31	-0.06374 0.7334 31	-0.08897 0.6341 31	-0.14344 0.4414 31

	P205	LOI	BA	CR203
SIO2	-0.53176 0.0021 31	-0.52053 0.0027 31	-0.43118 0.0154 31	0.69963 0.0001 31
AL203	-0.14984 0.4211 31	-0.08161 0.6625 31	0.59806 0.0004 31	-0.67969 0.0001 31
CAO	0.72592 0.0001 31	0.48559 0.0056 31	0.02207 0.9062 31	-0.26419 0.1509 31
MGO	0.73286 0.0001 31	0.52992 0.0022 31	0.10627 0.5694 31	-0.24576 0.1827 31
NA20	-0.42269 0.0178 31	-0.28942 0.1143 31	-0.50054 0.0041 31	0.14632 0.4322 31
K20	-0.01443 0.9386 31	0.06510 0.7279 31	0.75394 0.0001 31	-0.62654 0.0002 31
FE203	0.24482 0.1844 31	0.34149 0.0601 31	-0.06437 0.7308 31	-0.06374 0.7334 31
MNO	0.22070 0.2328 31	0.38934 0.0304 31	-0.12984 0.4863 31	-0.08897 0.6341 31
TIO2	0.06722 0.7194 31	0.26435 0.1507 31	0.22166 0.2307 31	-0.14344 0.4414 31
P205	1.00000 0.0000 31	0.36510 0.0434 31	0.17389 0.3495 31	-0.24561 0.1829 31
LOI	0.36510 0.0434 31	1.00000 0.0000 31	0.35177 0.0523 31	-0.32290 0.0764 31
BA	0.17389 0.3495 31	0.35177 0.0523 31	1.00000 0.0000 31	-0.61611 0.0002 31
CR203	-0.24561 0.1829 31	-0.32290 0.0764 31	-0.61611 0.0002 31	1.00000 0.0000 31

CORRELATION COEFFICIENTS / PROB > |R| UNDER HO:RHO=0 / NUMBER OF OBSERVATIONS

	SIO2	AL2O3	CAO	MGO	NA2O	K2O	FE2O3	MNO	TIO2	P2O5	LOI	BA	CR2O3
ZR	-0.32566 0.0738 31	-0.30803 0.0918 31	0.31420 0.0852 31	0.24727 0.1799 31	-0.04517 0.8093 31	-0.28753 0.1168 31	0.70034 0.0001 31	0.53082 0.0021 31	0.49989 0.0042 31	-0.07563 0.6859 31	-0.00133 0.9943 31	-0.13603 0.4656 31	0.13504 0.4689 31
SR	-0.53306 0.0020 31	0.65582 0.0001 31	0.16272 0.3818 31	0.13689 0.4628 31	-0.28893 0.1149 31	0.55066 0.0013 31	-0.06805 0.7160 31	-0.12171 0.5143 31	0.22646 0.2206 31	0.22957 0.2141 31	0.37573 0.0372 31	0.89742 0.0001 31	-0.69299 0.0001 31
RB	-0.39670 0.0271 31	0.22212 0.2298 31	0.11166 0.5498 31	0.11190 0.5490 31	-0.37028 0.0403 31	0.54106 0.0017 31	0.24131 0.1909 31	0.25762 0.1616 31	0.19748 0.2869 31	-0.14231 0.4451 31	0.02292 0.9026 31	0.37214 0.0392 31	-0.48223 0.0060 31
F	-0.58095 0.0006 31	-0.13111 0.4820 31	0.70599 0.0001 31	0.78042 0.0001 31	-0.24376 0.1863 31	-0.14692 0.4303 31	0.38586 0.0320 31	0.36843 0.0414 31	0.38659 0.0317 31	0.79081 0.0001 31	0.55091 0.0013 31	0.07306 0.6961 31	-0.17262 0.3531 31
CL	-0.20176 0.2764 31	0.15156 0.4157 31	0.18339 0.3234 31	0.19616 0.2902 31	0.12841 0.4912 31	-0.11271 0.5461 31	0.06672 0.7214 31	-0.02094 0.9110 31	0.17095 0.3578 31	0.30496 0.0953 31	0.07910 0.6723 31	-0.04220 0.8217 31	-0.08583 0.6462 31
U3O8	-0.22356 0.2267 31	-0.33492 0.0655 31	0.22670 0.2201 31	0.19596 0.2907 31	-0.03074 0.8696 31	-0.27909 0.1284 31	0.64420 0.0001 31	0.48251 0.0060 31	0.42786 0.0163 31	-0.09813 0.5995 31	-0.05846 0.7548 31	-0.17289 0.3523 31	0.21422 0.2472 31
THO2	-0.15959 0.3911 31	-0.32420 0.0752 31	0.17864 0.3363 31	0.12950 0.4875 31	0.05018 0.7886 31	-0.34271 0.0591 31	0.57583 0.0007 31	0.40921 0.0223 31	0.37346 0.0385 31	-0.11793 0.5275 31	-0.09327 0.6177 31	-0.18817 0.3107 31	0.24358 0.1867 31
CO3	-0.62253 0.0002 31	0.36676 0.0424 31	0.31896 0.0803 31	0.42304 0.0177 31	-0.51580 0.0030 31	0.53506 0.0019 31	0.22136 0.2314 31	0.18301 0.3244 31	0.35385 0.0508 31	0.37096 0.0399 31	0.67044 0.0001 31	0.88836 0.0001 31	-0.60557 0.0003 31
S	-0.36017 0.0506 30	0.12548 0.5088 30	0.31708 0.0878 30	0.17698 0.3495 30	-0.42470 0.0187 30	0.25937 0.1663 30	-0.00922 0.9614 30	-0.02984 0.8756 30	0.09865 0.6040 30	0.27562 0.1404 30	0.43409 0.0055 30	0.52954 0.0026 30	-0.32172 0.0830 30
SYMBOL	0.00000 1.0000 29	0.00000 1.0000 29	0.00000 1.0000 29	0.00000 1.0000 29	0.00000 1.0000 29	0.00000 1.0000 29	0.00000 1.0000 29	0.00000 1.0000 29	0.00000 1.0000 29	0.00000 1.0000 29	0.00000 1.0000 29	-0.00000 1.0000 29	-0.00000 1.0000 29

	ZR	SR	RB	F	CL	U3O8	THO2	CO3	S	SYMBOL
SIO2	-0.32566 0.0738 31	-0.53306 0.0020 31	-0.39670 0.0271 31	-0.58095 0.0006 31	-0.20176 0.2764 31	-0.22356 0.2267 31	-0.15959 0.3911 31	-0.62253 0.0002 31	-0.36017 0.0506 30	0.00000 1.0000 29
AL2O3	-0.30803 0.0918 31	0.65582 0.0001 31	0.22212 0.2298 31	-0.13111 0.4820 31	0.15156 0.4157 31	-0.33492 0.0655 31	-0.32420 0.0752 31	0.36676 0.0424 31	0.12548 0.5088 30	0.00000 1.0000 29

S T A T I S T I C A L   A N A L Y S I S   S Y S T E M   17:25 WEDNESDAY, SEPTEMBER 29, 1982

CORRELATION COEFFICIENTS / PROB > |R| UNDER HO:RHO=0 / NUMBER OF OBSERVATIONS

	ZR	SR	RB	F	CL	U3O8	THO2	CO3	S	SYMBOL
CAO	0.31420 0.0852 31	0.16272 0.3818 31	0.11166 0.5498 31	0.70599 0.0001 31	0.18339 0.3234 31	0.22670 0.2201 31	0.17864 0.3363 31	0.31396 0.0803 31	0.31708 0.0878 30	0.00000 1.0000 29
MGO	0.24727 0.1799 31	0.13689 0.4628 31	0.11190 0.5490 31	0.78042 0.0001 31	0.19616 0.2902 31	0.19596 0.2907 31	0.12950 0.4875 31	0.42304 0.0177 31	0.17698 0.3495 30	0.00000 1.0000 29
NA2O	-0.04517 0.8093 31	-0.28893 0.1149 31	-0.37028 0.0403 31	-0.24376 0.1863 31	0.12841 0.4912 31	-0.03074 0.8696 31	0.05018 0.7886 31	-0.51580 0.0030 31	-0.42670 0.0187 30	0.00000 1.0000 29
K2O	-0.28753 0.1168 31	0.55066 0.0013 31	0.54106 0.0017 31	-0.14692 0.4303 31	-0.11271 0.5461 31	-0.27909 0.1284 31	-0.34271 0.0591 31	-0.53506 0.0019 31	0.25937 0.1663 30	0.00000 1.0000 29
FE2O3	0.70034 0.0001 31	-0.06805 0.7160 31	0.24131 0.1909 31	0.38586 0.0320 31	0.06672 0.7214 31	0.64420 0.0001 31	0.57583 0.0007 31	0.22136 0.2314 31	-0.00922 0.9614 30	0.00000 1.0000 29
MNO	0.53082 0.0021 31	-0.12171 0.5143 31	0.25762 0.1618 31	0.36843 0.0414 31	-0.02094 0.9110 31	0.48251 0.0060 31	0.40921 0.0223 31	0.18301 0.3244 31	-0.02984 0.8756 30	0.00000 1.0000 29
TIO2	0.49989 0.0042 31	0.22646 0.2206 31	0.19748 0.2869 31	0.38659 0.0317 31	0.17095 0.3578 31	0.42786 0.0163 31	0.37346 0.0385 31	0.35385 0.0508 31	0.09865 0.6040 30	0.00000 1.0000 29
P2O5	-0.07563 0.6859 31	0.22957 0.2141 31	-0.14231 0.4451 31	0.79081 0.0001 31	0.30496 0.0953 31	-0.09813 0.5995 31	-0.11793 0.5275 31	0.37096 0.0399 31	0.27562 0.1404 30	0.00000 1.0000 29
LOI	-0.00133 0.9943 31	0.37573 0.0372 31	0.02292 0.9026 31	0.55091 0.0013 31	0.07910 0.6723 31	-0.05848 0.7548 31	-0.09327 0.6177 31	0.67044 0.0001 31	0.49409 0.0055 30	0.00000 1.0000 29
BA	-0.13603 0.4656 31	0.89742 0.0001 31	0.37214 0.0392 31	-0.07306 0.6961 31	-0.04220 0.8217 31	-0.17289 0.3523 31	-0.18817 0.3107 31	0.86836 0.0001 31	0.52954 0.0026 30	0.00000 1.0000 29
CR2O3	0.13504 0.4689 31	-0.69299 0.0001 31	-0.48223 0.0060 31	-0.17262 0.3531 31	-0.08583 0.6462 31	0.21422 0.2472 31	0.24358 0.1867 31	-0.60567 0.0003 31	-0.32172 0.0830 30	0.00000 1.0000 29
ZR	1.00000 0.0000 31	-0.11552 0.5360 31	0.12751 0.4942 31	-0.06178 0.7413 31	0.00103 0.9956 31	0.96240 0.0001 31	0.93400 0.0001 31	-0.01304 0.9445 31	-0.07761 0.6835 30	0.00000 1.0000 29
SR	-0.11552 0.5360 31	1.00000 0.0000 31	0.21831 0.2381 31	0.15752 0.3974 31	0.13716 0.4619 31	-0.20646 0.2651 31	-0.20339 0.2725 31	0.62818 0.0001 31	0.60678 0.0004 30	0.00000 1.0000 29

CORRELATION COEFFICIENTS / PROB > |R| UNDER HO:RHO=0 / NUMBER OF OBSERVATIONS

	ZR	SR	RB	F	CL	U308	THO2	CO3	S	SYMBOL
RB	0.12751 0.4942 31	0.21831 0.2381 31	1.00000 0.0000 31	-0.18949 0.3073 31	-0.43735 0.0139 31	0.09065 0.6277 31	-0.00691 0.9706 31	0.23851 0.1963 31	0.23625 0.2088 30	0.00000 1.0000 29
F	-0.06178 0.7413 31	0.15752 0.3974 31	-0.13949 0.3073 31	1.00000 0.0000 31	0.40380 0.0243 31	-0.10307 0.5811 31	-0.13468 0.4701 31	0.33353 0.0667 31	0.20288 0.2823 30	0.00000 1.0000 29
CL	0.00103 0.9956 31	0.13716 0.4619 31	-0.43735 0.0139 31	0.40380 0.0243 31	1.00000 0.0000 31	-0.06023 0.7476 31	-0.03928 0.8338 31	0.07548 0.6865 31	-0.12840 0.4989 30	0.00000 1.0000 29
U308	0.96240 0.0001 31	-0.20646 0.2651 31	0.09065 0.6277 31	-0.10307 0.5811 31	-0.06023 0.7476 31	1.00000 0.0000 31	0.96954 0.0001 31	-0.06911 0.7118 31	-0.14940 0.4307 30	0.00000 1.0000 29
THO2	0.93400 0.0001 31	-0.20339 0.2725 31	-0.00691 0.9706 31	-0.13468 0.4701 31	-0.03928 0.8338 31	0.96954 0.0001 31	1.00000 0.0000 31	-0.08357 0.6549 31	-0.19206 0.3093 30	0.00000 1.0000 29
CO3	-0.01304 0.9445 31	0.82818 0.0001 31	0.23851 0.1963 31	0.33353 0.0667 31	0.07546 0.6865 31	-0.06911 0.7118 31	-0.08357 0.6549 31	1.00000 0.0000 31	0.52075 0.0032 30	0.00000 1.0000 29
S	-0.07761 0.6835 30	0.60673 0.0004 30	0.23625 0.2088 30	0.20288 0.2823 30	-0.12840 0.4989 30	-0.14940 0.4307 30	-0.19306 0.3093 30	0.52075 0.0032 30	1.00000 0.0000 30	0.00000 1.0000 28
SYMBOL	0.00000 1.0000 29	0.00000 1.0000 29	0.00000 1.0000 29	0.00000 1.0000 29	0.00000 1.0000 29	0.00000 1.0000 29	0.00000 1.0000 29	0.00000 1.0000 29	0.00000 1.0000 28	0.00000 1.0000 29

Appendix 4

Station Location Map

Appendix 4

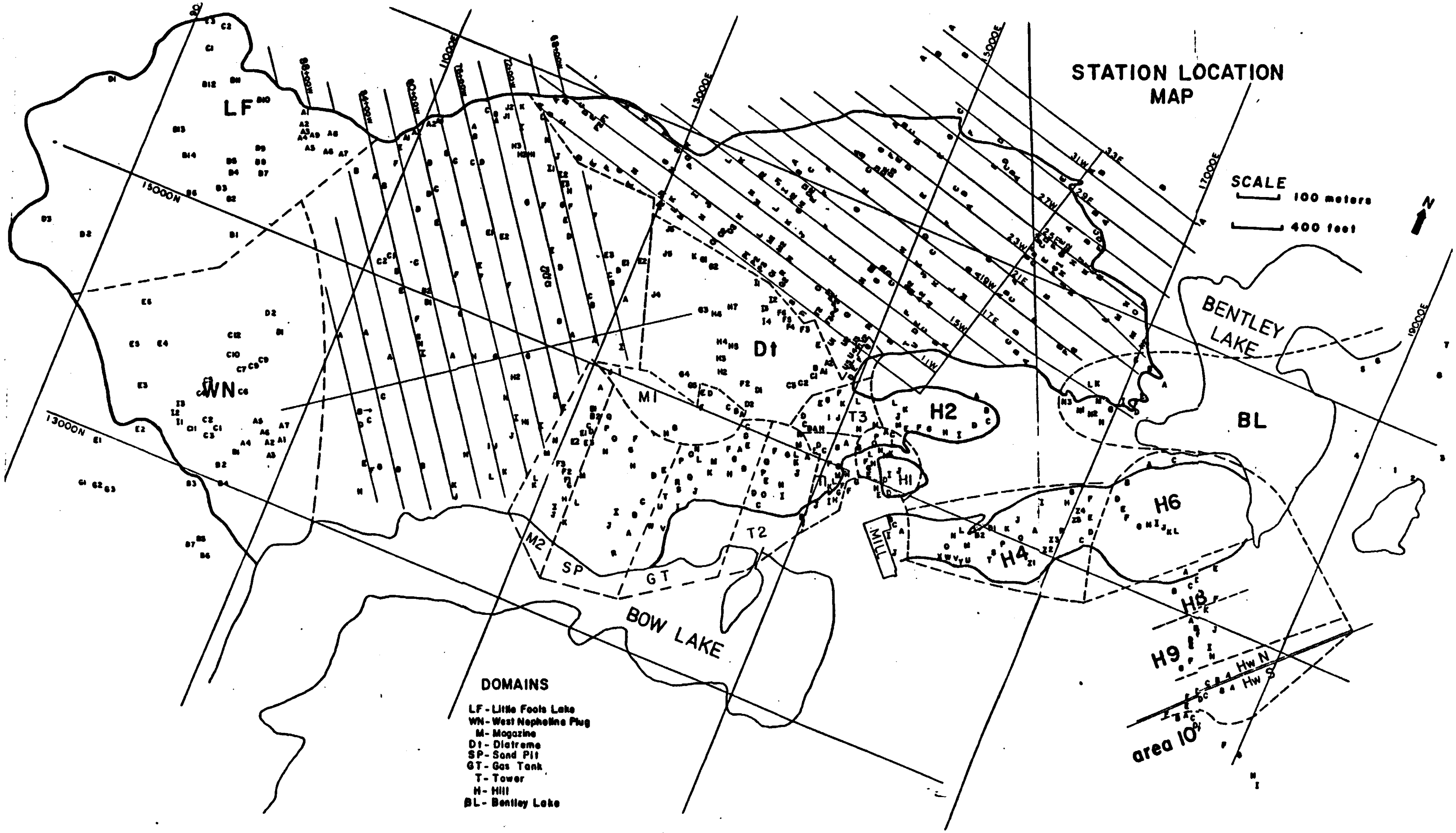
STATION LOCATION MAP
SCALE
100 meters
400 feet
N
BENTLEY LAKE
BL
BOW LAKE
LF
WN
D1
M1
M2
SP
GT
T2
T3
H1
H2
H4
H6
H8
H9
MILL
area 10
Hw N
Hw S
15000N
13000N
11000E
13000E
15000E
17000E
19000E
DOMAINS
LF - Little Fools Lake
WN - West Nepheline Plug
M - Magazine
D1 - Diatreme
SP - Sand Pit
GT - Gas Tank
T - Tower
H - Hill
BL - Bentley Lake

ACKNOWLEDGEMENTS

We would like to thank Patrick Ramsay and Steve Hall for assistance during the 1980 and 1981 field seasons respectively. R. Alexander, chief geologist, and staff geologists O. Zavesiczky and L. Richardson were particularly helpful in providing a great deal of information about the mine. M. Zurowski of Conwest provided data on the mine after its closure in 1982. Dr. S.B. Lumbers and V. Vertolli of the Royal Ontario Museum provided valuable assistance in discussions and on field trips about the regional geology. S. Masson of Laurentian University and N. Culshaw of Carlton University freely shared their knowledge of the area. We are most grateful to the Ontario Geological Survey for their financial as well as logistical support and like to thank particularly Cheryl Collins, Wendy Paquette, Hans Meyn, and J.A. Robertson.

BIBLIOGRAPHY

Appleyard, E.C. and Williams, S.E.
1981: Metasomatic Effects in the Faraday Metagabbro, Bancroft, Ontario, Canada; Tzchermaks Min. Petr. Mitt., Vol. 28. pp.81-87.

Ashwal, L.D.
1982: Mineralogy of Mafic and Fe-Ti Oxide Rich Differentiates of the Marcy Anorthosite Massif, Adirondacks, New York; American Mineralogist, Vol. 67. pp. 14-27.

Bedell, R.L. and Schwerdtner, W.M.
1981: Structural Controls of U-ore Bodies in the Madawaska Mines Area, Bancroft, Ontario; pp. 13-17, in Summary of Research, 1980-1981, edited by E.G. Pye, Ontario Geological Survey, Miscellaneous Paper 98.

Bedell, R.L.
1982: Influence of a Metamorphosed Gabbro in the Control of Uranium-Bearing Pegmatite Dykes, Madawaska Mines, Bancroft, Ontario; pp. 139-143, in Uranium in Granites, edited by Y.T. Maurice, Geological Survey of Canada, Paper 81-23.

Chapple, W.M.
1969: Fold Shape and Rheology: The Folding of an Isolated Viscous-Plastic Layer;Tectonophysics, Vol. 7, pp. 97-116.

Folk, R.L.
1974: Petrology of Sedimentary Rocks; Hemphill Publishing Company, Austin, Texas.

Hewitt, D. and Satterly, J.
1957: Haliburton-Bancroft Area, Ontario Department of Mines, Map No. 1957b.

Kamb, W.B.
1959: Ice Petrofabric Observations From Blue Glacier, Washington, in Relation to Theory and Experiment; J. Geophysical Res. Vol. 64, pp. 1891-1909.

Kretz, R.
1968: Study of Pegmatite Bodies and Enclosing Rocks, Yellowknife, Beaulieu Region, District of Mackenzie; Geological Survey of Canada, Bulletin 159. 108 p.

Kronenberg, A.K. and Shelton, G.L.
1980: Deformation Microstructures in Experimentally Deformed Maryland Diabase; Journal of Structural Geology, Vol. 2, pp. 341-353.

Little, H.W., Smith, E.E.N. and Barnes, F.Q.
1972: Uranium Deposits of Canada; International Geological Congress, Guidebook for 24th Exscursion C67.

Morris, H.R.
1956: Surface Geology of the Faraday Uranium Mine, Bancroft,

Ontario; unpublished M.Sc. Thesis, University of Toronto.

Price, N.
1966: Fault and Joint Development in Brittle and Semi-Brittle Rock. Pergamon Press.

Ross, M.R. and Huebner, J.S.
1975: A Pyroxene Geothermometer Based on Composition-Temperature Relationships of Naturally Occurring Orthopyroxene, Pigeonite and Augite; International Conference of Geothermometry and Geobarometry, Extended Abstracts Pennsylvania State University, University Park, Pa.

Schwerdtner, W.M., Sheehan, P.M., and Rucklidge, J.C.
1971: Variation in Degree of Hornblende Alignment Within Two Boudinage Structures; Can. Jour. Earth Sci., Vol. 8, pp. 144-149.

Schwerdtner, W.M., Bennett, P.J. and Janes, T.W.
1977: Application of L-S Tectonite Scheme to Structural Mapping and Paleostrain Analysis; Canadian Jour. Earth Sci., Vol. 14, pp. 1021-1032.

Schwerdtner, W.M. and Lumbers, S.B.
1980: Major Diapiric Structures in the Superior and Grenville Provinces of the Canadian Shield; in The Continental Crust and its Mineral Deposits, editor D. Strangway, Geological Association of Canada Special Paper 20, pp. 149-180.

N
SCALE
100 meters
400 feet
BENTLEY LAKE
BOW LAKE
MILL
HIGHWAY 28
metasediments
17000N
15000N
13000N
9000E
11000E
13000E
15000E
17000E
19000E


17000N
9000E
11000E
13000E
15000E
17000E
19000E
15000N
13000N
N
BENTLEY LAKE
BOW LAKE
MILL
Shear Zone
Foliation
Lineation
SCALE
100 meters
400 feet

N
BENTLEY LAKE
BOW LAKE
DIPS
0-22°
23-45°
46-68°
69-90°
SCALE
100 meters
400 feet